ISTANBUL TECHNICAL UNIVERSITY ★ GRADUATE SCHOOL OF EARTHQUAKE ENGINEERING AND DISASTER MANAGMENT

SOIL IMPROVEMENT BY POLYURETHANE-BITUMEN

M.Sc. THESIS

Atefeh SOROORI SARABI

Department of Earthquake Engineering and Disaster Management
Earthquake Engineering Programme

SEPTEMBER 2014

ISTANBUL TECHNICAL UNIVERSITY ★ GRADUATE SCHOOL OF EARTHQUAKE ENGINEERING AND DISASTER MANAGMENT

SOIL IMPROVEMENT BY POLYURETHANE-BITUMEN

M.Sc. THESIS

Atefeh SOROORI SARABI
(802121005)

Department of Earthquake Engineering and Disaster Management
Earthquake Engineering Programme

Thesis Advisor: Prof. Dr. Ayfer ERKEN

SEPTEMBER 2014

İSTANBUL TEKNİK ÜNİVERSİTESİ ★ DEPREM MÜHENDİLİĞİ VE AFET YÖNETİMİ ENSTİTÜSÜ

ZEMİN GÜÇLENDİRMESİ POLYURETHANE-BITUMEN ETKİSİNDE

YÜKSEK LİSANS TEZİ

Atefeh SOROORI SARABI
(802121005)

Deprem Mühendisliği ve Afet Yönetimi Anabilim Dalı
Deprem Mühendisliği Programı

Tez Danışmanı: Prof. Dr. Ayfer ERKEN

EYLUL 2014

Atefeh Soroori Sarabi, a **M.Sc.**student of ITU **Institute of Earthquake Engineering &Disaster Management / Graduate School of Earthquake Engineering**student ID **802121005**, successfully defended the **thesis** entitled “**SOIL IMPROVEMENT BY POLYURETHANE-BITUMEN**”, which she prepared after fulfilling the requirements specified in the associated legislations, before the jury whose signatures are below.

Thesis Advisor :	**Prof. Dr. Ayfer ERKEN** İstanbul Technical University	....
Jury Members :	**Assoc.Prof. Dr. Hasan YILDIRIM** İstanbul Technical University	....
	Assoc.Prof. Dr. Ayşe ENDINCLILER Boğaziçi University	....

Date of Submission : 5 MAY 2014
Date of Defense : 30 September 2014

To my mother and father,

FOREWORD

I would like to express my sincere gratitude to my thesis adviser Prof. Dr. Ayfer Erken and Assoc. Prof. Dr. Hasan Yıldırım for their advice and support. Further,I would like to thank the staff at the Geotechnical laboratory and Construction Materials Laboratory for their maintenance and help. I would like to thank Aytac Yasargun and Soheil Khoshkholghi for their help in the application of the test apparatus. Finally, I wish to express my greatest thanks to my family and friends who have supported me throughout my life.

SEPTEMBER 2014

Atefeh SOROORI SARABI
(Civil Engineer)

TABLE OF CONTENTS

Page

ABBREVIATIONS

ASTM : American Society for Testing and Materials
Ca: Apparent cohesion
C_u : Coefficient of uniformity
D : Damping ratio
D_{10} : Effective size
D_{30}: Diameter corresponding to 30% finer
D_{50}: The medium grain size
D_{60}: Diameter corresponding to 60% finer
D_r: Relative density
e : Void ratio
E : Elasticity modulus, Young's modulus
E_{max}: Maximum Elasticity modulus, Maximum Young's modulus
G : Shear Modulus
G_{max} : Maximum Shear Modulus
μ: Pore water pressure
UU : Unconsolidated undrained
In. : Inch
KN : Kilonewton
KPa : Kilopascal
MPa : Megapascal
P.B: polyurethane - Bitumen
PVD : Prefabricated vertical drain
P.W.P. : Pore water pressure
Psi : Pounds per square inch
SP : Poorly graded sand
V : Volume
VC:Vibro compaction
VCCs: Vibro concrete columns
Wt : Weight
α: parameter of the Ramberg-Osgood model
ε: Axial strain
ϕ : Shear strength angle, internal friction angle
μ : Poisson's ratio
τ : Shear stress
γ : Shear strain
σ_1: Major principle stress
σ_3: Minor principle stress

LIST OF TABLES

Page

LIST OF FIGURES

Page

IMPROVEMENT OF SANDS BY POLYURETHANE

SUMMARY

Many buildings have been damaged due to an extensive liquefaction of the sandy ground during the earthquakes. Civil engineering structures built on sites of loose saturated and dense cohesionless soils are therefore at risk of liquefaction with potential of damage to the structures and need improvement to safeguard against damages by liquefaction. In most of the constructions, the soil properties need to be improved in order to enable safe and economical constructions. Soil improvement techniques are used to improve the engineering properties of soils. Therefore a compressive laboratory program is required to study strength characteristics of both reinforced and unreinforced soils also to investigate their behaviors under cycle leading.

The objective of the present thesis is soil improvement of sands against liquefaction. The concept of reinforcement is not new. Early civilizations commonly used sun-dried soil bricks as a building material. Somewhere in their experience it became an accepted practice to mix the soil with straw or other fiber available to them to improve the properties. Various materials were used in reinforcement of both pavement materials and sub grade soils. They can vary greatly, either in form (strips, sheets, grids, bars, or fibers), texture(rough or smooth), and relative stiffness (high such as steel or relatively low such as polymeric fabrics).

In this research the improvement in the properties of uniform sand is achieved by the two-component, polyurethane – Bitumen. A fine sand sample was collected from Akpinar, Turkey. The mean diameter of sand is 0.3mm and e_{min} and e_{max} are 0.528 and 0.800 respectively. The mixture of sand and polyurethane-bitumen by various proportion (3%, 5% and 10% of dry weight of sand) has been prepare in two sizes by 10cm diameter, 20cm high and 5cm diameter, 10cm high.

In first section the liquefaction hazard and also the soil improvement and methods of improvement have discussed. Different methods are preferred according to the requirements and soil type. One of the most commonly used soil improvement type is the addition of substances.

In the second section dynamic properties of sand, methods for calculating the damping ratio of sand and also the factors that influence on soil's properties have been mentioned.

Throug last sections the dynamic and static tests that conducted in ITU laboratory described, the engineering properties of Akpınar sand are determined, a series of cyclic triaxial tests were performed using fine sands and mixing polyurethane-bitumen content. To study the effect of time on stress-strain behavior of the mixture sand specimens, unconfined axial loading tests have been conducted to the samples after 1st day, 7th day, 30th day, 5th ,6 th,7 th months. Also the triaxial loading test performed to 27 reinforced sand samples at three different curing time with different confining

pressure. The shear strength parameters calculated from static triaxial tests conducted on reinforced samples. And finally in last section the test's results have been discussed.

ZEMİN GÜÇLENDİRMESİ POLYURETHANE ETKİSİNDE
ÖZET

Gelişen teknoloji ve artan nüfusa bağlı olarak günümüzde zeminler yüksek miktarda yüklere maruz kalmaktadırlar. Birçok inşaat projesinde, güvenli ve ekonomik çözümler geliştirebilmek için zeminlerin mühendislik, özelliklerinin iyileştirilmesi gerekmektedir.

Depremler sırasında, bir çok binadaki hasar, kumlu zeminlerdeki meydana gelen geniş sıvılaşmadan kaynaklanmaktadır. İş bu haldeyken, gevşek suya doygun ve sıkı kohezyonsuz toprak üzerindeki yapılar, yapısal hasar potansiyeline sahip ve sıvılaşma riski altındadır. Böyle bir riske karşı korunmak için iyileştirilmeye ve güçlendirilmeye gerek duyulmaktadır.

Güvenli ve ekonomik yapıların sağlanması amacıyla, yapıtların çoğunda, toprak özelliklerinin iyileştirilmesi gerekir.

Zemin iyileştirme yöntemleri de zeminlerin mühendislik parametrelerini iyileştirmek için geliştirilen yöntemlerdir. Uygulanan zemin iyileştirme yöntemi, zemin cinsine ve uygulamanın gerekliliklerine bağlıdır. Toprağın mühendislik özelliklerini güçlendirmek için toprak iyileştirme teknikleri kullanılmaktadır. Bu nedenle, toprağın hem güçlendirilmiş ve hemde güçlendirilmemiş dayanım özelliklerini ve birde onların çevrimli yuk altındaki davranışını incelemek için bir laboratuar çalişmasina ihtiyaç duyulmaktadır.

İyileştirilme kavramı yeni bir yöntem değildir. İlkel uygarlıklar güneşte kurutulmuş toprak tüğlalarını yaygın bir şekilde yapı malzemesi olarak, kullanıyordu. Daha sonra deneyimlerde, toprk özelliklerinin iyilieştirilmesi için toprağın saman yada mevcut diğer elyaflar ile karıştırılması kabul edilebilir bir uygulama haline gelmiştir. Üst tabakalar (kaplamalar) ve alt sınıf tabakaların güçlendirimesinde çeşitli malzemeler kullanılmaktadır. Kullanılan malzemeler şekil (şeritler, levhalar, ızgaralar, çubuk yada lifler), doku (sert veya yumuşak dokular), göreceli rijitlik (çelik gibi yüksek yada polimer kumaş gibi düşük rijitliğe sahip) farklı açılardan değişik çeşitlerde olabilir.

Bu tezin amacı, kumlu zeminlerin sıvılaşmaya karşıt iyileştirilmesidir.

Bu çalışmada, iki-bileşenli Poliüretan - Bitüm ile homojen kumun özellikleri iyileştirilmiştir. Bu iki madde sıvı yalıtımından üretilmiştir. Burada temiz kum iyi derecelenmiş Akpınar kumundan örnekler elde edilmiştir. Burada standart kum kullanılmıştır. Kumun ortalama çapı 0.3 mm ve emin ve emax değerleri sırasıyla 0.528 ve 0.800 dir. Kum ve çeşitli oranlarda (kumun kuru ağırlığının 3%, 5% ve 10% i) Poliüretan – Bitüm karışımı, iki farklı çapta (10cm ve 20cm) ve 10cm yüksekliğinde hazırlanmıştır.

Bu karışımların davranışlarının incelenmesi için numunelerimize 1.günde, 7.günde, 30.günde ve 6 aylık zaman diliminden sonara serbest eksenel yük uygulanmistir. Elde ettiğmiz sonuçlara göre örneklerimizde hiç bir şekilde davranış farklılığı tesbit edilmemiştir. Kur suresi artırırken eksenel gerilmede artış gözlenmektedir.

Tezin ilk bölümünde, sıvılaşma tehlikesi ve toprak iyileştirlme kavramları ve iyilieştirme yöntemleri ele alınmıştır. Toprak tipine göre ve ihtiyaca göre, farklı yöntemler tercih edilmektedir. Günümüzde en çok kullanılan zemin iyileştirme yöntemlerinden biri de çeşitli
toprağa çeşitli malzemeler katılarak toprak iyileştirilmesidir.
İkinci bölümde kumun dinamik özellikleri, kumun sönüm oranının hesplanmasında kullanılan yöntemler ve birde toprağın özelliklerini etkileyen faktörlerden bahsedilmiştir.
Son bölümlerde, İTÜ laboratuarında yapılan dinamik ve statik testler anlatılmıştır. Akpınar kumunun mühendislik özellikleri hesaplanmıştır. İyi derecelenmiş kumlar ve Poliüretan - Bitüm karışımı üzerinde bir dizi çevrimsel üç eksenli deneyler yapılmıştır. Kum karışımı örneklerinde gerilme-deformasyon üzerindeki zaman faktörünün etkisini incelemek için, birinci, yedinci, otuzuncu günlerde ve beşinci, altıncı ve yedinci aylarda serbest eksenel yükleme testi uygulanmıştır.
Ayrıca 27 iyileştirilmiş kum örneğinde üç ayrı farklı kur suresi zamanında ve farklı basıncında üç eksenli yükleme deneyi uygulanmıştır. İyileştirilmiş örneklerin üzerinde yapılan statik üç eksenli deneyden, kayma mukavameti parametreleri elde edilmiştir ve son bölümde ise bahsi geçen deneylerden elde edilen sonuçlar tartışılmıştır.

1. INTRODUCTION

It is common knowledge that an earthquake can pose serious risks to population aggregates, as it can cause deaths, injuries, and property and infrastructure damage. One of the most recognizable forms of a soil in a cyclic loading situation happens during an earthquake. An earthquake is a propagation of seismic waves that radiate from an underground source, and are in most cases related to plate tectonics. These seismic waves, of which there are various kinds, impose on the soil small and large-scale movements that are both erratic and unpredictable. As such, studies that try to predict or evaluate the consequences of these phenomena are of extreme importance. Even though seismic waves travel through rock in the majority of its journey from the source of the quake to the ground surface, the small portion of soil that is often near the surface can have a significant impact on the magnitude and nature of shaking at ground surface (Kramer, 1996). The study of the material properties of soils is therefore very important to understand the influence that the soil can have on the seismic waves (often called site effects). Many of structures lie in regions of high liquefaction and ground displacement potential. Over recent years, Soil improvement techniques have been improved and support new foundations or increase the capacity of existing foundations. There are different methods to improve the engineering properties of soils.

In this thesis the improvement in the properties of uniform sand is achieved by the two-component, polyurethane - Bitumen is powered by a liquid waterproofing material.(In a very short time hardens and adheres to different surfaces perfectly elastic, creates a powerful film). Unconfined axial loading test, dynamic triaxial test and static triaxial test have been conducted to the samples for determining dynamic properties and static behavior of reinforced sand. The result of the experimental study will be discussed to present the effect of polyurethane-bitumen inclusion on the behaviour of sand.

2. LIQUEFACTION

2.1 Introduction

Liquefaction is a common cause of ground failure during earthquakes, which can be defined as a loss of strength and stiffness in soils. Liquefaction is one of the major causes of instability in buildings and structures during earthquakes and is one of the most important aspects of seismic research and design applied to foundations.

If saturated soil are subjected to earthquake, by an increase in pore water pressure and decreasing effective stress to zero, leading to the transformation of soil from a solid state to a viscous fluid mass. Under such conditions, sand liquefaction can occur, accompanied by related phenomena such as sand boiling, ground cracking, and lateral spread. Most susceptible would be very loose cohesionless soils. The low permeability of non-plastic silts and sands is a disadvantage. Moderate saturated soils below the water table, cohesion less soils such as sands and gravels, uniformly graded soils-fluvial, alluvial deposits are the soils that are prone to liquefaction previously, soils that are loosely deposited are most susceptible to liquefaction.

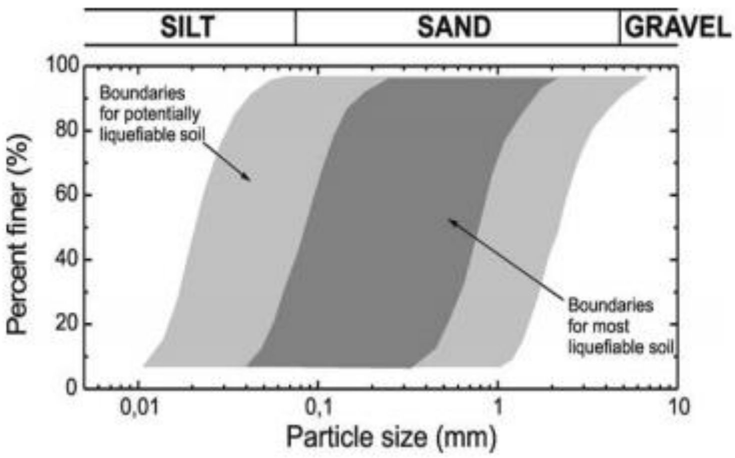

Figure2.1: Ranges of Grain Size Distribution for Liquefaction Susceptible Soils (Tsuchida, 1970).

Earthquake induced liquefaction is a major contributor to infrastructure seismic risk.The shaking causes increased pore water pressure which reduces the effective stress, and therefore reduces the shear strength of the sand. If there is a dry soil crust or impermeable cap, the excess water will sometimes come to the surface through cracks in the confining layer, bringing liquefied sand with it, creating sand boils. Liquefaction causes irregular settlements in the area liquified, which can damage buildings and break underground utility lines where the differential settlements are large. Sand boils can erupt into buildings through utility openings, and may allow water to damage the structure or electrical systems. Soil liquefaction can also cause slope failure. Areas of land reclamation are often prone to liquefaction because many are reclaimed with hydraulic fill, and are often underlain by soft soils which can amplify earthquake shaking. Liquefaction of saturated sands has been reported in a number of earthquakes, such as those in Niigata in 1964, Nihonkai-Chubu in 1983, and Hyogoken-Nanbu in 1995, Kocaali Earthquake in 1999 and Christchurch arthquake of February 22, 2011. Whitman (1971) and Seed and Idriss (1971) first developed the simplified liquefaction evaluation procedure to compute the factor of safety (FS) against liquefaction at a given depth in the soil profile. (Brett W. M., Russell A. G., Misko C. and Brendon A. B. 2014). Figur 2.2 shows devastating effect of earthquake by liquefaction induced bearing capacity failure during the Kocaeli earthquake in 1999.

Figure2.2: Kocaeli Earthquake in 1999 (EERC library of UC Berkeley)

Static loading also plays an important role in the initiation of liquefaction as well as the post-liquefaction flow slides in some cases. Liquefaction can occur under pure static loading conditions (Kramer and Seed, 1988; Hight et al., 1999; Jefferies and Been, 2006). After the initiation of liquefaction, the static shear stress in soil can be the driving force of flow slides (Ishihara, 1993, Jefferies and Been, 2006). It was also pointed out by Mohamad and Dobry (1986) that, when evaluating the cyclic strength of soils, the static undrained strength should be considered. Moreover, the statically sustained shear stress may cause pre-failure soil instability, leading to a run-away type of collapse (Chu and Leong, 2001; Chu and Wanatowski, 2008). Therefore, if desaturation is going to be a liquefaction mitigation method, the soil behavior with different degrees of saturation under static loading conditions should also be studied.

2.2 Liquefaction Phenomena

Liquefaction is a phenomenon where in a mass of a soil looses a large percentage of its shearing resistance , when subjected to monotonic, cyclic or shock loading , and flows in a manner resembling a liquid until the shear stresses acting on the mass are as low as the reduced shearing resistance (Sladen et.al,1985). The potential damage caused by liquefaction phenomena includes: Loss of bearing capacity, excessive settlement, lateral spreading, flow failure, and ground oscillation.Liquefaction features may vary in geometry, type, and dimension at different locations because of multiple factors, including anomalous propagation and amplification of the seismic waves, and geological conditions. (Galli 2000)

These phenomena can be divided into two main categories: flow liquefaction and cyclic mobility.

2.2.1 Flow liquefaction

Flow liquefaction is a phenomenon in which the static equilibrium is destroyed by static or dynamic loads in a soil deposit with low residual strength. Residual strength is the strength of a liquefied soil. Once triggered, the strength of a soil susceptible to flow liquefaction is no longer sufficient to withstand the static stresses that were acting on the soil before the disturbance. Flow liquefaction failures are characterized by the sudden nature of their origin, the speed with wich they develop, and the larg distance over which the liquefied materilas often move.

2.2.2 Cyclic mobility

Cyclic mobility is a liquefaction phenomenon, triggered by cyclic loading, occuring in soil deposits with static shear stresses lower than the soil strength. Deformations due to cyclic mobility develop incrementally because of static and dynamic stresses that exist during an earthquake.

Lateral spreading, a common result of cyclic mobility, can occur on gently sloping and on flat ground close to rivers and lakes. The 1976 Guatemala earthquake caused lateral spreading along the Motagua river, (Jörgen Johansson, 2011).

A special case of cyclic mobility is level-ground liquefaction. Because static horizontal shear stresses that could drive lateral deformation do not exist, level-ground liquefaction can produce large, chaotic movement known as ground oscillation during earthquake shaking, but produces little permanent lateral soil movement. Level-ground liquefaction failures are caused by the upward flow of water that occurs when seismically induced excess pore pressures dissipate. Depending on the length of time required to reach hydraulic equilibrium, level-ground liquefaction failure may occur well after ground shaking has ceased. (Kramer S.L, 1996)

2.3 Laboratory Studies to Simulate Field Conditions for Soil Liquefaction

If one considers a soil element in the field, as shown in Figure 2.3a, when earthquake effects are not present, the vertical effective stress on the element is equal to σ', which is equal to σ_u , and the horizontal effective stress on the element equals $k_0\sigma_u$, where k_0 is the at-rest earth pressure coefficient. Due to ground- shaking during an earthquake, a cyclic shear stress τ_h will be imposedon the soil element. This is shown in Figure 2.3b. Hence, any laboratory test to study the liquefaction problem must be designed in a manner so as to simulate the condition of a constant normal stress and a cyclic shear stress on a plane of the soil specimen. Various types of laboratory test procedure have been adopted in the past, such as the dynamic triaxial test (Seed and Lee, 1966, Lee and Seed, 1967), cyclic simple shear test (Peacock and Seed, 1968, Finn, Bransby, and Pickering, 1970, Seed and Peacock, 1971), cyclic torsional shear test (Yoshimi and Oh-oka, 1973; Ishibashi and Sherif, 1974), and shaking table test (Prakash and Mathur, 1965). However, the most commonly used laboratory test procedures are the dynamic triaxial tests and the simple shear tests.

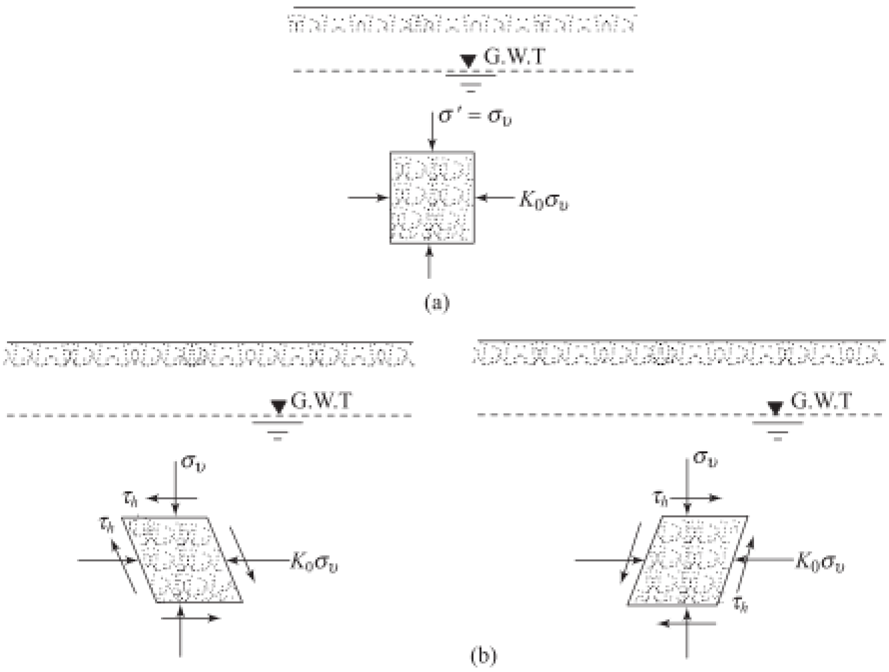

Figure2.3: Application of cyclic shear stress on a soil element due to an earthquake (Das, B.M, Principles of soil Dynamics, 1993)

2.4 Techniques for Mitigating Liquefaction Hazards

If hazard evaluations indicate that there is a liquefaction risk, then soil improvement methods should be considered for the mitigation of these hazards. Potentially suitable methods of mitigation may include the following: removal and replacement, dewatering, in-situ soil improvement, containment or encapsulation structures, modification of site geometry, deep foundations, structural systems and, if possible, alternate site selection. In general, soil improvement methods reduce the liquefaction susceptibility of sandy soils by increasing the relative density, providing conduits for the dissipation of excess pore pressures generated during earthquakes, and/or providing a cohesive strength to the soil.

3. SOIL IMPROVEMENT

3.1 Introduction

Soil improvement includes systems that use the ground or some modification of it, to transfer or support loads. Current technology affords many ground improvement techniques to suit a variety of soil conditions, structure type and performance criteria. The techniques are divided into three categories:

Compaction: techniques that typically are used to compact or densify soil in situ.

Reinforcement: techniques that typically construct a reinforcing element within the soil mass without necessarily changing the soil properties. The performance of the soil mass is improved by the inclusion of the reinforcing elements.

Fixation: techniques that fix or bind the soil particles together thereby increasing the soil's strength and decreasing its compressibility and permeability. Techniques have been placed in the category in which they are most commonly used even though several of the techniques could fall into more than one of the categories.

3.2 Compaction

3.2.1 Dynamic compaction

The Dynamic Compaction Technique achieves deep ground densification involves dropping a heavy weight on the surface of the ground to compact soils to depths as great as 40 ft or 12.5m . Dynamic compaction is most effective in permeable, granular soils.Cohesive soils tend to absorb the energy and limit the technique's effectiveness.The procedure involves repetitively lifting and dropping a weight on the ground surface.

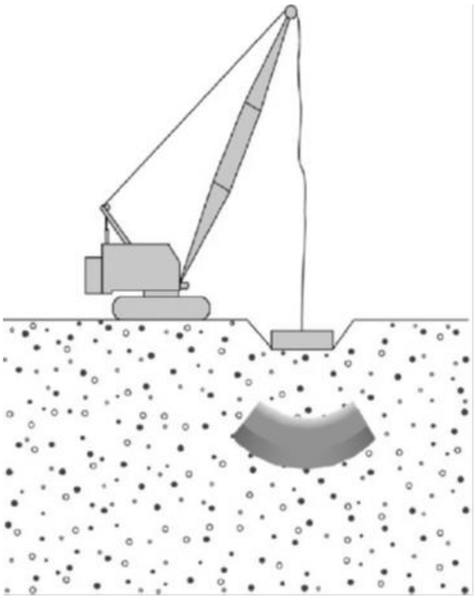

(a) (b)

Figure3.1: Deep dynamic compaction: (a) schematic, (b) field implementation (Hussin D.J, 2006)

3.2.2 Vibro compaction

Vibro compaction (VC), also known as Vibroflotation TM was developed in the 1930s in Europe. The process involves the use of a down-hole vibrator (vibroflot), which is lowered into the ground to compact the soils at depth (Figure 3.2).

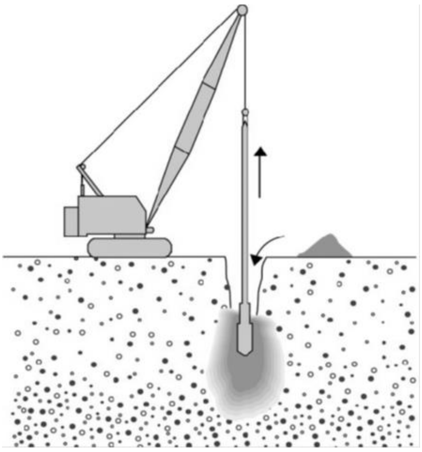

(a) (b)

Figure3.2: Vibroflotation: (a) schematic, (b) field implementation. (Hussin D.J, 2006)

The VC process is most effective in free draining granular soils. The vibroflot consists of a cylindrical steel shell with and an interior electric or hydraulic motor, which spins an eccentric weight.The vibrator, is lowered into the ground, assisted by its weight, vibration, and typically water jets in its tip.

3.2.3 Compaction grouting

Compaction grouting has been used to control surface settlements by pregrouting to densify and stress the soils to the point of heave.This technique densifies soils by the injection of a low mobility, low slump mortar grout. The grout bulb expands as additional grout is injected, compacting the surrounding soils through compression. Besides the improvement in the surrounding soils, the soil mass is reinforced by the resulting grout column, further reducing settlement and increasing shear strength. Compaction grouting is most effective in free draining granular soils and low sensitivity soils. Compaction grouting is typically started at the bottom of the zone to be treated and precedes upward. The treatment does not have to be continued to the ground surface and can be terminated at any depth. The technique is very effective in targeting isolated zones at depth. Compaction grouting is also now widely accepted as a site improvement technique, both for the mitigation of liquefaction potential and for soil densification to increase bearing capacity and reduce settlements, (Chastanet and Blakita, 1992).

3.2.4 Compaction grouting process.

Generally, the compaction grout consists of Portland cement, sand, and water. Additional fine-grained materials can be added to the mix, such as natural fine-grained soils, fly ash, or bentonite (in small quantities). The grout strength is generally not critical for soil improvement, and if this is the case, cement has been omitted and the sand replaced with naturally occurring silty sand. A minimum strength may be required if the grout columns or mass are designed to carry a load.

3.2.5 Surcharging with prefabricated vertical drains

Surcharging consists of placing a temporary load (generally soil fill) on sites to preconsolidate the soil prior to constructing the planned structure, the process improves the soil by compressing the soil, increasing its stiffness and shear strength. In partially or fully saturated soils, prefabricated vertical drains (PVDs) can be placed prior to surcharge placement to accelerate the drainage, reducing the required surcharge time. Preloading is best suited for soft, fine-grained soils. Soft soils are generally easy to penetrate with PVDs and layers of stiff soil may require predrilling.

3.3 Reinforcement

3.3.1 Stone columns

Stone columns refer to columns of compacted, gravel size stone particles constructed vertically in the ground to improve the performance of soft or loose soils. The stone can be compacted with impact methods, such as with a falling weight or an impact compactor or with a vibroflot, the more common method. Stone columns improve the performance of soils in two ways, densification of surrounding granular soil and reinforcement of the soil with a stiffer, higher shear strength column.

The column construction starts at the bottom of the treatment depth and proceeds to the surface. The vibrator penetrates into the ground, assisted by its weight, vibration, and typically water jets in its tip, the wet top feed method, (Figure 3.3).

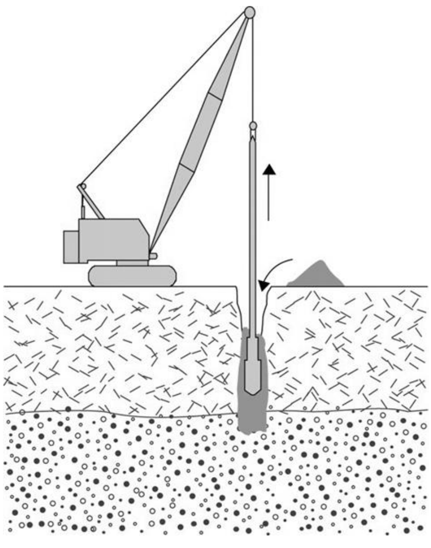

(a)

(b)

Figure3.3: Installation of stone columns: (a) schematic, (b) field implementation. (Hussin D.J, 2006)

3.3.2 Vibro concrete columns

Vibro concrete columns (VCCs) involve constructing concrete columns in situ using a bottom feed vibroflot. The method will densify granular soils and transfer loads through soft cohesive and organic soils. VCCs are best suited to transfer area loads, such as embankments and tanks, through soft and/or organic layers to an underlying granular layer. The depth of the groundwater table is not critical.

3.3.3 Micropiles

Micropiles, also known as minipiles and pin piles, are used in almost any type of ground to transfer structural load to competent bearing layers (Figure 3.4). Micropiles were originally small diameter (2 to 4 inch, or 5 to 10 cm), low-capacity piles. Micropiles can be used for a wide range of applications; however, the most common applications are underpinning existing foundations or new foundations in limited headroom and tight access locations. The micropile typically consists of a steel rod or pipe. Portland cement grout is often used to create the bond zone and fill the pipe.

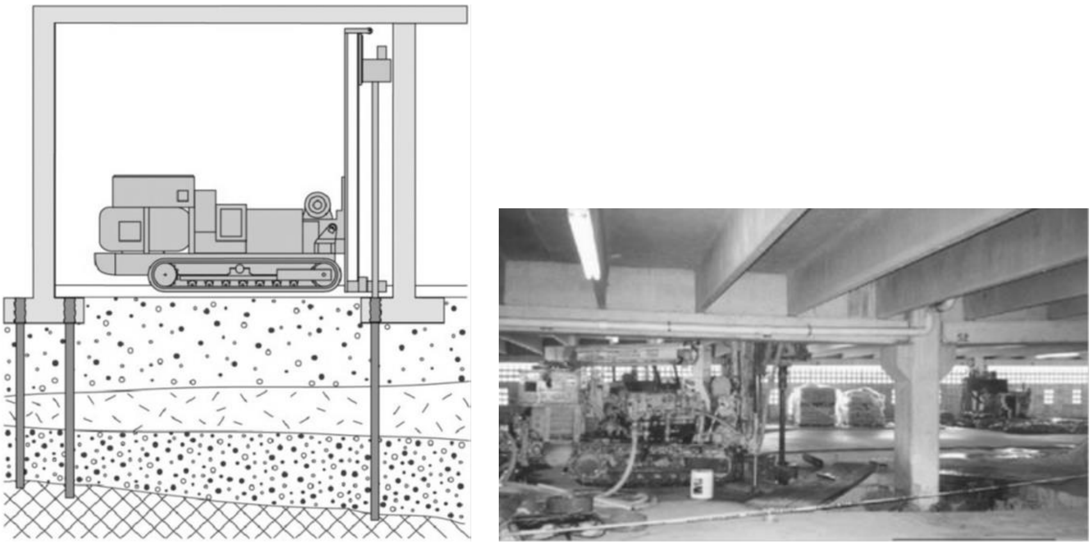

(a) (b)

Figure3.4: Micropiling: (a) schematic, (b) field implementation. (Hussin D.J, 2006)

3.3.4 Fracture grouting

Fracture grouting, also known as, compensation grouting, is the use of a grout slurry to hydro-fracture and inject the soil between the foundation to be controlled and the process causing the settlement.Grout slurry is forced into soil fractures, thereby causing an expansion to take place counteracting the settlement that occurs or producing a controlled heave of the foundation. Multiple, discrete injections at multiple elevations can create a reinforced zone. A variation of fracture grouting is injection systems for expansive soils. The technique reduces the post-treatment expansive tendencies of the soil by either raising the soils’moisture content, filling the desiccation patterns in the clay or chemically treating the clay to reduce its affinity to water. Since the soil is fractured, the technique can be performed in any soil type.

3.3.5 Fibers and biotechnical

Fiber reinforcement consists of mixing discrete, randomly oriented fibers in soil to assist the soil in tension. The use of fibers in soil dates back to ancient time but renewed interest was generated in the 1960s. Laboratory testing and computer modeling have been performed; however, field testing and evaluation lag behind. There are currently no standard guidelines on field mixing, placement and compaction of fiber-reinforced soil composites, (Hussin D.J, 2006).

Biotechnical reinforcement involves the use of live vegetation to strengthen soils. This technique is typically used to stabilize slopes against erosion and shallow mass movements. The practice has been widely used in the United States since the 1930s. Recent applications have combined inert construction materials with living vegetation for slope protection and erosion control. Research has been sponsored by the National Science Foundation to advance the practice.

3.4 Fixation

3.4.1 Permeation grouting

Permeation grouting is the injection of a grout into a highly permeable, granular soil to saturate and cement the particles together. The permeability requirement restricts the applicable soils to sands and gravels, with less than 18% silt and 2% clay. The mixing plant and grout pump vary depending on the type of grout used.

3.4.2 Jet grouting

The technique hydraulically mixes soil with grout to create in situ geometries of soilcrete. Jet grouting offers an alternative to conventional grouting, chemical grouting, slurry trenching, underpinning, or the use of compressed air or freezing in tunneling. A common application is underpinning and excavation support of an existing structure prior to performing an adjacent excavation for a new, deeper structure.Jet grouting is effective across the widest range of soils. Because it is an erosion-based system, soil erodibility plays a major role in predicting geometry, quality, and production. Granular soils are the most erodible and plastic clays the least. Jet grout is a bottom-up process.

3.4.3 Soil mixing

Soil mixing mechanically mixes soil with a binder to create in situ geometries of cemented soil. Mixing with a cement slurry was originally developed for environmental applications; however, advancements have reduced the costs to where the process is used for many general civil works, such as in situ walls, excavation support, port development on soft sites, tunneling support, and foundation support. Mixing with dry lime and cement was developed in the Scandinavian countries to treat very wet and soft marine clays. The system is most applicable in soft soils. Cohesionless soils are easier to mix than cohesive soils. The ease of mixing cohesive soils varies inversely with plasticity and proportionally with moisture content.

3.4.4 Freezing and vitrification

Ground freezing involves lowering the temperature of the ground until the moisture in the pore spaces freezes. The frozen moisture acts to ‘‘cement’’ the soil particles together.The process typically involves placing double walled pipes in the zone to be frozen. A closed circuit is formed through which a coolant is circulated. A refrigeration plant is used to maintain the coolant’s temperature. Since ice is very strong in compression, the technique has been most commonly used to create cylindrical retaining structures around planned circular excavations. Vitrification is a process of passing electricity through graphite electrodes to melt soils in situ. Electrical plasma arcs have also been used and are capable of creating temperatures in excess of 40008C. The soil becomes magma, and after several days of cooling it hardens into an artificial igneous rock. Although laboratory testing is ongoing, the electrical usage of the process to date appears to make it uneconomical. It is possible that the process could find application in the field of environmental cleanup.

4. LITERATURE REVIEW

4.1 Introduction

Characterizing soil behavior under seismic loading was one of the first issues that led part of the geotechnical community to focus on dynamic problems. Seismic waves can induce strong motions in the upper ground layers, even far from the epicenter. These motions may even be amplified within particular topographical and geological conditions.

Dynamic shear modulus and damping are important properties to determine the response of the soils under cyclic loading. The recent developments in the numerical analyses for the non-linear dynamic response of grounds due to strong earthquake motions have increased the demand for the dynamic soil properties corresponding to large strain level also. In this part of the thesis, brief information about the dynamic properties of sand is included.

4.2 Dynamic Soil Properties

The physical and mechanical properties of the soil play an important role in the dynamic response of soil. Two of the most important parameters in any dynamic soils analysis are the shear modulus and the damping ratio. Soil properties depend on different parameters such as the state of stress, void ratio, confining stress and water content, stress history, strain levels, drainage condition and the dynamic amplitude and frequency of the applied load. In addition, liquefaction susceptible parameters are important dynamic soil properties.

It has been observed that the dynamic soil properties are affected by many factors like: method of sample preparation in the laboratory (whether intact and reconstituted samples), relative density, confining pressure, methods of loading, overconsolidation ratio, loading, frequency, soil plasticity, percentage of fines and soil type.

Determination of dynamic soil properties is an important aspect in geotechnical earthquake engineering problems. Laboratory soil tests for dynamic soil properties developed in the past three decades disclosed that soils change from a linear material to a nonlinear material as induced shear strain grows from 10^{-6} to 10^{-3} and finally reach failures at strain larger than10^{-2}. Figure 4.1 provides is a useful reference for geotechnical engineers, as it gives the amplitude of shear strain levels, type of applicable dynamic tests, and the area of applicability of these test results. Despite the fact that laboratory testing is not ideal, it will continue to be important because soil conditions can be better controlled in the laboratory, (Das, B.M, 1993).

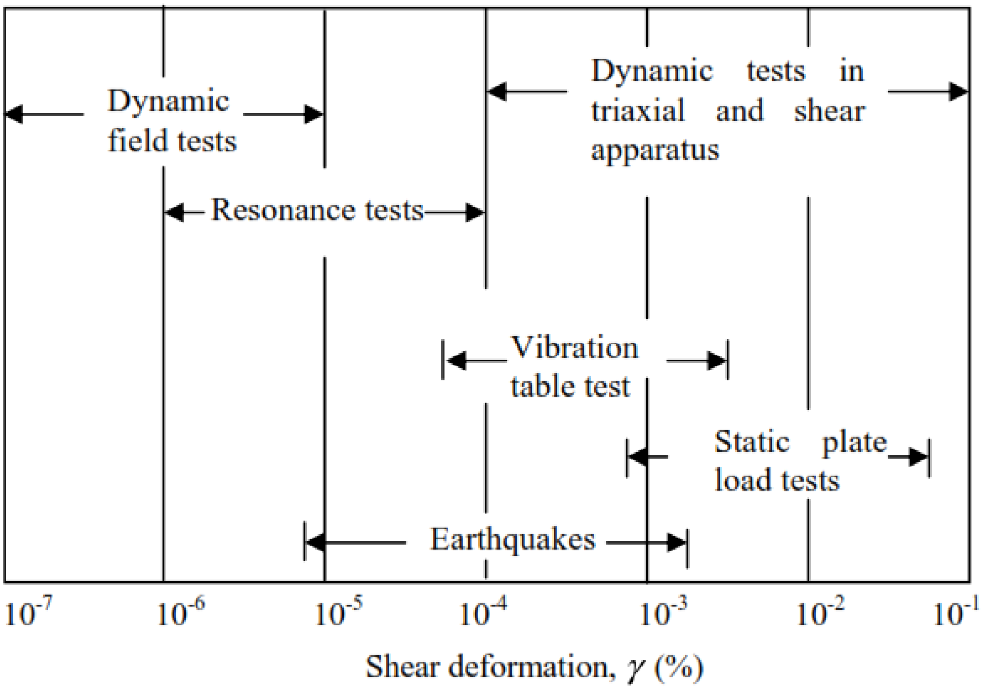

Figure 4.1: Range and applicability of dynamic laboratory tests (Das, B.M, 1993)

The dynamic triaxial test is a useful method for estimating the Damping ratio. In this test, first hydraulic pressure is applied to cylindrical sample, and then reversed loading is applied to the cylinder in its longitudinal direction. From the stress-strain curve, the elastic modulus E is estimated (Figure 4.2).

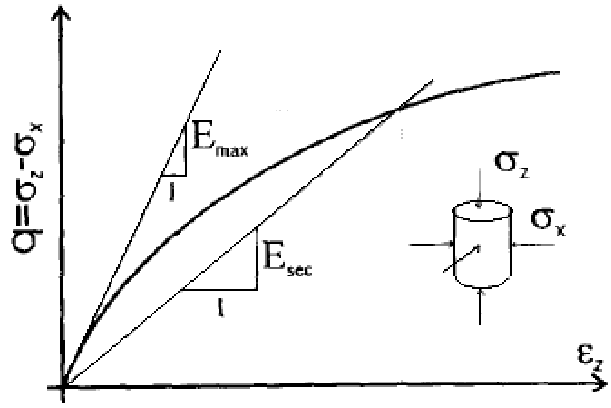

Figure 4.2: Definition of Young's modulus (Tatsuoka et. al, 1994)

The shear modulus G can be computed from E and the measured Poisson's ratio. The Shear Modulus (G) can be calculated as:

$$G = \frac{E}{2(1+\mu)} \tag{4.1}$$

Shear modulus G and damping ratio D change as schematically shown in Figure 4.3. In current engineering practice, shear modulus G is normalized by initial shear modulus G_0, (Takaji kokusho, nonlinear site response and strain-depentdent soil properties)

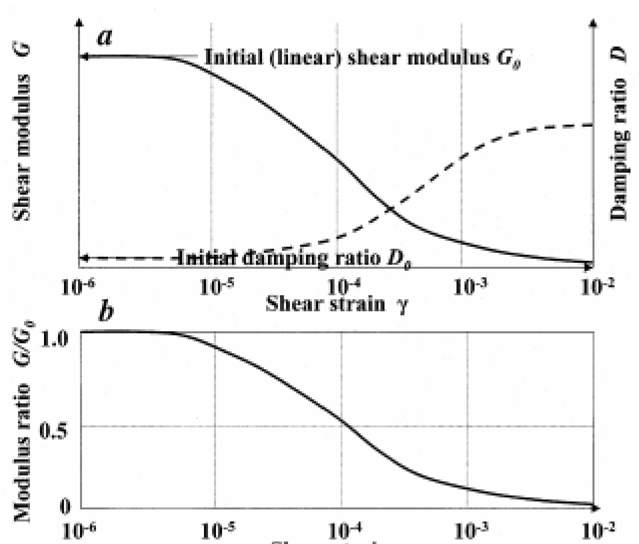

Figure 4.3: Shear modulus/damping ratio versus shear strain relationship (a)and modulus degradation curve(b). Kokusho 1980

The cyclic behavior of soils is nonlinear and hysteretic, this hysteresis behaviour is idealised as a simple hysteresis loop as shown in figure 4.4. The shear modulus is usually expressed as the secant modulus determined is the slop of hysteresis loop, while the damping ratio is proportional to the area inside the hysteresis loop. It is apparent that each of these properties will depend on the amplitude of the strain for which the hysteresis loop is determined, and thus both shear moduli and damping ratio must be determined as functions of the induced strain in a soil specimen.

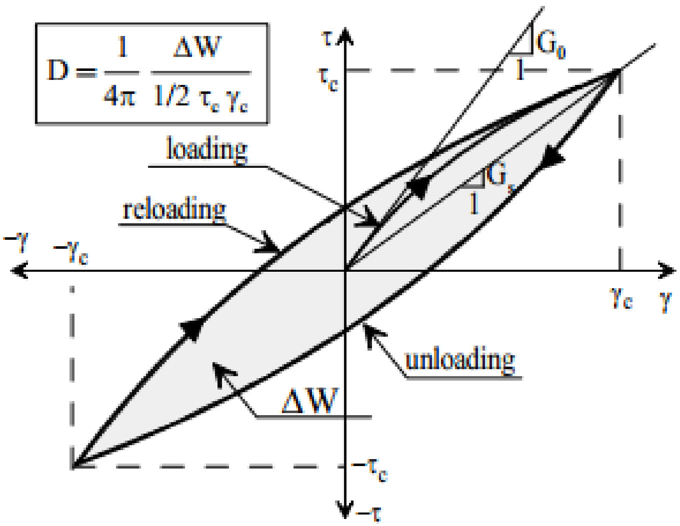

Figure 4.4: Idealised cyclic stress-strain loop, (B. D'Elia, G. Lanzo & A. Pagliaroli, 2003)

In the lab/in-situ tests, the magnitude of excess pore pressure build up to initiate liquefaction depends on the amplitude and duration of the cyclic loading, the number of cycles, the type of tests and soil type. There are two most common approaches to evaluate the liquefaction potential, one is cyclic stress approach and other is cyclic strain approach, in which earthquake induced loading expressed in terms of cyclic shear stress and cyclic shear strain respectively, (Kramer, S.L, 1996). Several researchers have reported that the cyclic stress ratio and pore pressure generation are liquefaction parameters and experimentally investigated that loose soil liquefy in few cycles if large cyclic shear stress is applied; however, dense soils require large number of cyclic shear stress or cyclic stress ratio.

4.2.1 Damping Ratio of Soil

Most methods that deal with the characterisation of the soil under cyclic loading conditions focus on determining the evolution of damping characteristics. Damping, in the context of cyclic loading, can be understood as the dissipation of energy that follows a loading of the soil. Studies performed by Hardin and Drnevich (1972), Seed and Idriss (1970), and others have shown that although such factors as grain size characteristics, degree of saturation, void ratio, lateral earth pressure coefficient, angle of internal friction, and number of stress cycles have minor effects on the damping ratios for sands,(Seed H.B, 1986). It has a very important effect on the consequences of the cyclic loading of soils. For example, if a soil that had no damping were to be excited by an external momentary load that would cause it to vibrate, it would vibrate indefinitely and with unchanging amplitude. Soil damping allows such an excitation to decrease over time until it is no longer felt. Similarly, for loading frequencies close to the soil's resonance frequency, the amplification phenomenon is less grievous the more damping the soil exhibits. This is especially important to mitigate the consequences of, for example, seismic activity.

When talking about damping, it is important to distinguish between material damping and radiation damping, the former being the dissipation of energy through internal soil friction, and the latter the dissipation of energy from the natural spreading of energy/motion waves through space. Of these types of damping, only material damping is dependent on the soil's characteristics and not on the soil's overall geometry and boundaries. Therefore, material damping will be the type of damping that is given the most focus in this work. Unless stated otherwise, from now on any mentions of damping in this work should be taken to mean material damping. In the context of cyclic loading behaviour, damping is often considered to increase with strain (Kramer, 1996; Ishihara, 1996). This evolution of damping characteristics with strain is a fundamental target of analysis when working with models that deal primarily with this kind of behaviour.

While the amplitude of shear strain is small enough, the strain level can be sufficiently high so that the soil does not behave as a linear elastic material, but instead exhibits non-linear behaviour. This kind of behaviour seems to manifest itself for shear strains in the range approximately between 10-5 and 10-3, (Ishihara, 1996). A type of model that is typically used to simulate soil behaviour in this strain range is defined as the non-linear cycle independent model (Ishihara, 1996). Two models that can be classified as non-linear cycle-independent are the Hyperbolic model (Kondner, 1963) and the Ramberg-Osgood model (Ramberg and Osgood, 1943).

4.3 Models for Nonlinear Stress and Strain Relations

The nonlinear stress-strain behavior of soils can be represented more accurately by cyclic nonlinear models that follow the actual stress-strain path during cyclic loading. Such models are able to represent the shear strength of the soil, and with an appropriate pore pressure generation model, changes in effective stress during undrained cyclic loading, (Kramer S.L.1996). Two kinds of material models have been used to describe the nonlinear stress-strain relations of soils. The first is a two-parameter model as represented by the hyperbolic or exponential functions. The second is a four-parameter model known as the RambergOsgood model.The basic aspect of these models is discussed below:

4.3.1 Hyperbolic model

The performance of cyclic nonlinear can be illustrated by a very simple example in wich the shape of the backbone curve is described by $\tau=F_{bb}(\gamma)$. The shape of any backbone curve is tied to two parameters, the initial (low-strain) stiffness and the (high-strain) shear strength of the soil. For the simple example, the backbone function, $F_{bb}(\gamma)$, can be described by hyperbola:

$$F_{bb}(\gamma)=\frac{G_{max}\gamma}{1+(\frac{G_{max}}{\tau_{max}})\gamma} \qquad (4.2)$$

The shape of the hyperbolic backbone curve is illustrated in figure 4.5.

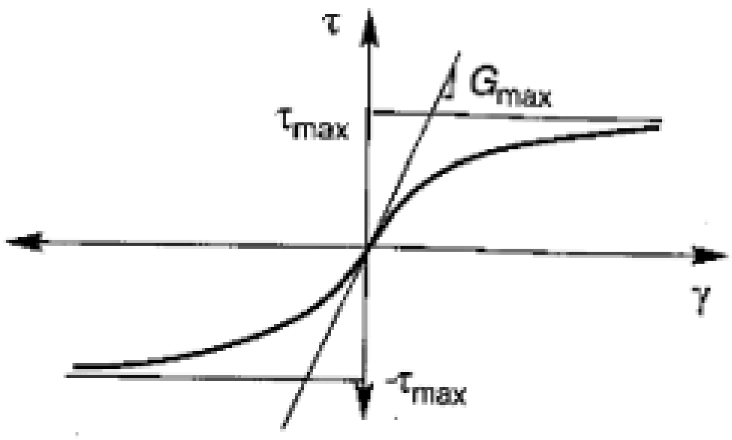

Figure 4.5: Hyperbolic backcone curve asymptotic $\tau=G_{max}\gamma$ and to $\tau=\tau_{max}$ (Kramer et.al., 1996)

Then a relationship between the secant shear modulus and damping ratio is obtained as:

$$D = \frac{4}{\pi}\frac{1}{1-\frac{G}{G_0}}\left[1 + \frac{\frac{G}{G_0}}{1-\frac{G}{G_0}}\,ln\left(\frac{G}{G_0}\right)\right] - \frac{2}{\pi} \tag{4.3}$$

This relationship is numerically calculated and plotted in Fig. 4.6.

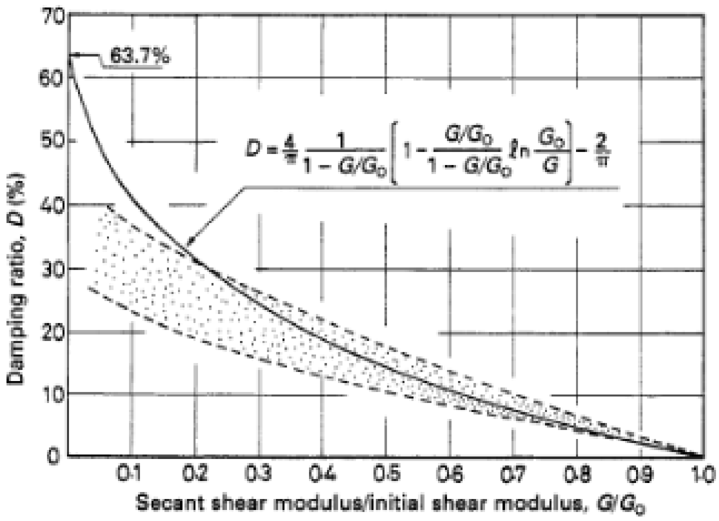

Figure 4.6: Relation between damping ratio and shear modulus ratio, (Ishihara, 1996)

4.3.2 Ramberg-osgood model

The Ramberg-Osgood formula was developed by Ramberg and Osgood (1943), as a way to define the stress-strain relationship of certain materials in terms of three parameters (namely, Young’s modulus and two secant yield strengths). This model was developed with metal alloys in mind, but – with appropriate adaptations – has since been proven to also adequately represent a soil’s backbone curve in certain conditions, such as in the small to medium strain range (Ishihara,1996). This model simulates elastoplasticity by having the elastic parameters change with strain and behave differently for first loading and for unloading/reloading. The model express the hysteresis curve using yield strain γy, and yield stress τ_y shown in figure 4.7, the expression of damping ratio for the R-O model is:

$$D = \frac{2}{\pi}\,\frac{r-1}{r+1}\;.\alpha.\frac{\left|\frac{G}{G_0}.\frac{\gamma_a}{\gamma_r}\right|^{r-1}}{1+\alpha\left|\frac{G}{G_0}.\frac{\gamma_a}{\gamma_r}\right|^{r-1}} \tag{4.4}$$

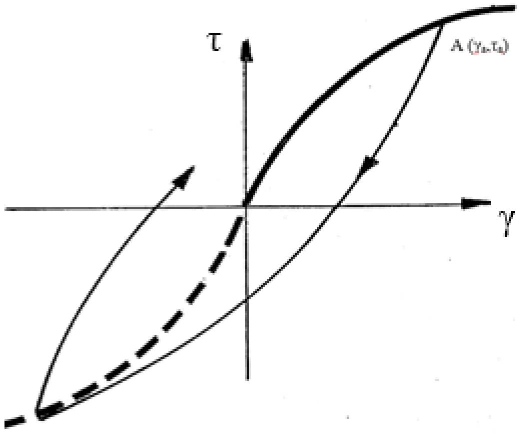

Figure 4.7: Ramberg-Osgood model

For typical sets of values for α and r, the relations of equation (4.4) is presented numerically in figure 4.8, where it can be seen that G/G_0 value tends to decrease and the damping ratio to increase with increasing shear strain ratio γ_a/γ_r.

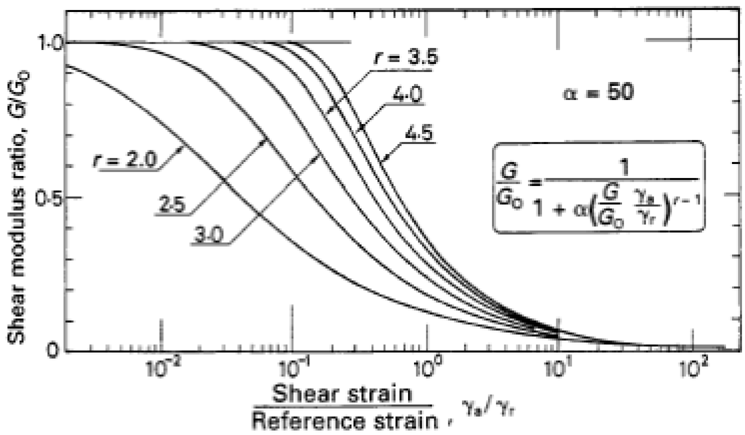

Figure 4.8: Numerical example of Ramberg_Osgood model, (Ishihara, 1996)

As in the case of the hyperbolic model, the secant shear modulus as well as the damping ratio is expressed as a function of shear strain ratio γ_a/γ_r and therefore by eliminating γ_a/γ_rbetween equation (4.4), the damping ratio D will be:

$$D = \frac{2}{\pi}\,\frac{r-1}{r+1}\,[1 - \frac{G}{G_0}] \qquad (4.5)$$

4.4 Critical Factors Influencing The Dynaimic Properties of Soil

Dynamic properties of soil are affected by many factors such as method of sample preparation, relative density, confining pressure, methods of loading, overconsolidation ratio, loading frequency, soil plasticity, percentage of fines and soil type.

4.4.1 Methods of sample preparation

Several researchers have proposed different method for sample preparation like air-pluviation, wet-tamping, moist-vibration, trimming, spooning and raining technique. It has also been reported that the methods of sample preparation and methods of also affect the strength of soil the strength of soil. Mulilis et al. Mulilis, J.P., Seed, H.B., Chan, C.K., Mithch, J.K., and Arulanandan, K., (1977) have observed that the variation of sample diameters does not significantly affect the cyclic strength. However, Wong, R.T., Seed, H.B. and Chan, C.K., (1975) compared the effects of size considering 70 mm and 300 mm (2.8 in. and 12 in.) diameter specimens with similar height-to-diameter ratios and showed that the 300 mm (12 in.) diameter specimen was approximately 10% weaker than the 70 mm (2.8 in.) diameter specimen (Fig. 4.9.).

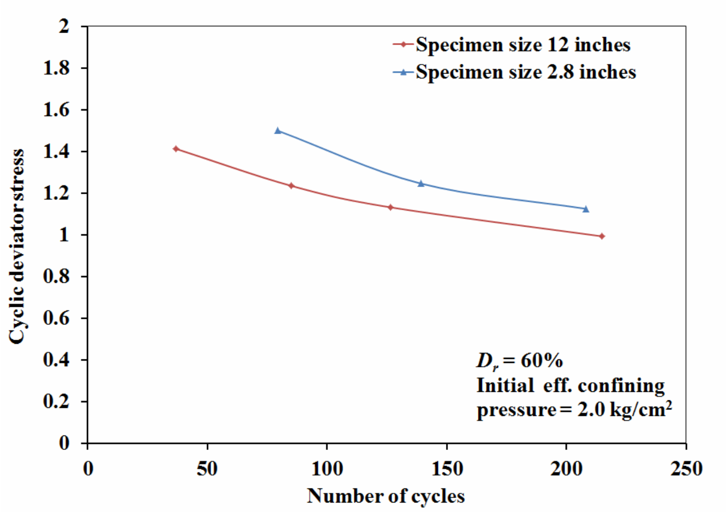

Figure 4.9: Cyclic ratio versus number of cycles for different compaction procedures (Wong, R.T., Seed, H.B. and Chan, C.K.,1975)

4.4.2 Effects of confining pressure

Effects of Shear modulus, damping ratio and liquefaction are significantly affected by confining pressure. As the confining pressure increases, the shear modulus increases and damping ratios decreases because of the densification/compactness of soil sample

(Figs. 4.10 and 4.11). Densification causes an increase in the relative density, which further results in the increment of shear modulus and number of cycles required to initiate liquefaction. A series of different tests have been performed on soils to observe the effect of confining pressure over its strain-dependent dynamic properties. In the range of shear strains tested, it has been observed and reported that as the confining pressure increases, the shear modulus increases significantly and the damping ratio decreases.(Silver, M.L. and Ishihara, K.,1977)

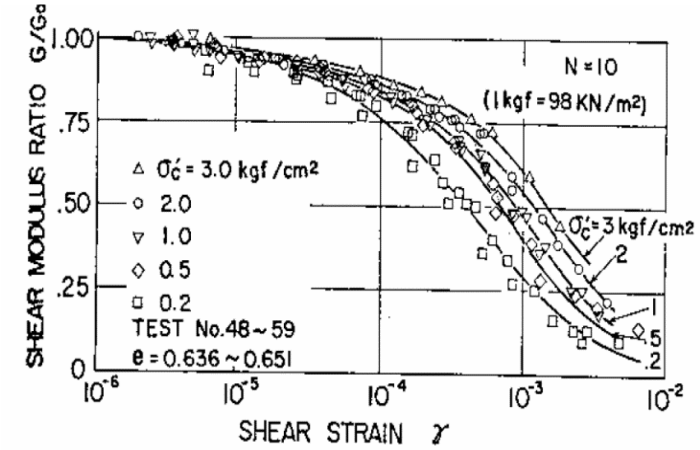

Figure 4.10: Variation of shear modulus ratio and shear strain for dense sand with different confining pressures,(Kokusho, et.al .,1980)

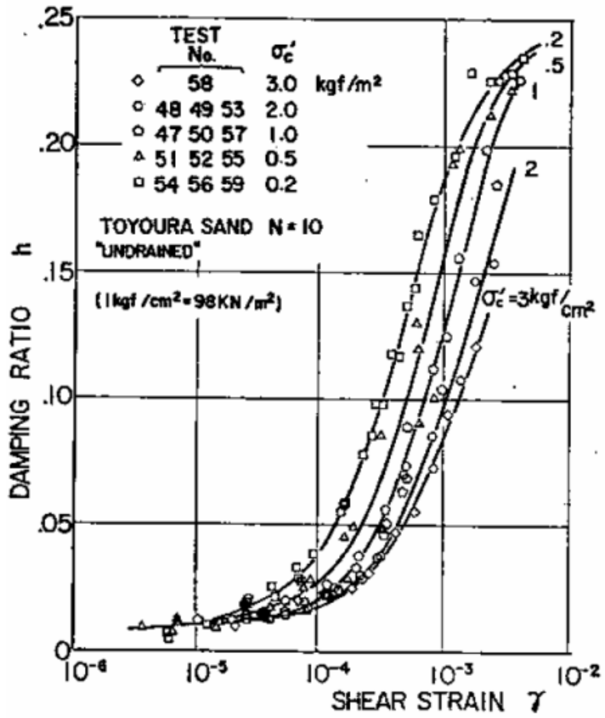

Figure 4.11: Variation of damping ratio and shear strain for dense sand withdifferent confining pressures, (Kokusho, et.al ., 1980)

4.4.3 Effects of void ratio

Void ratio is one of the mechanical properties of soil which is mainly influenced by the static/dynamic actions of loading. As the void ratio becomes lesser under the application of load, soil particles come closer to each other resulting in densification of soil sample. Densification or reduction in void ratio of soils due to confining pressure and method of sample preparation are the main causes increasing the cyclic strength. Kokusho.T, (1980) performed a series of cyclic triaxial tests on isotropically consolidated saturated Toyoura sand (void ratios: 0.64 – 0.80) subjected to specified effective confining stress (19.6 kPa - 294 kPa) and frequency (0.02 Hz - 0.1 Hz) and reported about the influence of void ratio on the strain dependent shear modulus and damping ratio (Fig. 4.12).

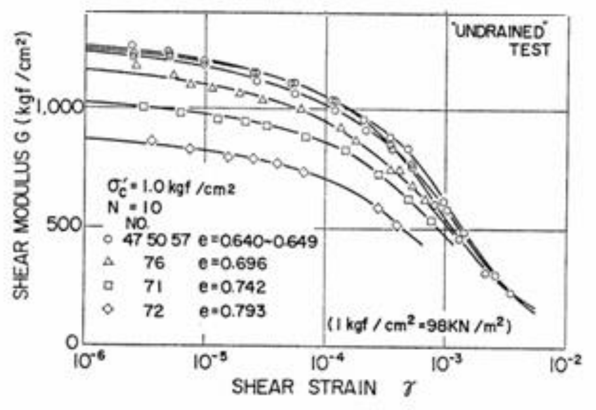

Figure 4.12: Shear modulus versus shear strain for σ' = 98 kN/m with different void ratios, (Kokusho, et.al ., 1980)

4.4.4 Effects of excitation frequency

Based on the experimentation for a wide range of excitation frequency, Hardin, B.O., (1965) had reported that the damping behaviour of dry sand is independent of the frequency. This concept has been widely accepted and applied in the ground response analysis in frequency domain. However, if the soil damping becomes frequency dependent, the analysis in frequency domain is not valid, and it will be very complicated toanalyse the ground response and soilstructure interaction accounting for frequency effect of soil damping. Based on the cyclic triaxial tests performed by GovindaRaju (Figs. 4.13 and 4.14), it has been observed that the shear modulus is not significantly affected while damping ratios are significantly affected by the excitation frequency.

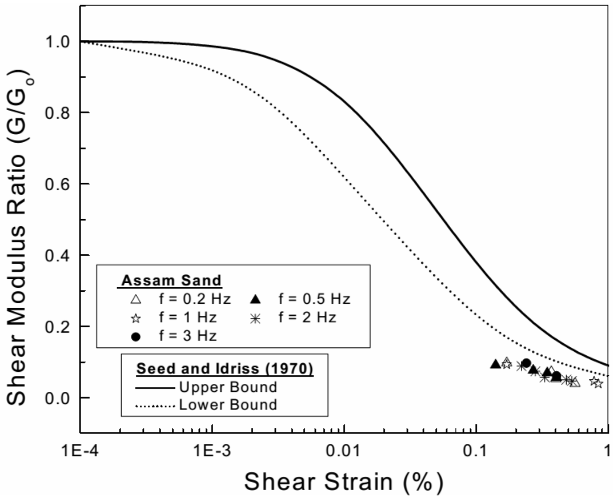

Figure 4.13: Variation of normalized modulus ratio with shear strain for different frequencies (GovindaRaju, L., 2005)

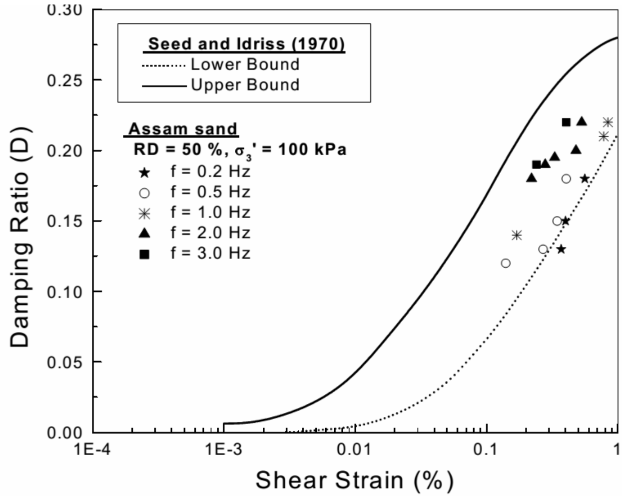

Figure 4.14: Variation of damping ratio with shear strain for different frequencies (GovindaRaju, L, 2005)

4.4.5 Effects of soil plasticity

In the early year of geotechnical earthquake engineering, the modulus reduction behaviors of coars-and fine-grained soils were improved separately (e.g., Seed and Idriss, 1970).Recent research, however, has revealed a gradual transition between the modulus reduction behavior of nonplastic coarse-grained soil and plastic fine-grained soil.

After reviewing experimental results from a board range of materilas, Dobry and Vuetic (1987) concluded that the shape of the modulus reduction curve is effected more by the plasticity index than by the void ratio and presented curves of the type shown in figure 4.15. These curves show that the linear cyclic shear strain is greater for highly plastic soils than for soils of low plasticity.

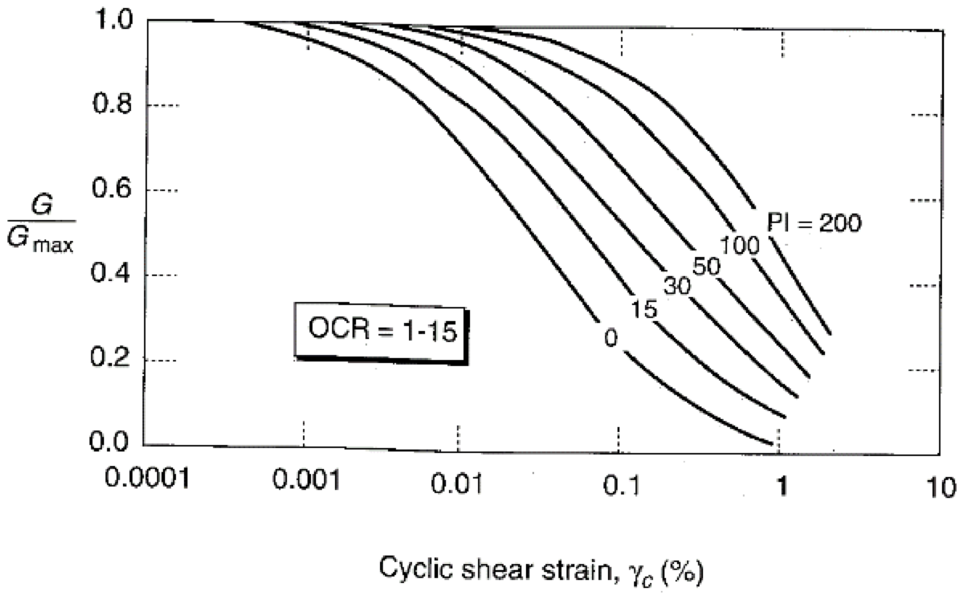

Figure 4.15: Modulus reduction curves for fine-grained soils of different plasticity.(After Vucetic and Dobry ,1991)

4.4.6 Effects of percentage fines

Most of the earlier researches were focused on clean sands with an idea that presence of fines in a sand deposit resists the development of pore water pressure. However, large scale liquefaction related failures in silty sand deposits in earthquakes of recent past changed this idea and most of the present research are more focused on the influence of fines in controlling the pore pressure response and hence the liquefaction behaviour of sandy soils. The pore pressure generation is dependent on the deformational characteristics of silty sands, which is quite different from that of clean sands. Seed, H.B., Tokimatsu, K., Harder, L.F., and Chung, R.M., (1985) have reported that fines do not influence the liquefaction resistance of sand unless the fines comprise more than 5% of the soil. Ishihara and Koseki Ishihara, K. and Koseki, J., (1989) have also observed that the low plasticfines (PI<4) does not influence the liquefaction potential. Hanumantharao and Ramana (2008) performed stress and strain controlled undrained cyclic triaxial tests on remoulded sand and sandy slit specimens of 70 mm diameter and 140 mm height under a sinusoidal loading at 1 Hz frequency for evaluating the modulus reduction and damping curves (Fig. 4.16 and 4.17) and reported that the shear modulus is not significantly affected, although with the increase in silt content, the damping ratio was observed to decrease.

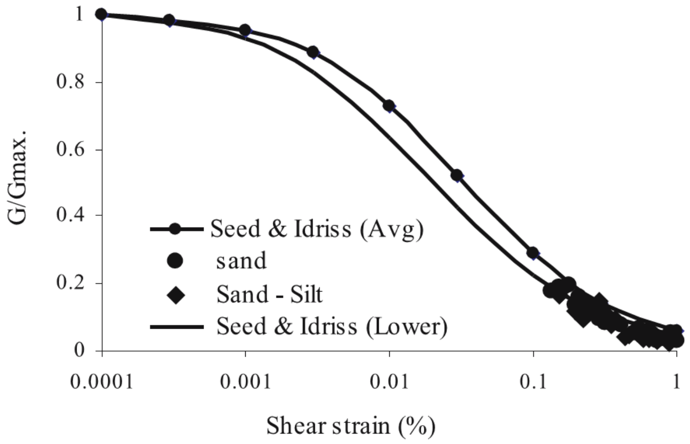

Figure 4.16: Normalized shear modulus (G/Gmax) versus shear strain (Hanumantharao,C. and Ramana, G.V., 2008)

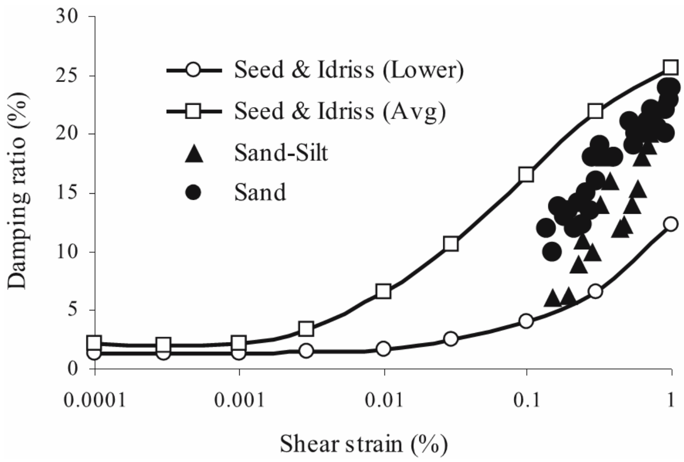

Figure 4.17: Damping ratio versus shear strain (Hanumantharao,C. and Ramana, G.V., 2008)

5. EXPERIMENTAL STUDY

The experimental study consists of static and dynamic laboratory tests on reinforced sand specimens. First, the grain size distribution of the sand that will be used in the unconfined axial Loading Test is performed to evaluation the shear strength of samples. To study the affect of time on stress-strain behavior of the mixture sand specimens, unconfined axial loading tests have been conducted to the samples after 1st day, 7st day, 30st day and 6st months. After Unconfined axial Loading Test, the triaxial test is performed to 27 samples at first, 7th and 30th days for three different P.B ratio contents.

The thirth part of experimental study the dynamic triaxial test is conducted to samples. At the first part, the maximum initial Elasicity Modulus is determined for confining pressure of 100kPa. The same samples were subjected to Cyclic triaxial test to determine the the Dynamic properties of reinforced sand.

5.1 Triaxial Test Apparatus

The triaxial tests apparatus is used for both monotonic and cyclic loading conditions. The details of a typical triaxial cell are shown in figure 5.1. The main components of a triaxial test apparatus are cell base, cell body and top, loading piston and loadingcaps (Head, 1998). The cyclic triaxial test apparatus Model DTC-311, shown in figure 5.1., was developed by the Japanese company “Seiken Inc.” and was brought to Istanbul Technical University Soil Dynamics Laboratory within the scope of ITU-JICA (Japan International Cooperation Agency) cooperation.

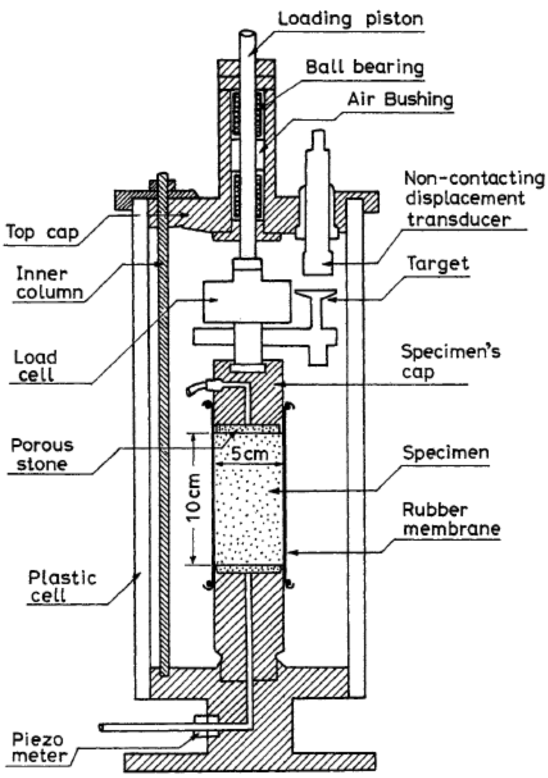

Figure 5.1: Details of a Triaxial Test Apparatus (Head, 1998)

The device is capable of applying cyclic and monotonic loads. The load cell has a vertical load capacity of 500 kgf and lateral load capacity of 10 kg/cm². It is possible to form specimens with diameters of 50 mm, 60 mm, 75 mm and heights of 100 mm, 120 mm and 150 mm by changing the top and bottom caps. The vertical loading apparatus is capable of applying 200 kgf dynamic load. For monotonic loading conditions, the loading capacity is 500 kgf and rate of loading is between 0.002mm/min and 2.0mm/min. It is possible to apply pressures between 0-10 kg/cm2. The air pressure is transmitted to water leading to triaxial chamber and the pressure regulator controls its amount. The drainage valves connected to the top and bottom caps are used for supplying water into the specimen and applying the backpressure. The 25ml burette pipe is connected to the drainage valves and it is used for calculating the amount of water drained during consolidation. The test apparatus also includes a water tank and a vacuum tank with volumes of 5 lt.

Figure 5.2: Dynamic triaxial Test Apparatus in ITU Soil Dynamics Laboratory

The cyclic loading is applied to the specimen by uniform sinusoidal load and its frequency ranges between 0.001 Hz and 2.0 Hz. The load, displacement and pore water pressure transducers are used for monitoring the specimen behaviour and the data is directly transferred to the computer. The computer program, Virtuel Bench Logger, is used for transferring the data and also drawing the graphics. The schematically drawing of the loading unit and triaxial chamber are shown in figure 5.3.

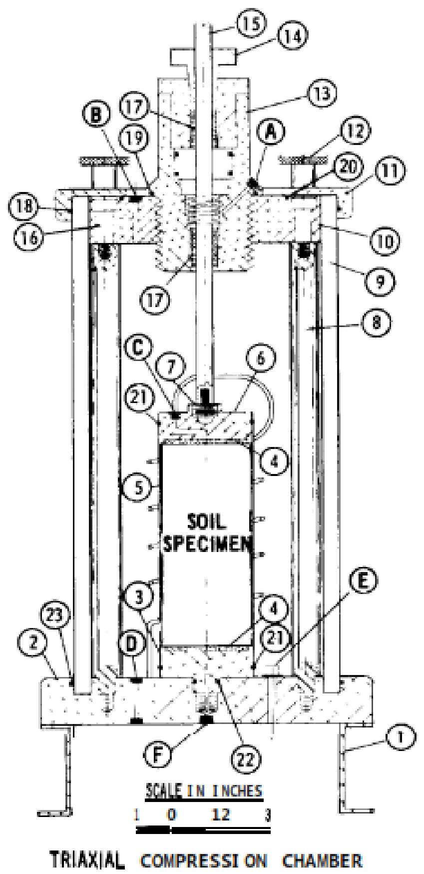

A. HYDROSTATIC SEAL AIR SUPPLY PORT
B. VENT
C. TOP DRAINAGE PORT
D. CHAMBER FLUID DRAIN
E. TRANSDUCER CABLE CONNECTOR
F. BOTTOM DRAINAGE PORT

PART NO.	NAME	MATERIAL	QUANTITY
1	CHAMBER FOOT	ALUMINUM CHANNEL	2
2	CHAMBER BASE	ALUMINUM PLATE	1
3	SPECIMEN BASE	ALUMINUM	1
4	POROUS PLATE	STAINLESS STEEL	2
5	SPECIMEN MEMBRANE	RUBBER	1
6	SPECIMEN CAP	ALUMINUM	1
7	SPECIMEN CAP CONNECTOR	BRASS	1
8	BEARING SUPPORT ROD	STAINLESS STEEL	2
9	CYLINDER	CLEAR ACRYLIC	1
10	CHAMBER CAP	ALUMINUM	1
11	CYLINDER SEALING RING	ALUMINUM	1
12	LOCKING KNOBS	STEEL	3
13	AIR BEARING ASSEMBLY	ALUMINUM	1
14	PISTON LOCK	BRASS	1
15	LOADING PISTON	STAINLESS STEEL	1
16	SHOULDER SCREW	STEEL	2
17	BALL BUSHING	STAINLESS STEEL	2
18	O-RING	RUBBER	1
19	O-RING	RUBBER	1
20	O-RING	RUBBER	1
21	O-RING	RUBBER	2
22	O-Ring	RUBBER	1
23	O-RING	RUBBER	1

Figure 5.3: Triaxial compression chamber used for cyclic triaxial tests (U. S. Army Corps of Engineers,Washington, D. C. 20314-1000)

The digital system shown in figure 5.4 is used for calibrating the data. When the digital system starts to operate, the condition of gain button, ATT5 button and CAL.με button must be controlled. The ATT button controls the sensitivity of measurements. The CAL.με button calibrates the μ ε input. The CAL.με button is switched by pressing the CALL.ON button and it starts the calibration. First, the AUTO button is switched and the digital voltmeter should show the value of “0.00”. Then CALL.ON button is switched and the value of voltmeter is arranged as “5.00” by using the GAIN control button which controls the sensitivity of the amplifier. The ZERO-C-BAL button controls the changes in the measurement and after it is switched to zero, the ZERO CONTROLLER is used for setting the voltmeter value shown on digital indicator (DV) to “0.00”. The ZERO-C-BAL button is kept constant at the C-BAL position and the voltmeter value is set to “0.00” by using CBAL button. At the same time, for calibrating the sensitivity of the measurements, ATT 1, 2 or 5 button is calibrated. The MEANS button is pushed for adjusting the indicator to the rated value of the sensor. After that, CAL.ON is switched and DV value is set to “10.00” with turning MEAS controller. At The end CAL button is switched off and so the device will be ready to record experimental data. The mechanical gauges are also placed to be used for experimental calculations.

Figure 5.4: Digital system of the triaxial apparatus

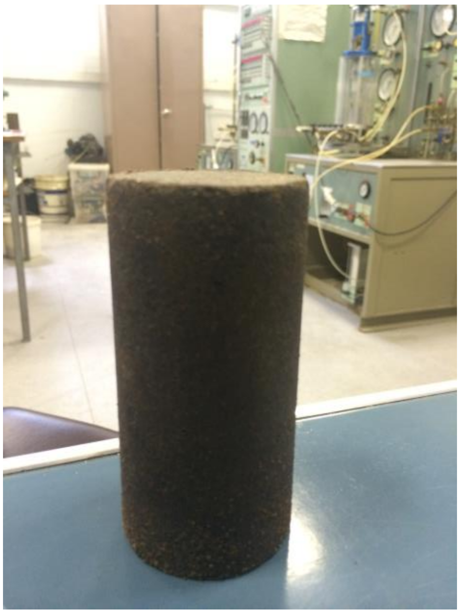

Figure 5.5: Dynamic triaxial test 1st day reinforced sand with 10% of P.B

5.2 Test Material

Representative sand samples were collected from the locations to the right bank of the Akpinar in Turkey . The grain size distribution curve of Akpınar Sand is shown in figure 5.6 . The parameters of the sand shown in the table 5.1.

Table 5.1 Properties of sand

Property	value
Specific Gravity	2.45
Maximum Void ratio	0.8
Minimum void ratio	0.528
D_{50}(mm)	0.3
D_{10}(mm)	0.23
D_{30}(mm)	0.27
D_{60}(mm)	0.33
Coefficient of uniformity ,C_u	1.43
Coefficient of curvature ,C_c	0.96

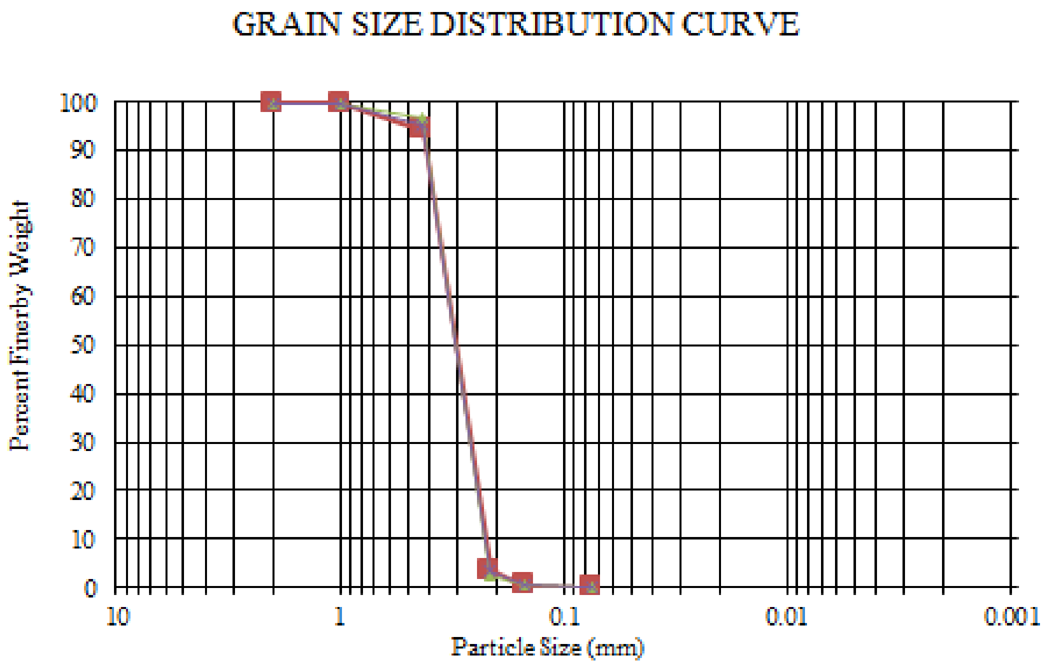

Figure 5.6: Grain size distribution curve of akpınar sand

The polyurethane used as the reinforcement is called HYPERDESMO-PB-2K. It is a fast-curing, two-component, bitmuen-extended polyurethane fluid. It produces a highly elastic membrane with strong adesion to many types of surfaces and excellent mechanical and chemical resistance properties.

Table 5.2 Polyurethane-bitmuen properties

Specific weight of the mixture	gr/cm^3	ASTM D1475 / DIN 53217 / ISO 2811, @ 20 °C	0.97
Flash point	°C	ASTM D93, closed cup	> 40
Tack-free time, @ 77 °F (25 °C) & 55% RH	hours	-	1-2
Recoat time	hours	-	6-24

5.3 Sample Preparation

In the research, the improvement in the properties of uniform sand is achieved by the two-component, polyurethane- Bitumen is powered by a liquid waterproofing material. The mixture of sand and polyurethane by various proportion (3%, 5% and 10% of dry weight of sand) has been prepare in two sizes by 10cm diameter, 20cm high and 5cm diameter, 10cm high.

The polyurethane and sand are mixed thoroughly by mixer until a uniform mixture is obtained. The Polyurethane reinforced sand sample is transferred to the mold with a spoon in three layers and compacted with 25 impacts for each layer. To study the effect of time of the mixture sand specimens, tests have been conducted to the samples after 1^{st} day, 7^{th} day, 30^{th} day and 7^{th} months. Figures 5.7, 5.8 and 5.9 show the microscopic pictures of the samples which have been resized to 200 and 500 times larger, respectively.

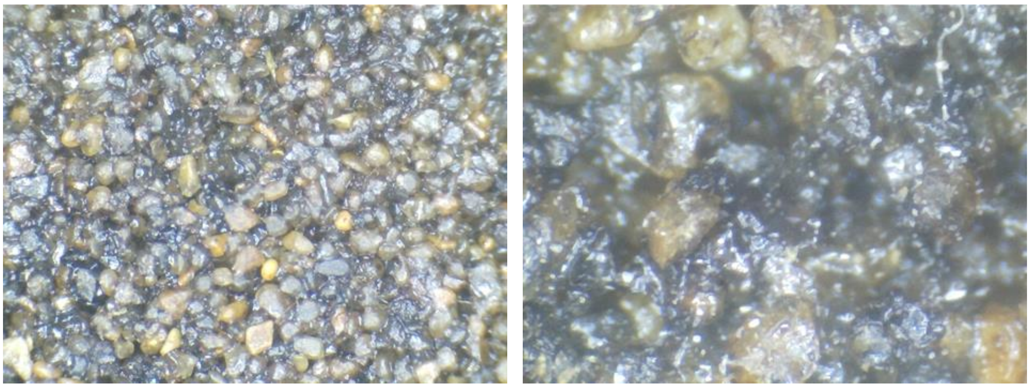

Figure 5.7: Microscopic images of reinforced sand with 10% of polyurethane

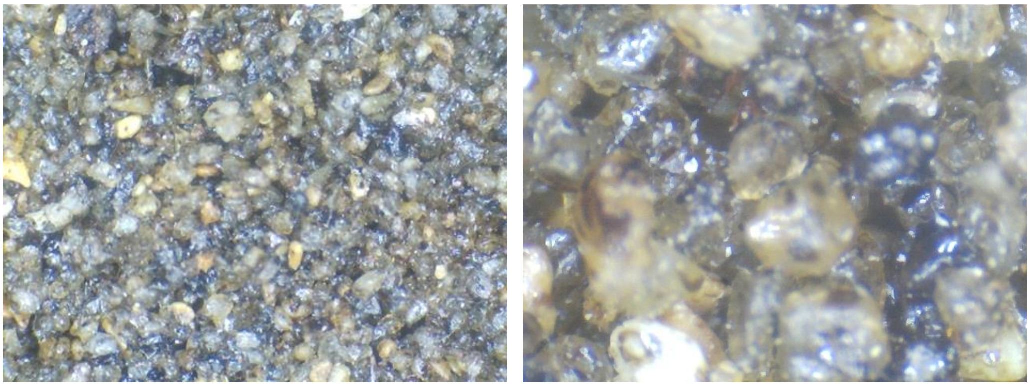

Figure 5.8: Microscopic images of reinforced sand with 5% of polyurethane

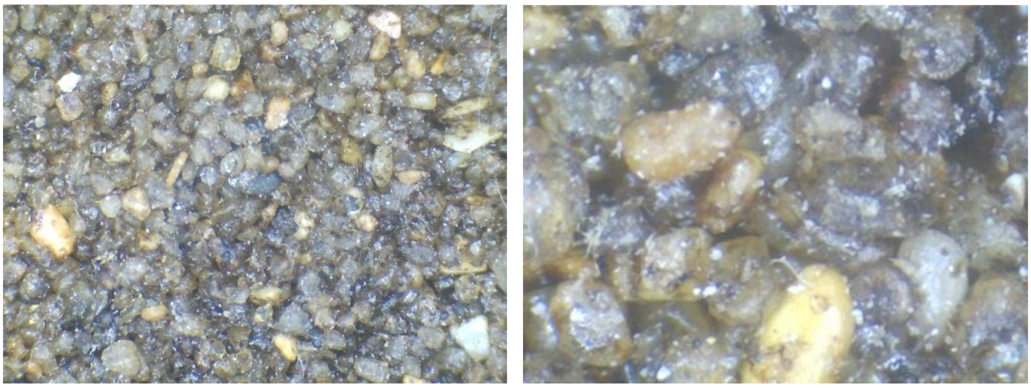

Figure 5.9: Microscopic images of reinforced sand with 3% of polyurethane

5.4 Cyclic Triaxial Test

Controlled cyclic triaxial test is used to evaluate the liquefaction potential and strength of a soil under shear stresses representative of those induced by an earthquake. The samples prepared at 5cm diameter and 10 cm high. For any particular test, the sample weight, diameter and height are measured and recorded. The height should be measured, at two or more diametrically opposed locations. The diameter is measured at several locations with a vernier caliper. The membrane is slid over the sample and lower platen. Then an O-ring is used to seal the membrane and secure it in place. The membrane stretcher is removed. The top cap is put in place on the sample and the membrane rolled onto the top cap. With a split ring tube, the O-ring is snapped onto the top cap to seal and secure the membrane. The tests were conducted on the 100 KPa pressure and the specimen is consolidated isotropically, after saturation and consolidation to the required stress, in general the sample is sheared by increasing the vertical load until failure. The controlling and data acquisition software provides certain predefined testing options according to respectively standard ASTM D3999. Following the standards the cyclic loading is to be performed under undrained conditions. During cyclic loading, the cell pressure is kept constant.

Any loading or unloading on the specimen must be controlled from the digital unit system. After the drainage valves are turned off, the test will start. The effective stress applied is 100kPa, The cyclic stress has a peak-to-peak amplitude of 5% of effective stress, (the first amplitude is 5, every 5 periods the amplitude will be 10 more than the previous period's amplitude).As the number of cyclic loading increases, the effective stress decreases and thus axial deformations occur. The test is performed until the pore water pressure value is equal to the net pressure or the axial strains reach to a value of ±2.5, whichever is earlier. The shear stress applied to the specimen is equal to the half of the axial stress (σ_d).

$$\text{C.S.R.}= \frac{\sigma d}{2 \times \sigma\prime} \qquad (5.2)$$

Where σ_d is the axial stress and σ' is the existing effective confining stress (Ishihara K., Soil Behavior in Earthquake Geotechnics, 1996). If the test needs to stop at a certain number of loading cycles, it must be arranged thus the test will stop automatically when it reaches that number of cycles. If the number of cycles is set to “000000” at the beginning of the test, the test must be stopped manually. The frequency is arranged as 0.1 Hz. After the dynamic loading unit is prepared, the digital system must be initialized by pressing AUTO buttons. The power supply is turned on and a pressure of 100 KPa is applied to the system. The top loading piston is lowered until it touches the specimen cap by using the static regulation button. The piston must be lowered really slowly, otherwise load will apply to the specimen and the specimen will be deformed. After completing the cyclic triaxial test, the air pressure applying to the top loading piston is lowered by using the static regulation button. The vertical pressure valve must be opened to applying a balancing pressure. The back pressure on the specimen is lowered to zero and the confining pressure is lowered to evacuate the water inside the chamber. The cables connecting to the digital system are disconnected. The cell cap, cell chamber and the specimen are removed. The recorded time history of stresses and deformations is translated to effective stresses and strains for further analysis. From these axial values shear stress and shear strain can be calculated. For undrained test conditions it can be shown that the shear strain is 1.5 times the axial strain, that is $\gamma=1.5\varepsilon$. This relation is connected to Poisson’s ratio $\upsilon = 0.5$ in undrained test conditions. The hysteresis loop is achieved by plotting cyclic stress against axial strain. It is used for the calculation of damping ratio and elasticity modulus for each cycle. The Elasticity Modulus values are calculated as:

$$E = \frac{\Delta_\sigma}{\Delta_\varepsilon} \tag{5.3}$$

And also the shear modulus G can be computed from E and the measured Poisson’s ratio. The Shear Modulus (G) can be calculated as:

$$G = \frac{E}{2(1+\mu)} \tag{5.4}$$

The damping ratio are calculated using the following equations:

$$D = \frac{A_{loop}}{4\pi A_\Delta} \tag{5.5}$$

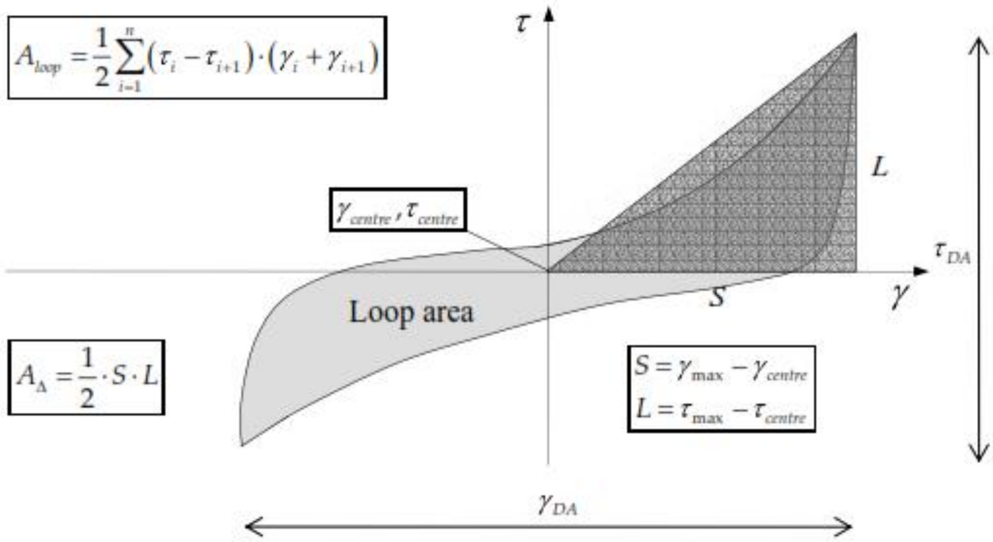

Figure 5.10: Hysteresis loop with triangle area

Also the ramber-osgood model used to calculate the damping ratio as equation 5.6, (r=2).

$$D = \frac{2}{\pi}\,\frac{r-1}{r+1}\,[1-\frac{G}{G_0}] \qquad (5.6)$$

5.5 Unconfined Axial Loading Test

The Unconfined Compression Test is a simplest and quickest laboratory test method for evaluation of the shear strength of cohesive soil. Unconfined Test Apparatus is normally useful in soil mechanics laboratories. In this test, cylindrical specimens are tested in compression with no lateral support while undergoing vertical compression.

The unconfined compressive strength is computed from the following formula:

Equation Set (5.7): Unconfined strength

$$\sigma = \frac{P}{A} \qquad \mathbf{(5.7)}$$

σ = unconfined compressive strength (kgf/cm^2)

P=compressive force (kgf/cm^2)

A=cross sectional area (cm^2)

The area of the specimen changes to maintain constant volume through the test (bulging). Thus, the average cross sectional area at a particular deformation during the test is calculated using:

$$A = \frac{A_0}{1-\varepsilon} \tag{5.8}$$

A=average cross sectional area (cm^2)

A_0=initial cross sectional area (cm^2)

ε =axial strain

ΔL =change in length (cm)

L_0=initial length (cm)

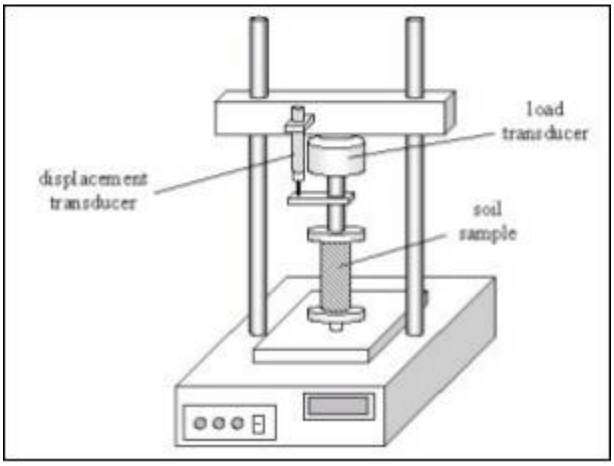

Figure 5.11: Sketch of an unconfined compression test device

To study the affect of time on stress-strain behavior of the mixture sand specimens, unconfined axial loading tests have been conducted to the samples after first day, 7th day, 30th day, 4th month,5th month and 7th months. Results have shown there is no affect the sizes on stress-strain behavior. As the ratio of Polyurethane-Bitumen increase peak axial stress increase at every curing time and also the peak axial stress increase during the times.

Figure 5.12: Unconfined axial test 7th Day reinforced sand with 3% of P.B

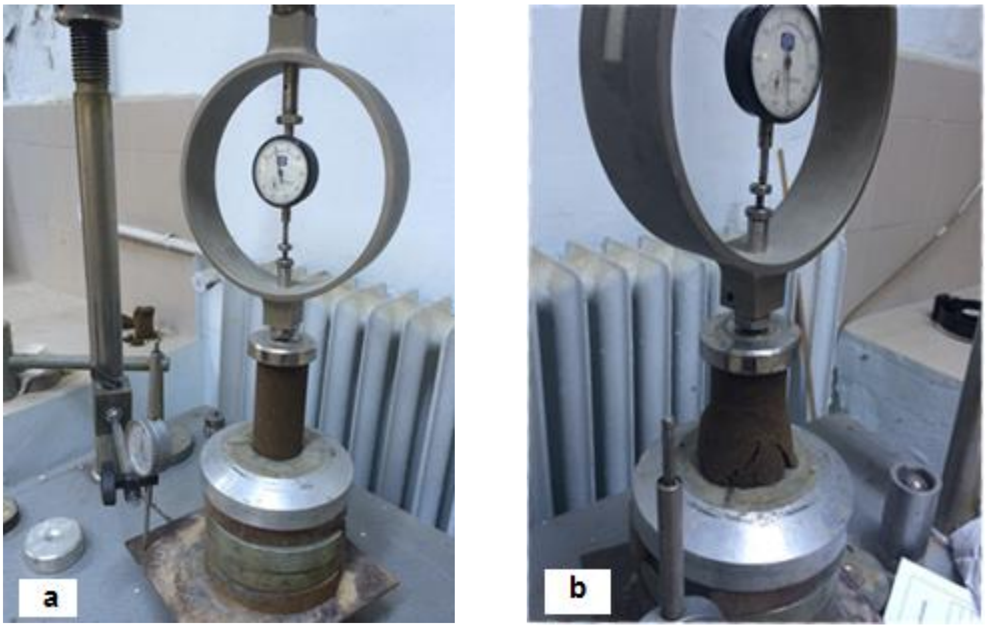

Figure 5.13: Unconfined axial test 110th Day reinforced sand with 5% of P.B a)before test,b)after test

5.6 Unconfined Undrained Triaxial Test

Determining the mechanical properties of soils is a very important step to design foundations, embankments and other soil structures. UU triaxial test was performed to samples to determine the cohesion intercept and the friction angle. The tests were performed in general accordance with ASTM D 2850 – Standard Test Method for Unconsolidated Undrained Triaxial Compression Test on Cohesive Soils.

For the UU test, the specimens are subjected to a confining fluid pressure in a triaxial chamber. Once the specimen is inside the triaxial cell, the cell pressure is increased to a predetermined value by rotating the knob, and the specimen is brought to failure by increasing the vertical stress by applying a constant rate of axial strain. Saturation and consolidation are not permitted to keep the original structure and water content of sample untouched. Pore pressures are not measured during this test and therefore the results can only be interpreted in terms of total stress. These tests are carried out on three specimens of the same sample subjected to different confining stresses,(1 kg/cm²,2Kg/cm² and 3Kg/cm²). The results of the test are plotted as curves of axial stress against strain. For conditions of maximum principal stress difference (taken as failure) Mohr circles are plotted in terms of total stress. The failure envelope drawn tangential to the Mohr circles in order to find the "undrained cohesion intercept" and undrained "angle of shearing resistance".

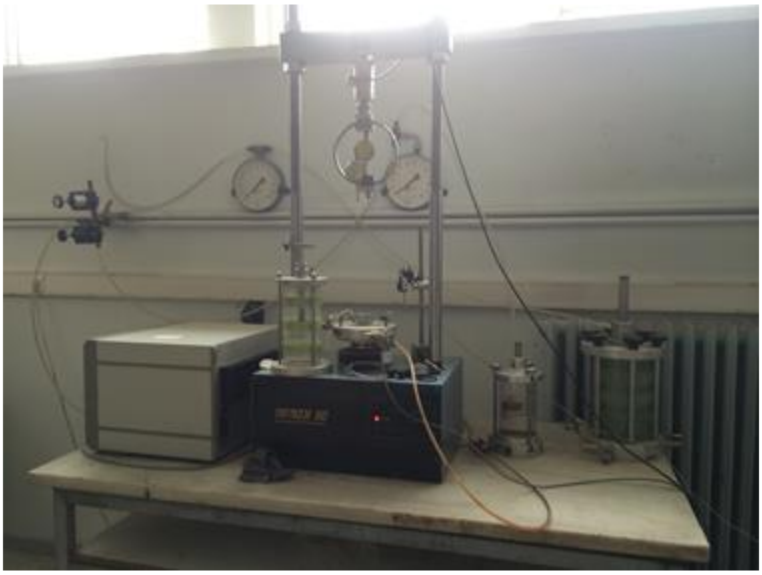

Figure 5.14: Triaxial Test Apparatus in ITU Soil Dynamics Laboratory

To plot a Mohr circle from triaxial data, obtain σ_1, and σ_3 from the triaxial test and draw a circle connecting the two points centered at $(\sigma_1+\sigma_3)/2$. Repeat for every stress state tested. Plotting the results from three triaxial tests at three different confining stresses on the same graph, drawing the circles, and drawing a tangent to the circles constructs the failure envelope. The failure envelope is stress dependent, i.e. because the triaxial tests are performed at significantly different confining stresses the failure envelope will not be a straight line. For this reason it is important that all triaxial tests be performed in the anticipated field stress range (Figure 5.15).

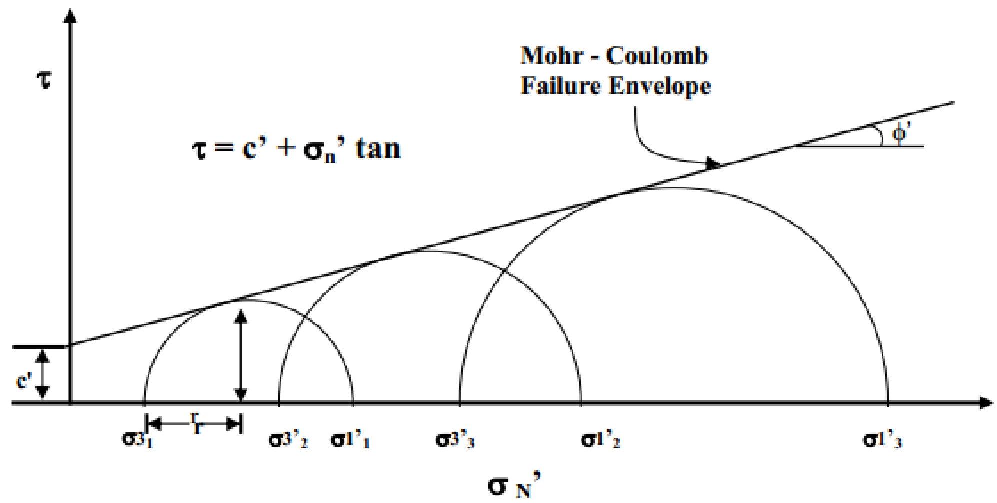

Figure 5.15: Mohr Coulomb Plot (CIV E 353 - Geotechnical Engineering,Shear Strength of Soils, 2006)

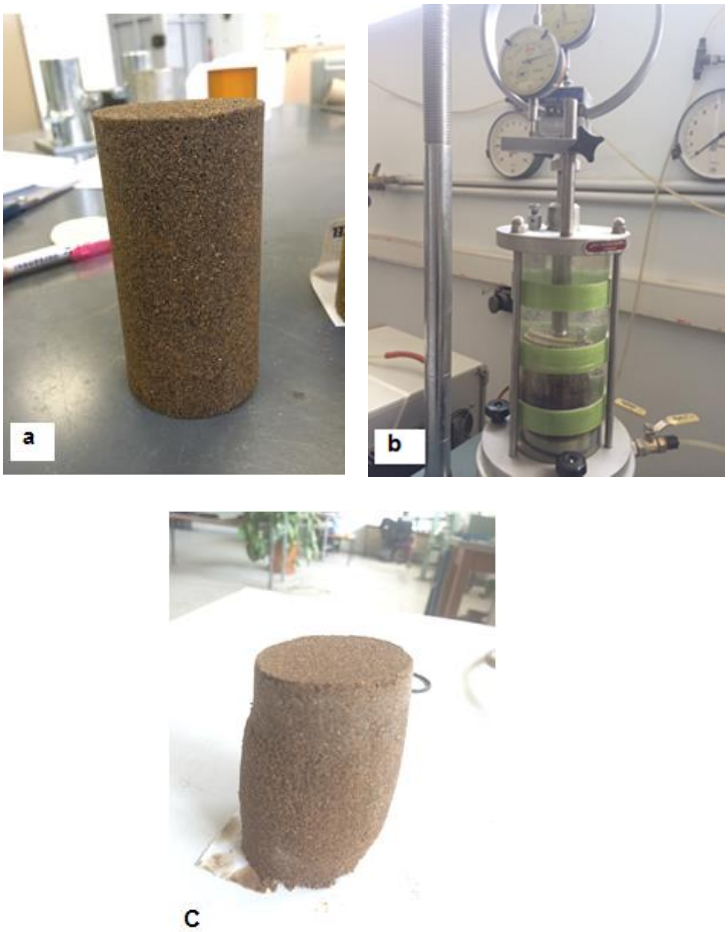

Figure 5.16: Triaxial test first Day reinforced sand with 3% of P.B a)before test,b)during the test,c)after test

6. EXPERIMENTAL RESULTS

In this part of the thesis, the experimental results of the laboratory tests conducted at ITU Soil Mechanics Laboratory are presented.

6.1 Cyclic Triaxial Test Result

A common triaxial test is performed for the determination of the elasticity modulus and damping ratio of the samples. After saturation and consolidation to the required stress, in general the sample is sheared by increasing the vertical load until failure. From the stress-strain curve, the elastic modulus E is estimated and the damping ratio calculated from rumberg-osgood model. Figure 6.1, shows the cyclic test results for sample with 5% of P.B at first day. A cyclic stress vs. number of cycles is shown at the first figure, in the first 5 cycles amount of stress is ±0.02 and increased to ±0.25 at last 5 cycles,(cycles 20-25). The test has been finished at twenty fifth cycle. The second figure shows axial strain vs. number of cycles, there is a downward stretch after 15^{th} cycle, because of rigidity of the sample, (this rigidity causes membrane to stretch). The thrid figure shows the stress-strain relationship, because of stretching of membrane in the test, the results cut off at 20^{th} cycle. The fourth figure shows the elasticity modulus of sample vs. axial strain, the value of E_{max} was determined which has been 83.4 MPa.

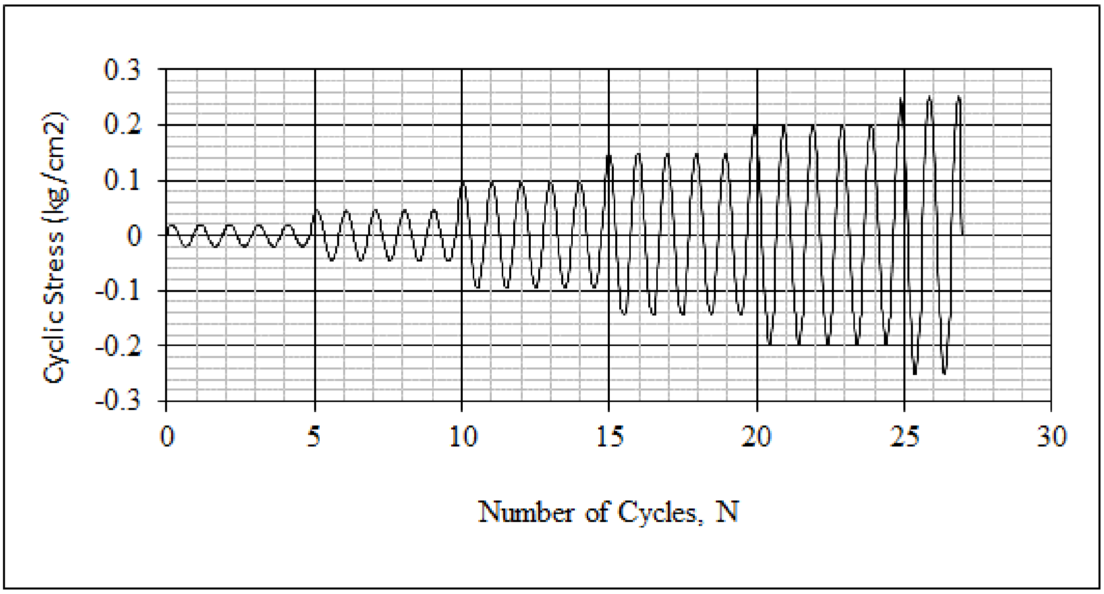
0.3
0.2
0.1
0
-0.1
-0.2
-0.3
Cyclic Stress (kg/cm2)
0
5
10
15
20
25
30
Number of Cycles, N

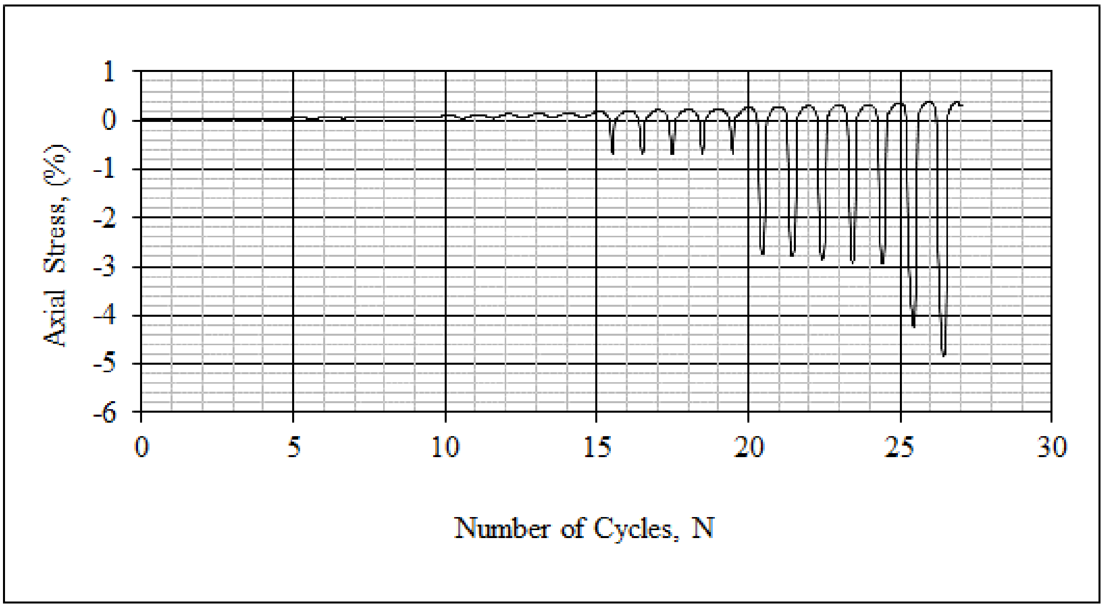
1
0
-1
-2
-3
-4
-5
-6
Axial Stress, (%)
0
5
10
15
20
25
30
Number of Cycles, N

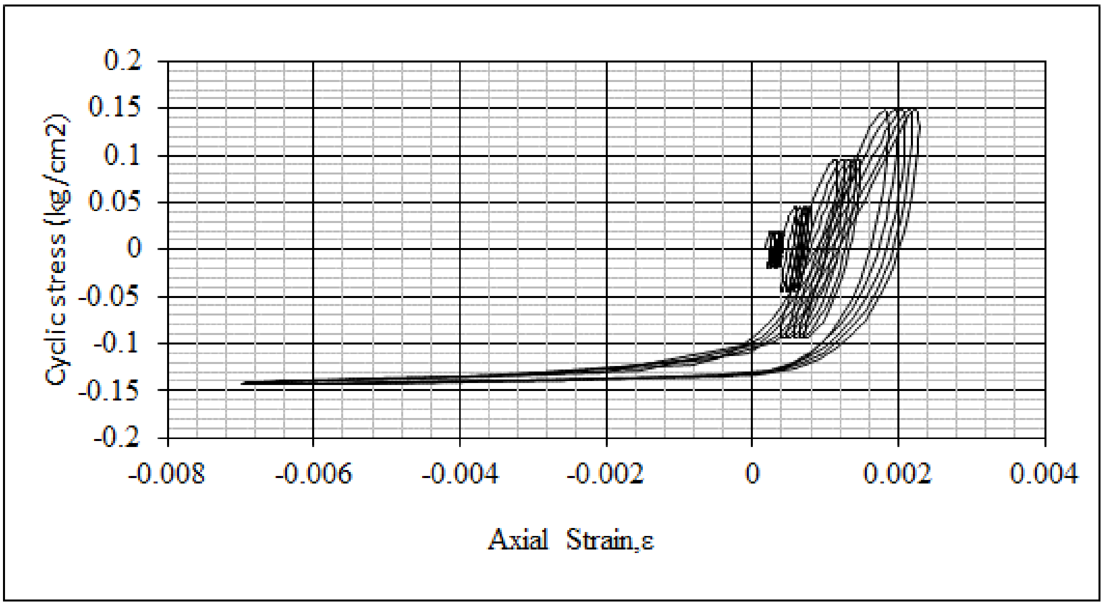
0.2
0.15
0.1
0.05
0
-0.05
-0.1
-0.15
-0.2
Cyclic stress (kg/cm2)
-0.008
-0.006
-0.004
-0.002
0
0.002
0.004
Axial Strain,ε

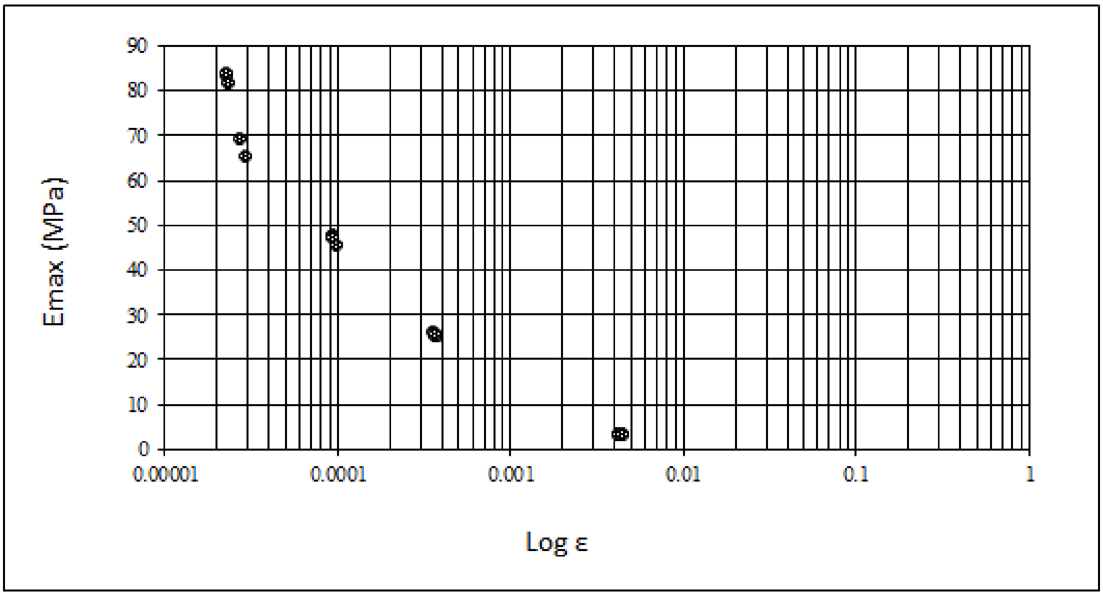

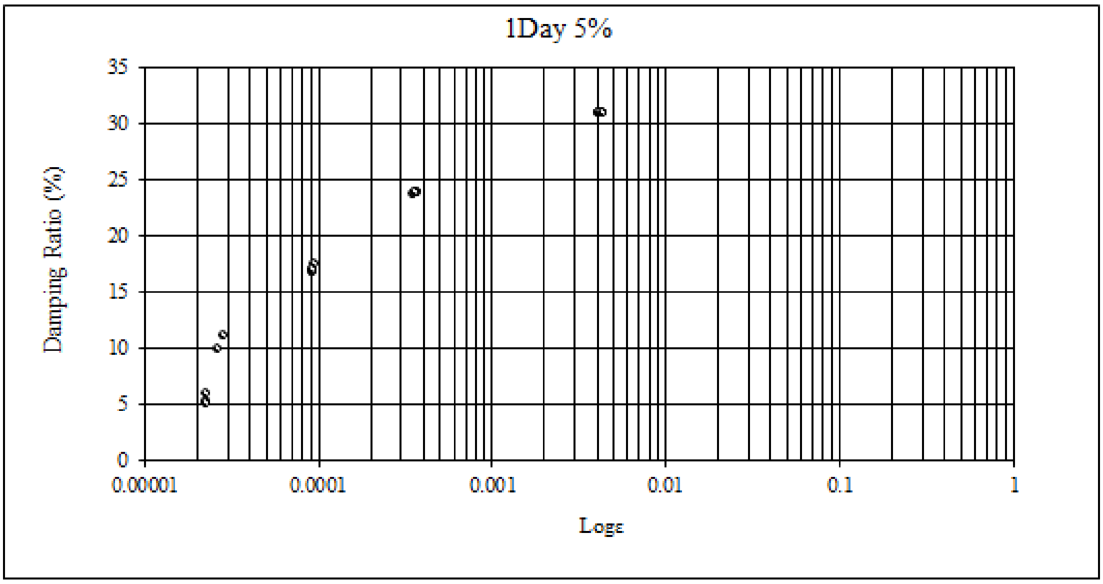

Figure 6.1 : Experimental result for sample with 5% of P.B at 1st day, (Test No.1.2)

Table 6.1 Experimental results of cyclic load on Sample with 5% P.B at first day(σ_c=100)

Cycles No.	P.B (%)	A (cm²)	V (cm³)	γ	ε	σ (kg/cm²)
5.04	5	19.64105	196.4105	0.000844	0.000562	0.043314
11.02	5	19.65427	196.5427	0.001852	0.001235	0.095767
14.94	5	19.66425	196.6425	0.002612	0.001741	0.144022
19.92	5	19.68142	196.8142	0.003919	0.002613	0.198364

Figure 6.2, shows the cyclic test results for sample with 10% of P.B at first day. A cyclic stress vs. number of cycles is shown at the first figure, in the first 9 cycles amount of stress is ±0.01 and increased to ±0.4 at last cycles. The test has been finished at 40th cycle. The second figure shows axial strain vs. number of cycles, there is a downward stretch after 22nd cycle. The thrid figure shows the stress-strain relationship, because of stretching of membrane in the test, the results cut off at 30th cycle. The fourth figure shows the elasticity modulus of sample vs. axial strain, the value of E_{max} was determined which has been 230 MPa.

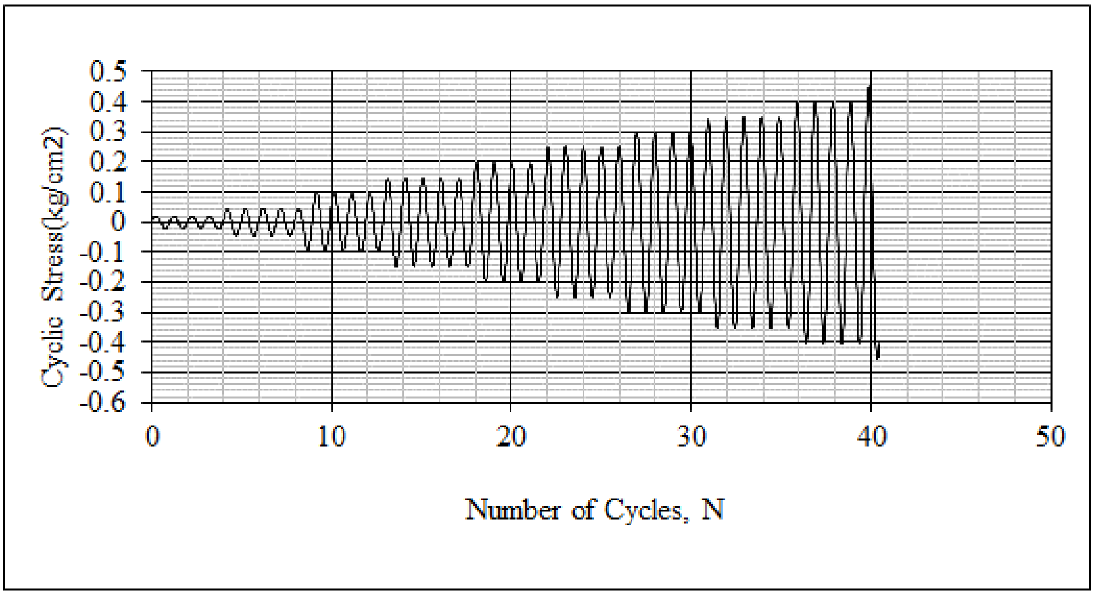

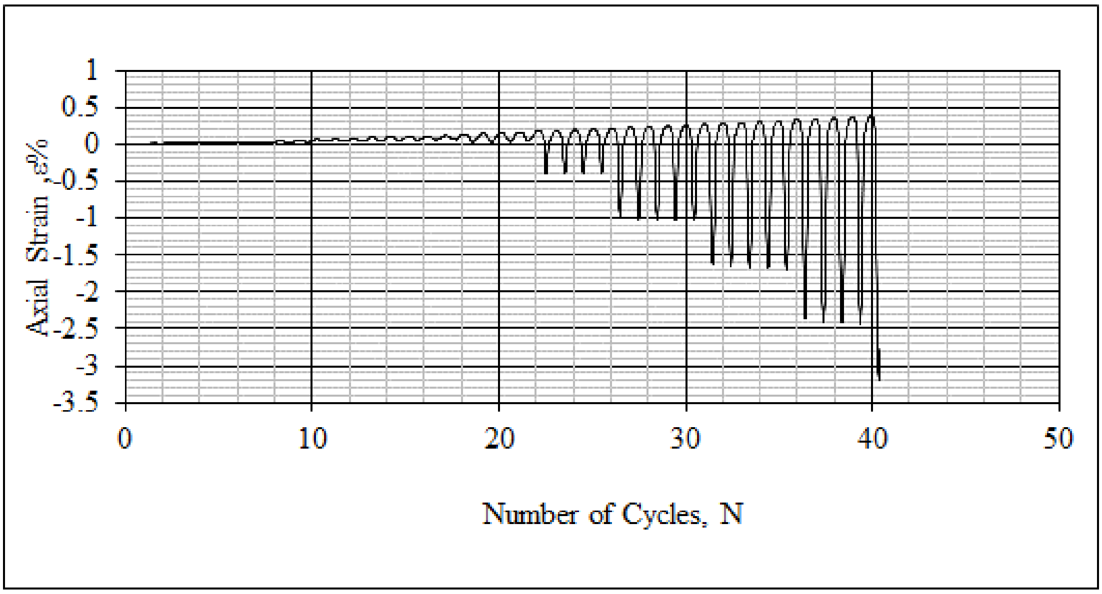

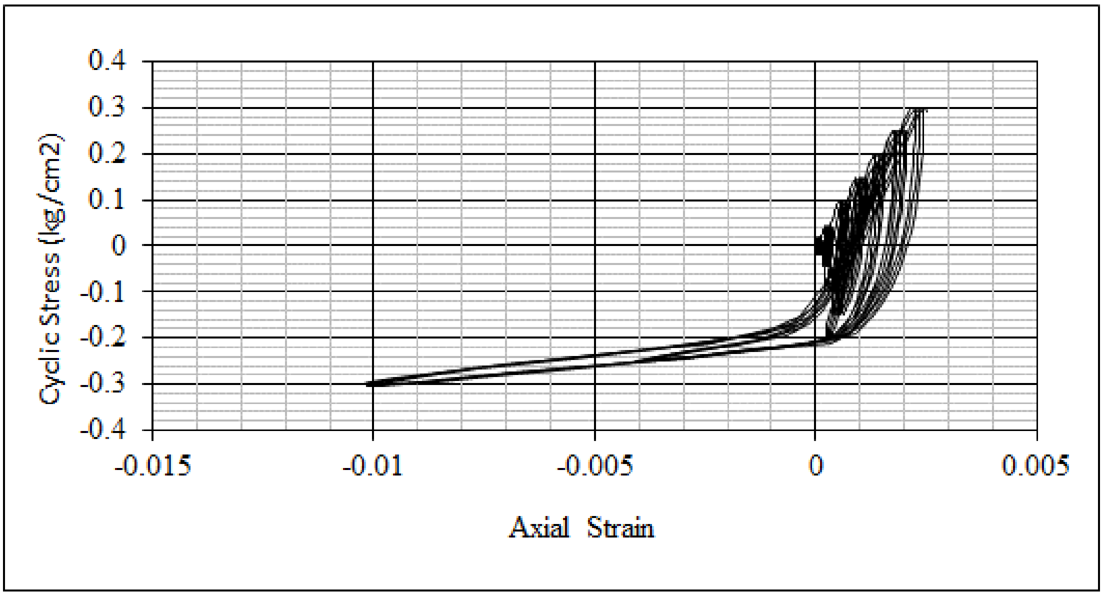

0.4
0.3
0.2
0.1
0
-0.1
-0.2
-0.3
-0.4
Cyclic Stress (kg/cm2)
-0.015
-0.01
-0.005
0
0.005
Axial Strain

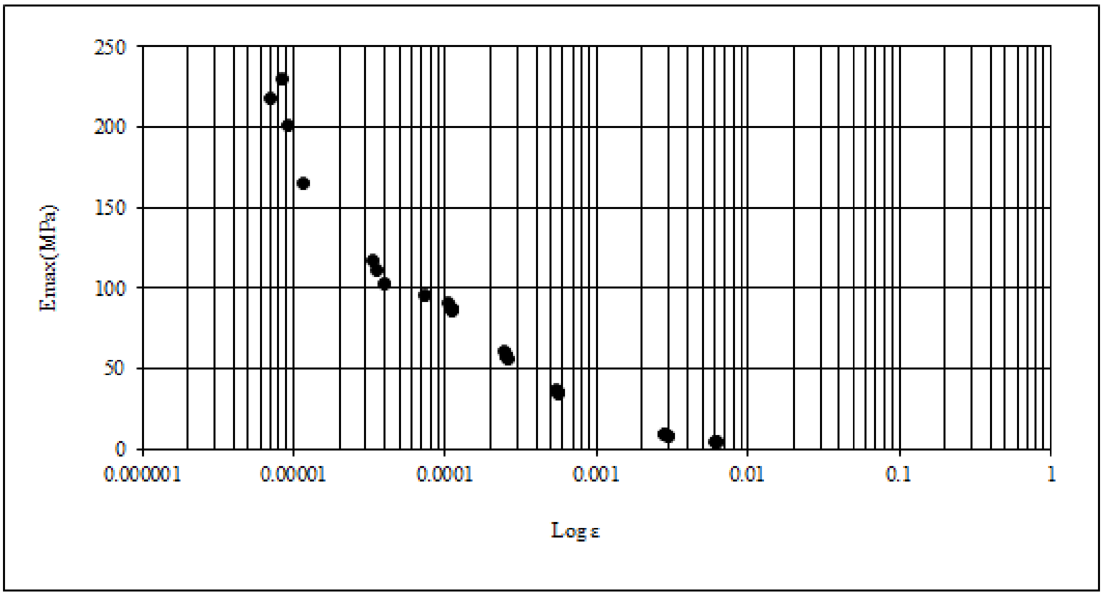

250
200
150
100
50
0
Emax(MPa)
0.000001
0.00001
0.0001
0.001
0.01
0.1
1
Log ε

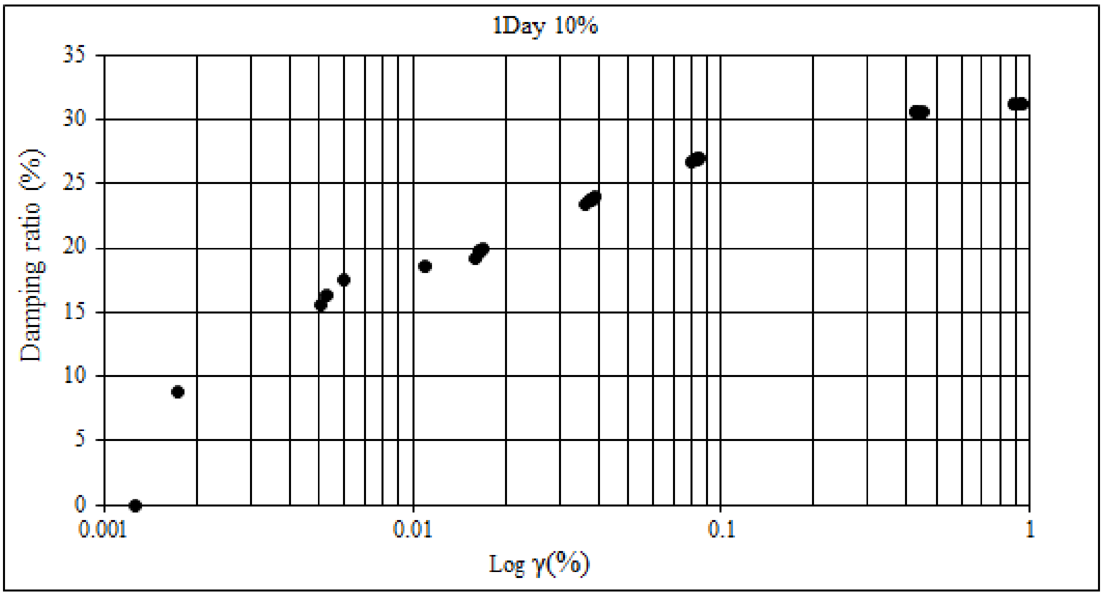

Figure 6.2 : Experimental result of cyclic triaxal test for sample with 10% of P.B at 1st day,(Test No.1.3)

Table 6.2 Experimental results of cyclic loading on sample with 10% P.B at first day(σ_c=100KPa)

Cycles No.	P.B (%)	A (cm^2)	V (cm^3)	γ	ε	σ (kg/cm^2)
1.2	10	19.63129	196.3129	0.000098	0.000065	0.018219
4.18	10	19.63399	196.3399	0.000305	0.000203	0.042363
9.12	10	19.63979	196.3979	0.000748	0.000498	0.092217
13.1	10	19.64739	196.4739	0.001328	0.000885	0.144348
18.06	10	19.65583	196.5583	0.001971	0.001314	0.196112
26.94	10	19.6709	196.709	0.003119	0.002079	0.288434

Figure 6.3, shows the cyclic test results for sample with 3% of P.B at 7th day. A cyclic stress vs. number of cycles is shown at the first figure, in the first cycles amount of stress is ±0.02 and increased to ±0.3 at last cycles. The test has been finished at 32nd cycle. The second figure shows axial strain vs. number of cycles, there is a downward stretch after 20th cycle. The thrid figure shows the stress-strain relationship, because of stretching of membrane in the test, the results cut off at 25th cycle. The fourth figure shows the elasticity modulus of sample vs. axial strain, the value of Emax was determined which has been 183 MPa.

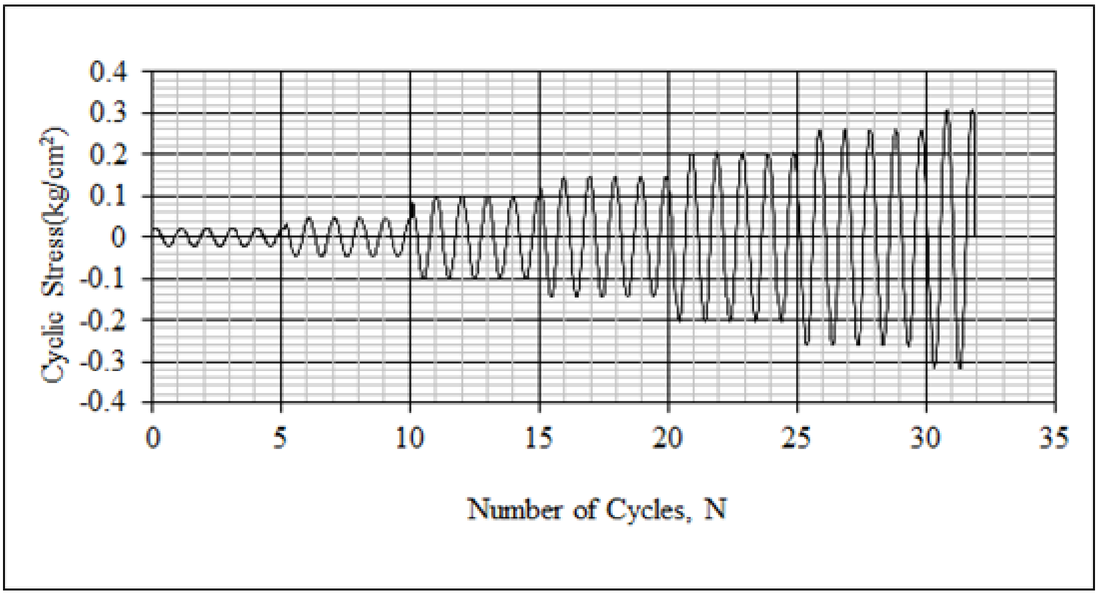

Cyclic Stress(kg/cm^2)
Number of Cycles, N

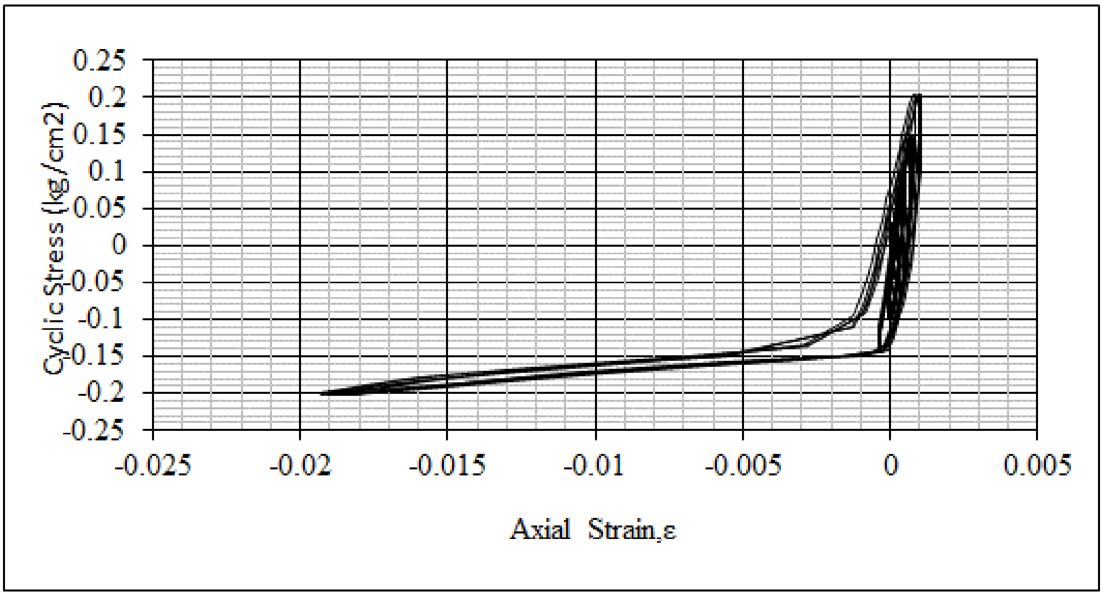

Cyclic Stress (kg/cm2)
Axial Strain,ε

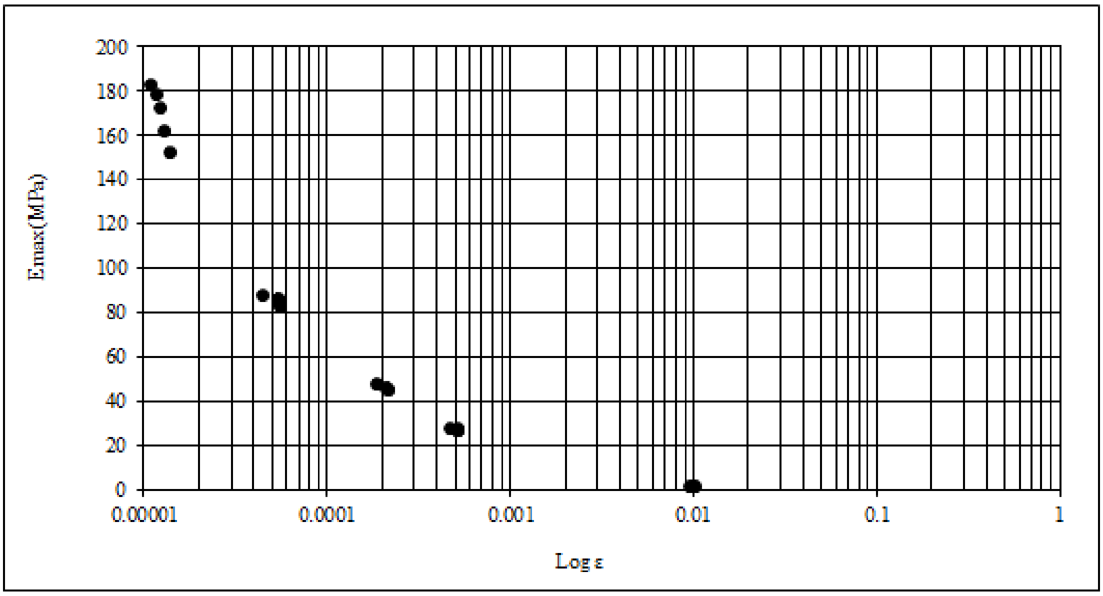

Emax(MPa)
Log ε

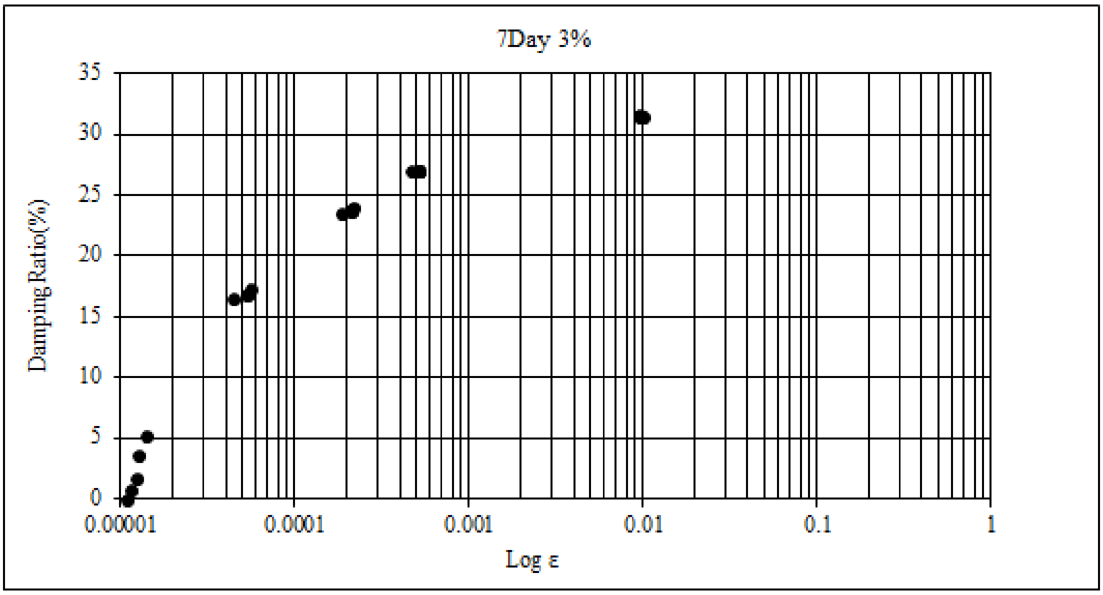

Figure 6.3 : Experimental result of cyclic triaxal test for sample with 3% of P.B at 7th day, (Test No.7.1)

Table 6.3 Experimental results of cyclic loading on sample with 3% P.B at7th day(σ_c=100KPa)

Cycles No.	P.B (%)	A (cm^2)	V (cm^3)	γ	ε	σ (kg/cm^2)
1.1	3	19.24098	190.4857	7.65455E-	5.103E-	0.021046
10.12	3	19.24562	190.5316	0.000438	0.000292	0.082605
15.96	3	19.25208	190.5956	0.000941	0.000627	0.145184
20.98	3	19.25674	190.6418	0.001305	0.000869	0.19266
24.88	3	19.26039	190.6779	0.001588	0.001059	0.203807

Figure 6.4, shows the cyclic test results for sample with 5% of P.B at 7th day. A cyclic stress vs. number of cycles is shown at the first figure, in the first cycles amount of stress is ±0.02 and increased to ±0.95 at last cycles. The test has been finished at 98th cycle. The second figure shows axial strain vs. number of cycles, there is a downward stretch after 75th cycle. The thrid figure shows the stress-strain relationship, because of stretching of membrane in the test, the results cut off at 85th cycle. The fourth figure shows the elasticity modulus of sample vs. axial strain, the value of Emax was determined which has been 250 MPa.

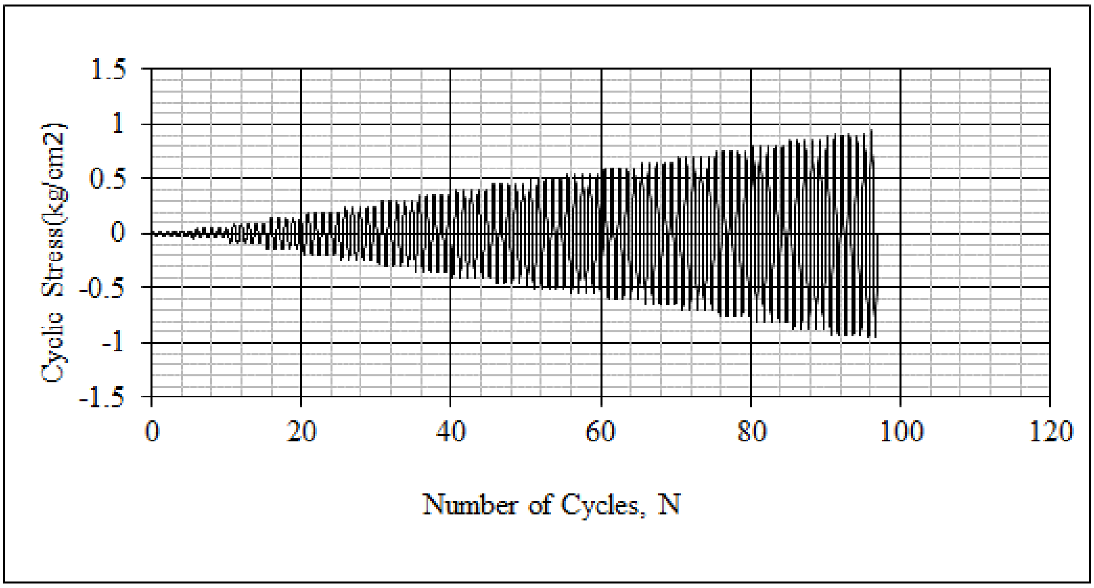
Cyclic Stress(kg/cm2)
1.5
1
0.5
0
-0.5
-1
-1.5
0
20
40
60
80
100
120
Number of Cycles, N

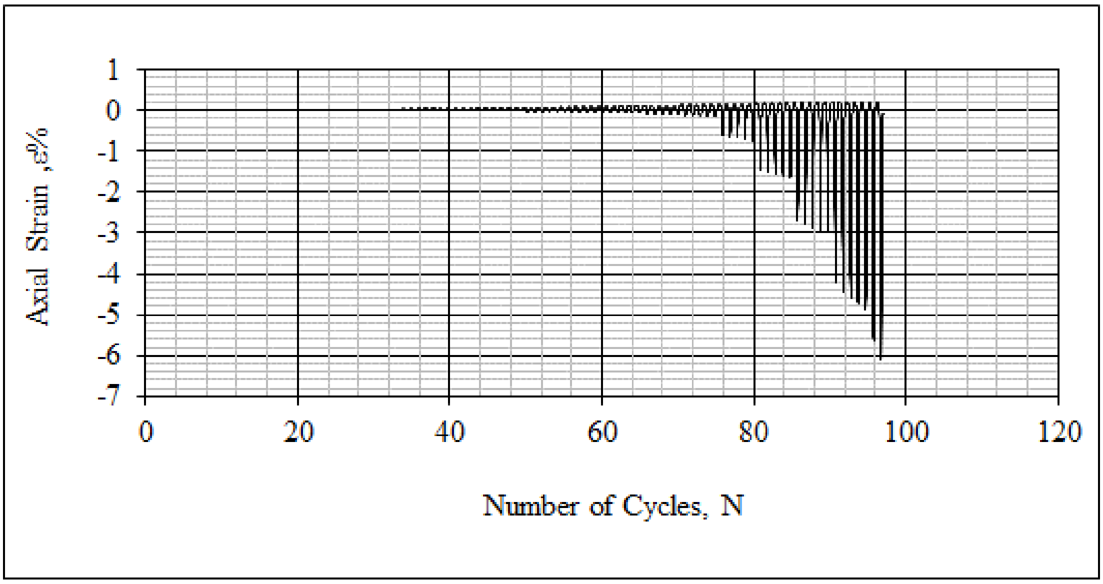
Axial Strain ,ε%
1
0
-1
-2
-3
-4
-5
-6
-7
0
20
40
60
80
100
120
Number of Cycles, N

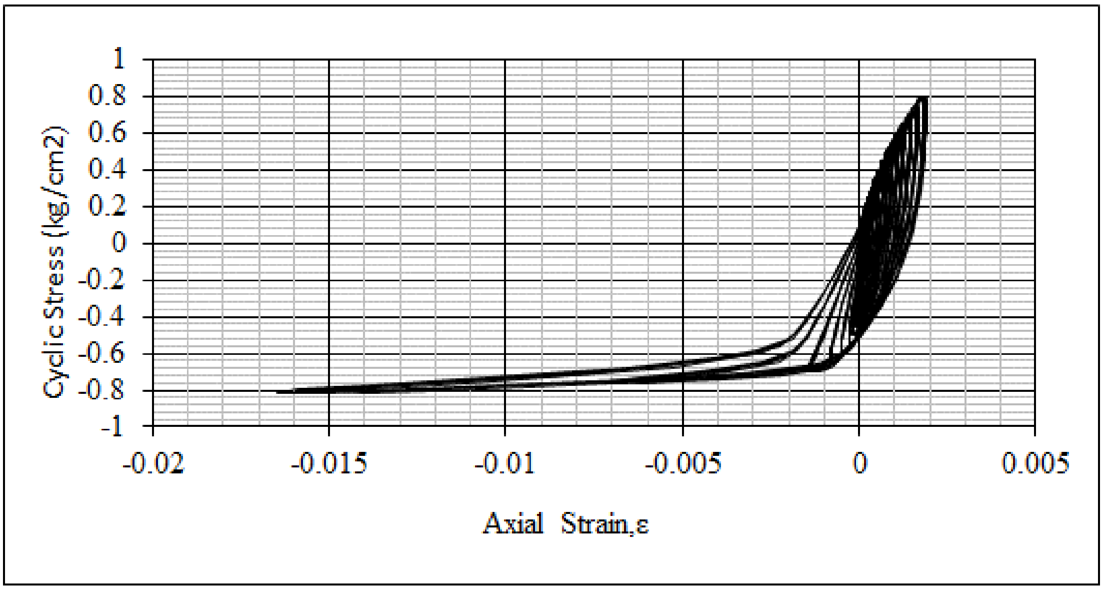
Cyclic Stress (kg/cm2)
1
0.8
0.6
0.4
0.2
0
-0.2
-0.4
-0.6
-0.8
-1
-0.02
-0.015
-0.01
-0.005
0
0.005
Axial Strain,ε

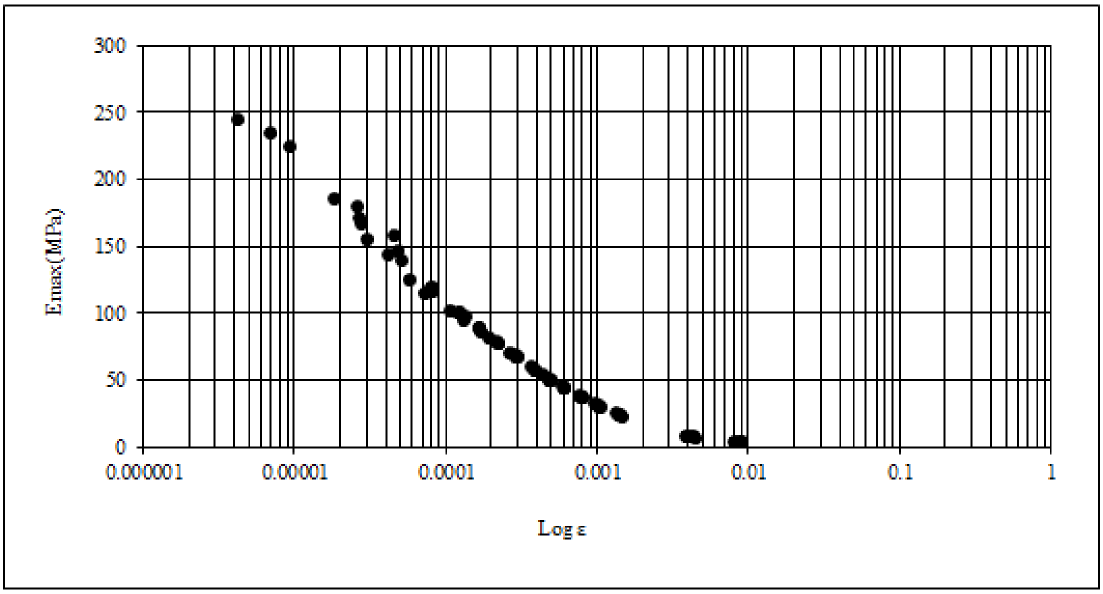

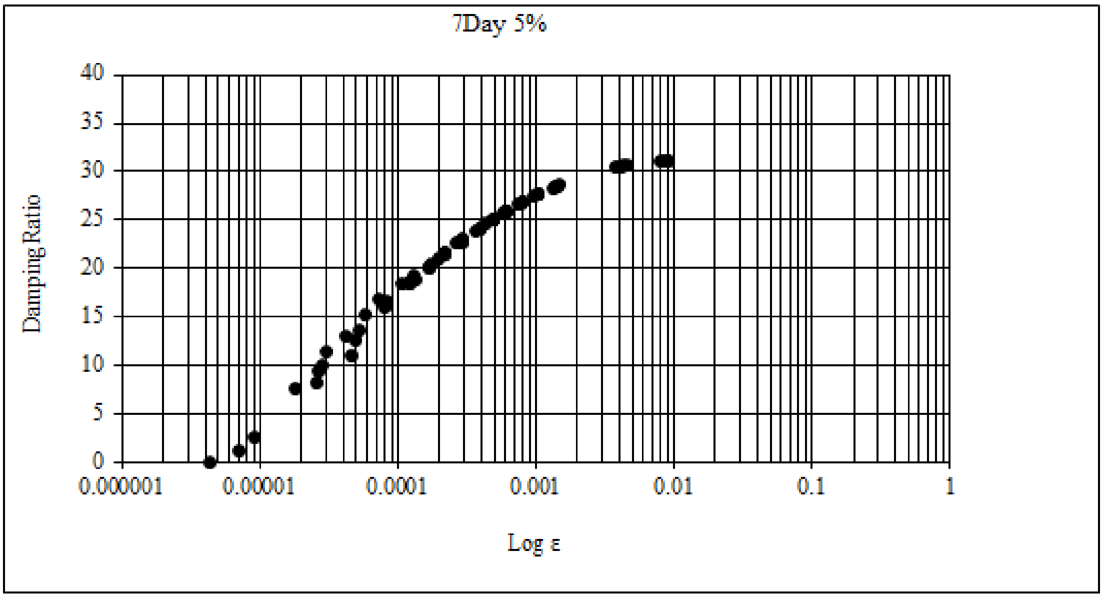

Figure 6.4 : Experimental result of cyclic triaxal test for sample with 5% of P.B at 7^{th} Day, (Test No.7.2)

Table 6.4 Experimental results of cyclic loading on Sample with 5% P.B at7th day(σ_c=100KPa)

Cycles No.	P.B (%)	A (cm^2)	V (cm^3)	γ	ε	σ (kg/cm^2)
11	5	19.63052	196.3052	3.96E-05	2.64E-05	0.093797
15.96	5	19.63136	196.3136	0.000104	6.94E-05	0.14529
20.92	5	19.63282	196.3282	0.000216	0.000144	0.195592
30.82	5	19.63618	196.3618	0.000472	0.000315	0.300767
40.72	5	19.64023	196.4023	0.000782	0.000521	0.402415
66.46	5	19.65398	196.5398	0.00183	0.00122	0.653232
75.38	5	19.66087	196.6087	0.002355	0.00157	0.753926
81.32	5	19.66554	196.6554	0.002711	0.001807	0.805155

Figure 6.5, shows the cyclic test results for sample with 10% of P.B at 7th day. A cyclic stress vs. number of cycles is shown at the first figure, in the first cycles amount of stress is ±0.022 and increased to ±0.98 at last cycles. The test has been finished at 101st cycle. The second figure shows axial strain vs. number of cycles, there is a downward stretch after 86th cycle. The thrid figure shows the stress-strain relationship, because of stretching of membrane in the test, the results cut off at 90th cycle. The fourth figure shows the elasticity modulus of sample vs. axial strain, the value of Emax was determined which has been 362 MPa.

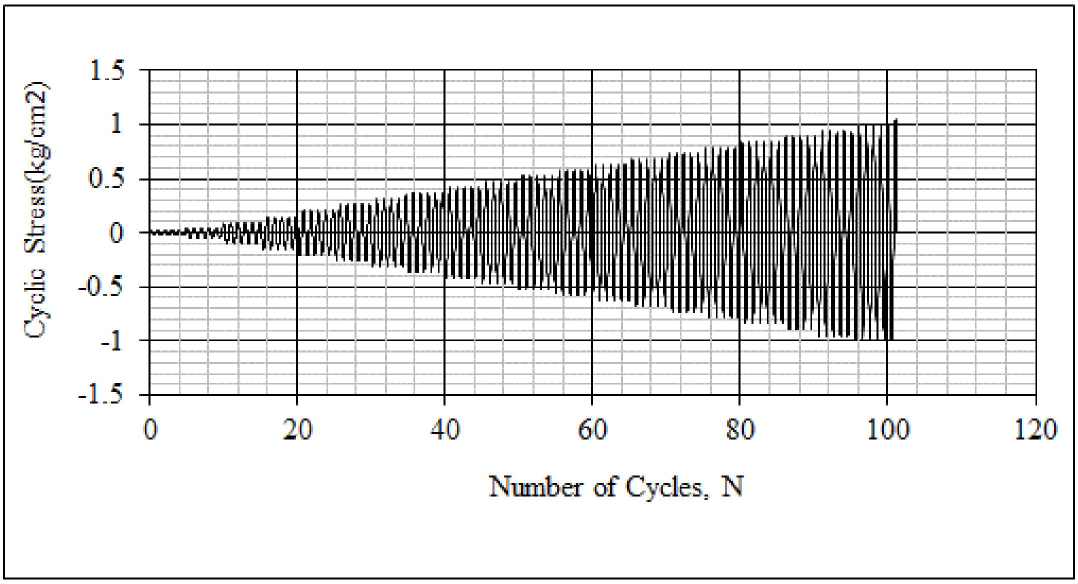

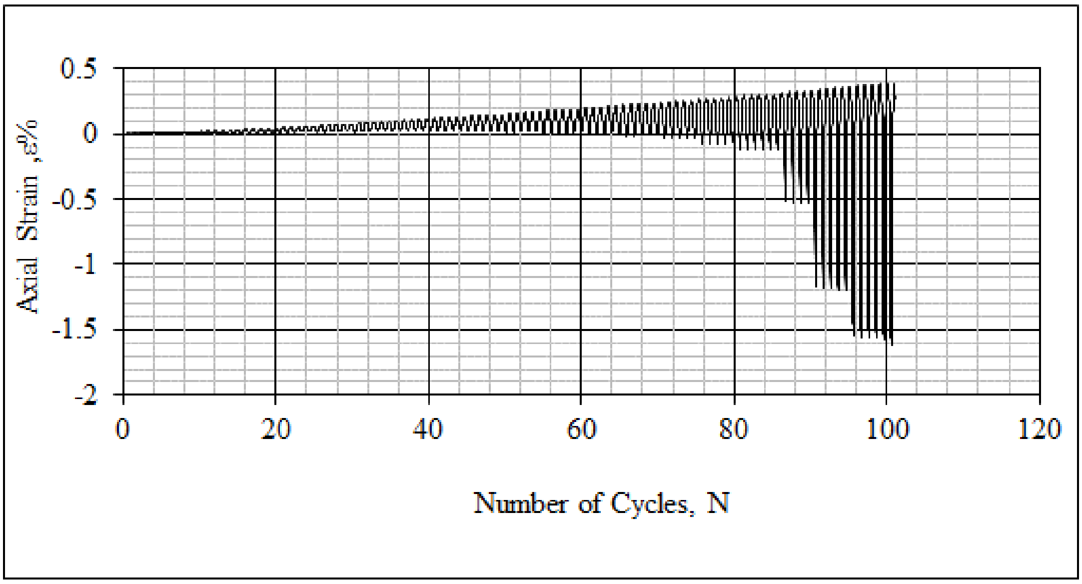

Axial Strain ,ε%
Number of Cycles, N

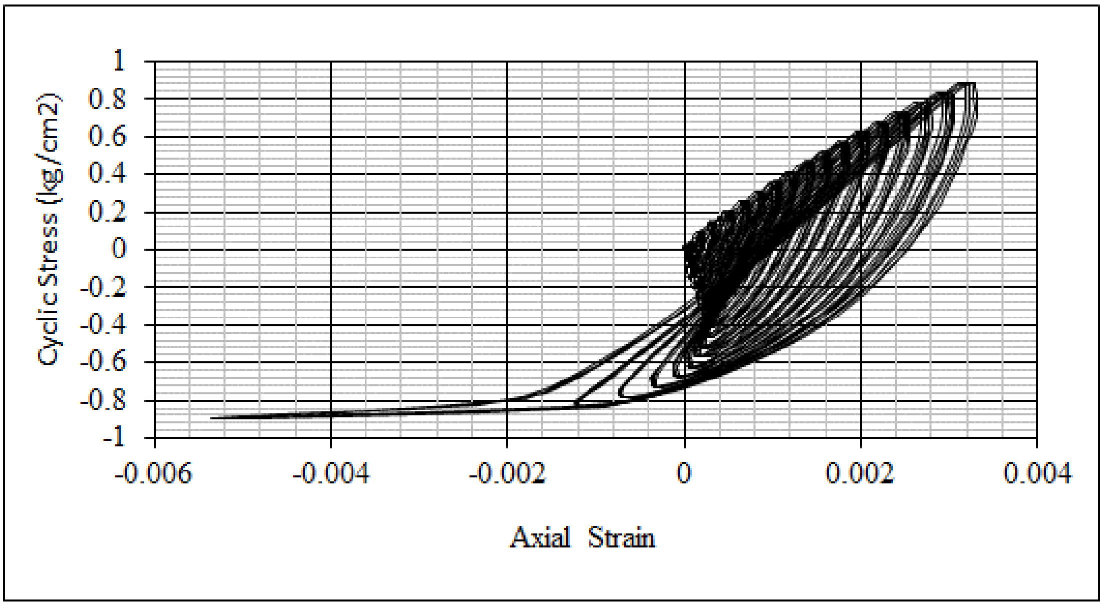

Cyclic Stress (kg/cm2)
Axial Strain

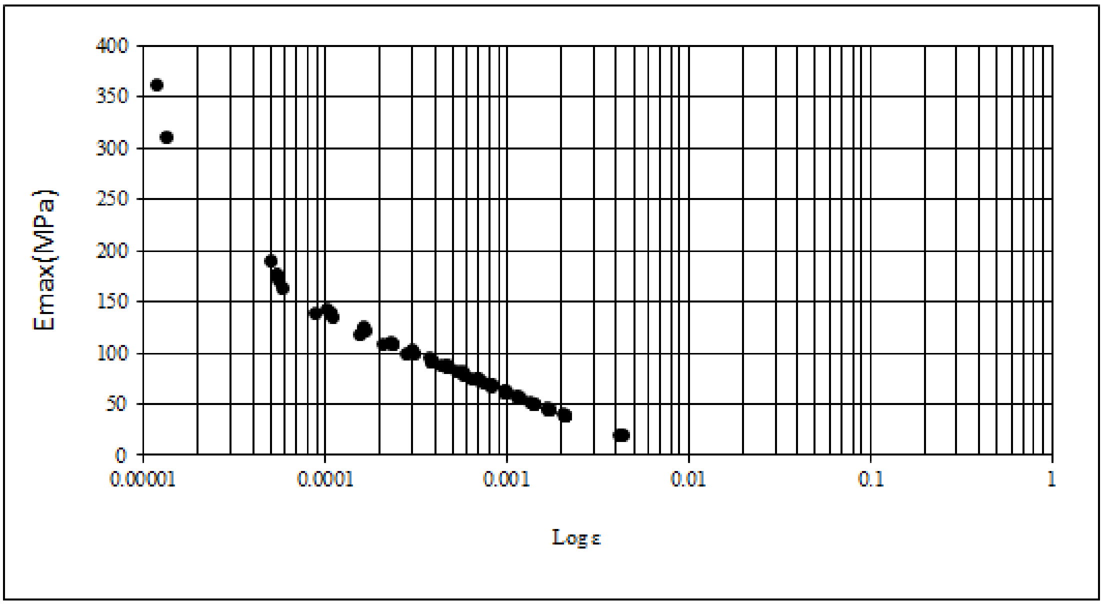

Emax(MPa)
Log ε

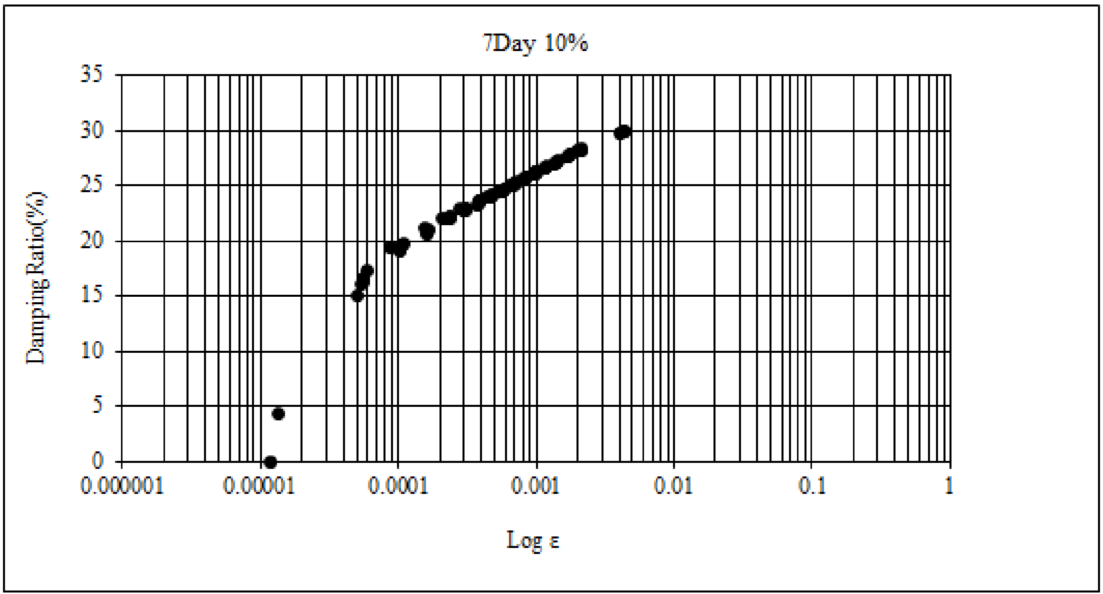

Figure 6.5 : Experimental result of cyclic triaxal test for sample with 10% of P.B at 7th Day,(Test No.7.3)

Table 6.5 Experimental results of cyclic loading on Sample with 10% P.B at7th day(σ_c=100KPa)

Cycles No.	P.B (%)	A (cm^2)	V (cm^3)	γ	ε	σ (kg/cm^2)
1	10	18.85028	187.5603	2.2794E-5	1.5196E-5	0.016416
10.02	10	18.85281	187.5854	0.000224	0.000149	0.097467
15.9	10	18.85511	187.6083	0.000407	0.000271	0.141889
20.86	10	18.85813	187.6383	0.000647	0.000431	0.197809
25.82	10	18.86186	187.6755	0.000944	0.000629	0.255843
30.74	10	18.86457	187.7025	0.001159	0.000773	0.294101
40.66	10	18.87163	187.7727	0.001719	0.001146	0.408326
50.56	10	18.87874	187.8435	0.002284	0.001523	0.516921
60.46	10	18.88643	187.92	0.002894	0.001929	0.623684
70.38	10	18.89551	188.0103	0.003613	0.002409	0.731142
87.18	10	18.90965	188.151	0.004732	0.003155	0.886304

Figure 6.6 and 6.7 show the maximum elasticity modulus of 5 samples with different P.B ratio at 1st and 7th curing time, as it's clear the E_{max} value increase by increasing the polyurethane-bitumen ratio, and also as curing time increase the E_{max} increased.

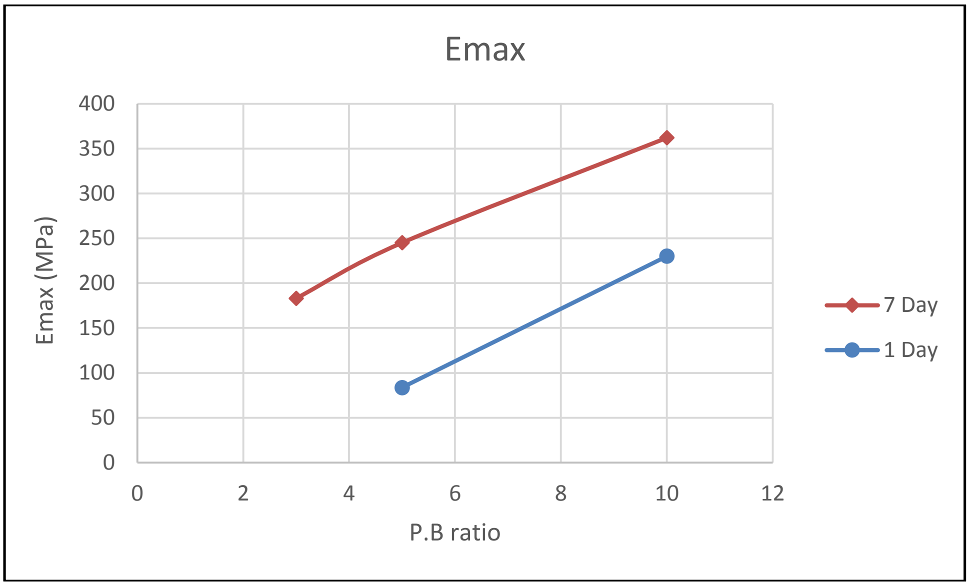

Figure 6.6 : Effect P.B inclusion in Emax

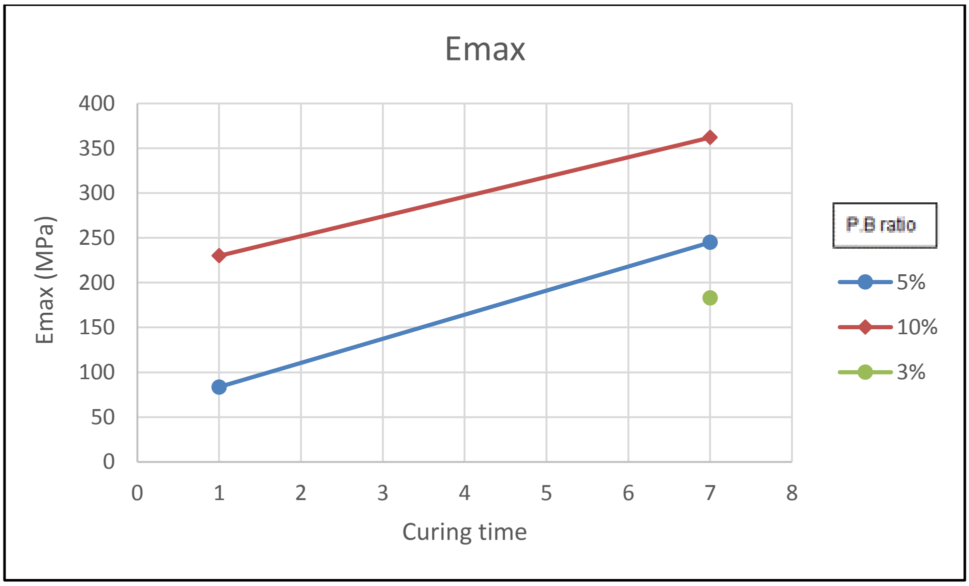

Figure 6.7 : Effect of time in Emax

The experimental results of dynamic triaxial show in table 6.6, with increasing the P.B ratio the maximum elasticity modulus increased.

Table 6.6 Experimental result of dynamic triaxial test

Test number	D×H (cm)	P.B (%)	Curing time	W (Kg)	ɣ	Emax (Mpa)
7.1	4.95×9.9	3	7	302	1.58	183
1.2	4.48×9.95	5	1	312.9	1.99	83.46
7.2	5×10	5	7	321.03	1.63	245
1.3	5×10	10	1	343.98	1.75	230
7.3	4.9×9.95	10	7	337.4	1.79	362

Figure 6.8 and 6.9 show the modulus reduction and damping ratio curves of different sands and also the samples in this thesis. With comparing all available result of damping ratio curves in reinforced samples with lower and upper bound of Seed and Idriss (1970) and also Toyoura sand (kokusho, 1980) curves, it has been observed that the reinforced sand with polyurethane-bitumen has higher values of damping ratio.

In figure 6.10 and 6.11 the modulus reduction and damping ratio curves are compared with damping curves of three samples of clay, it has been seen that the reinforced sand with polyurethane-bitumen has higher values of damping ratio.

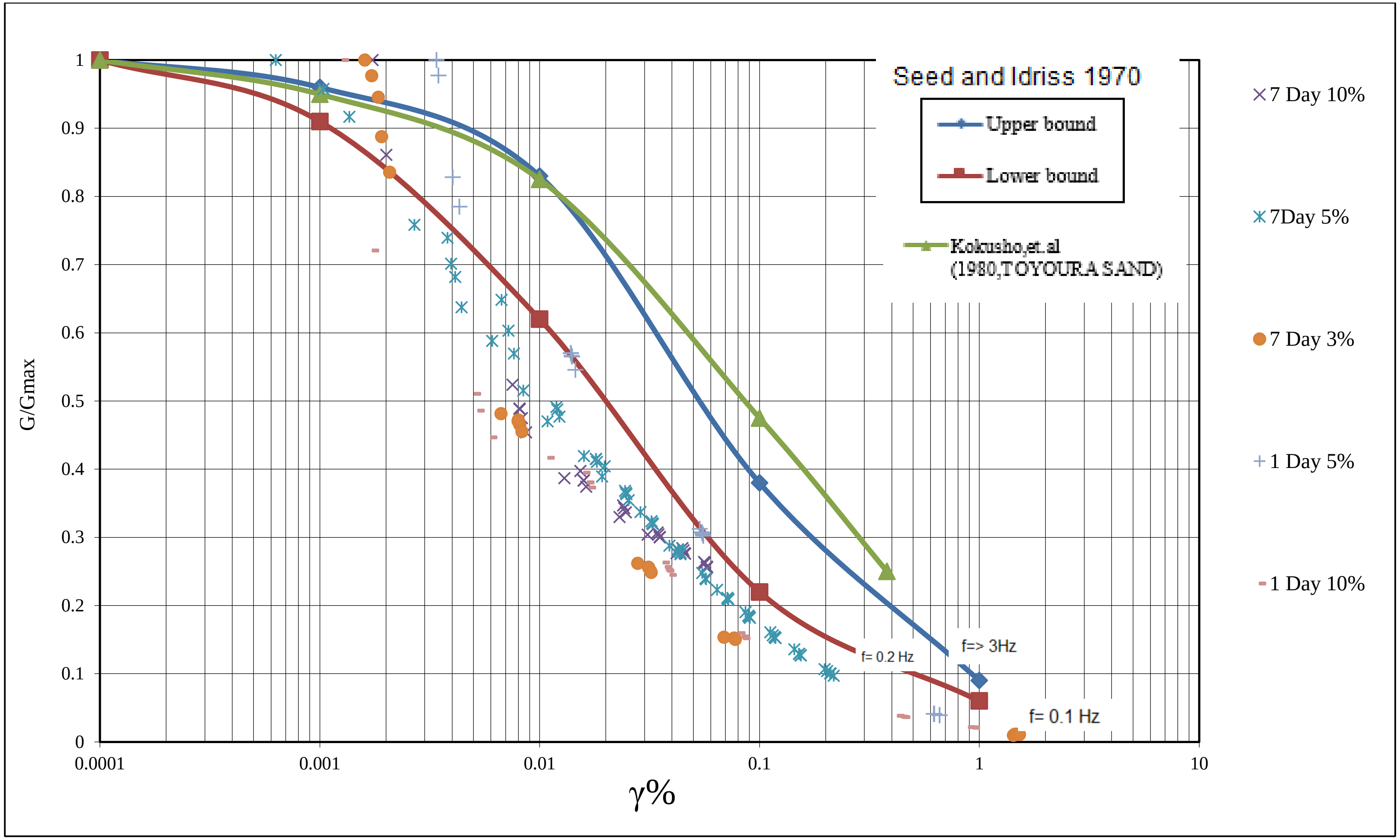

Figure 6.8 : Variation of G/Gmax and shear strain for different sands and reinforced sand with P.B. with diffrent ratio

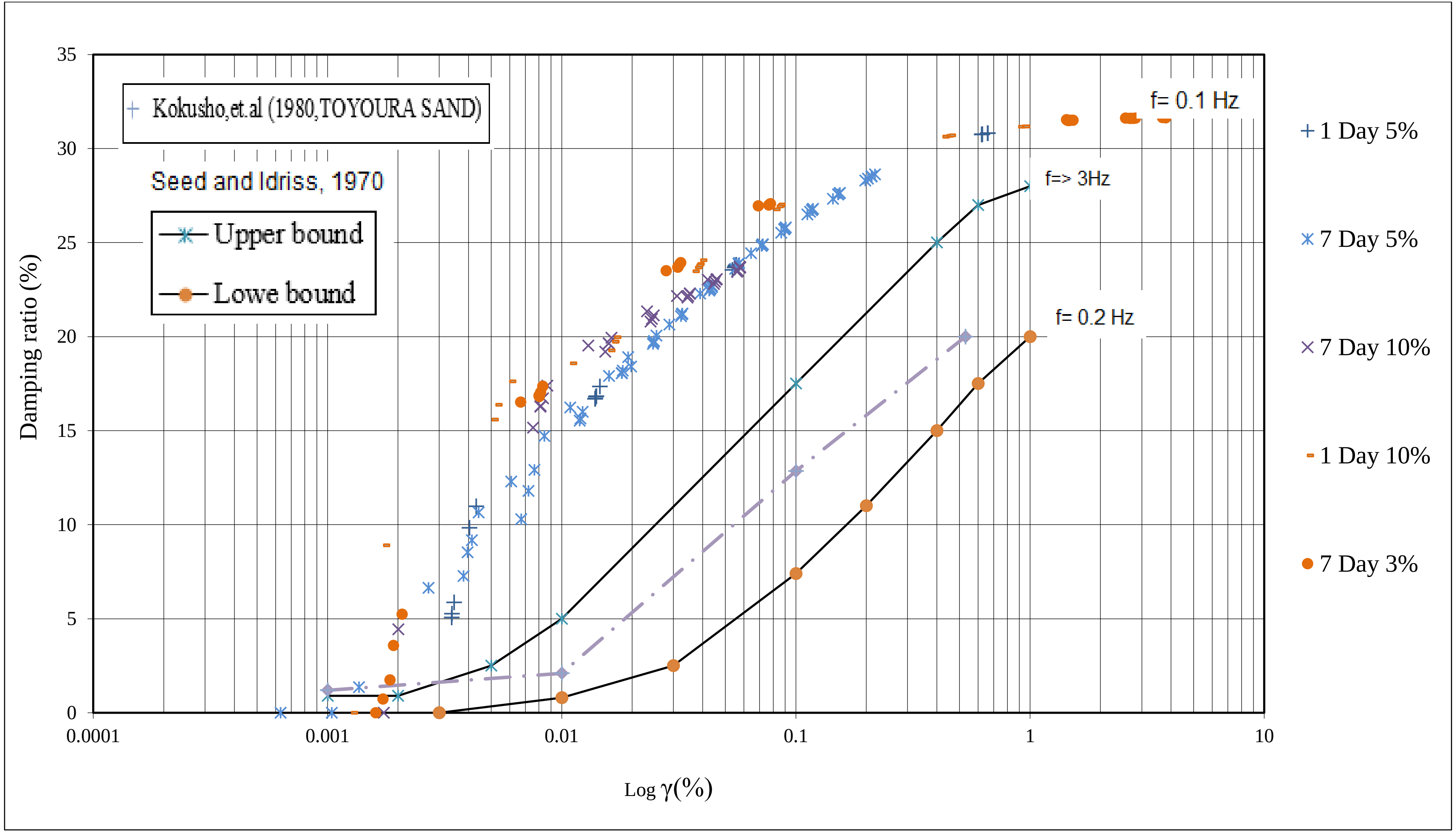

Figure 6.9 : Variation of damping ratio and shear strain for different sands and reinforced sand with P.B. with diffrent ratio

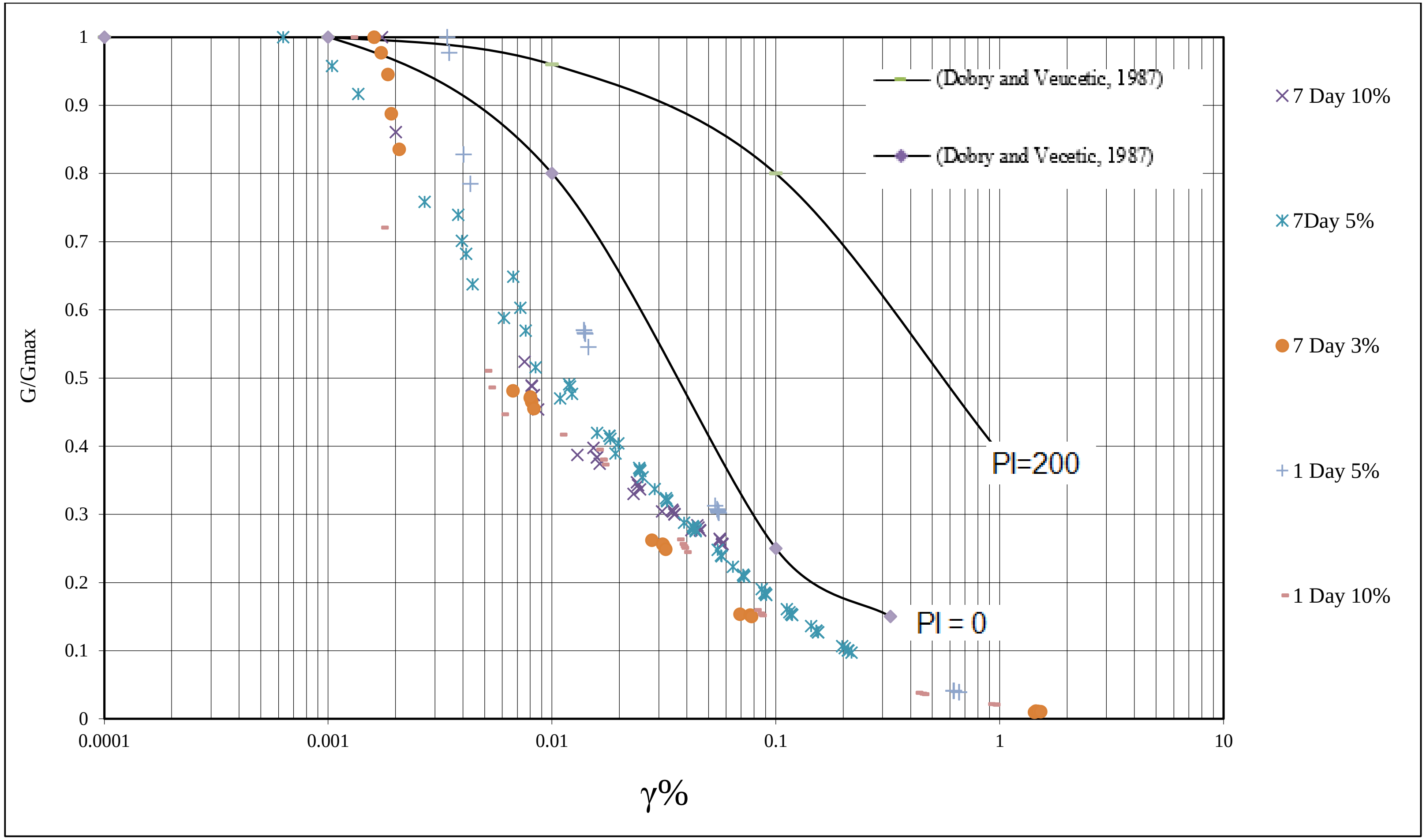

Figure 6.10 : Variation of G/Gmax and shear strain for different clays and reinforced sand with P.B. with diffrent ratio

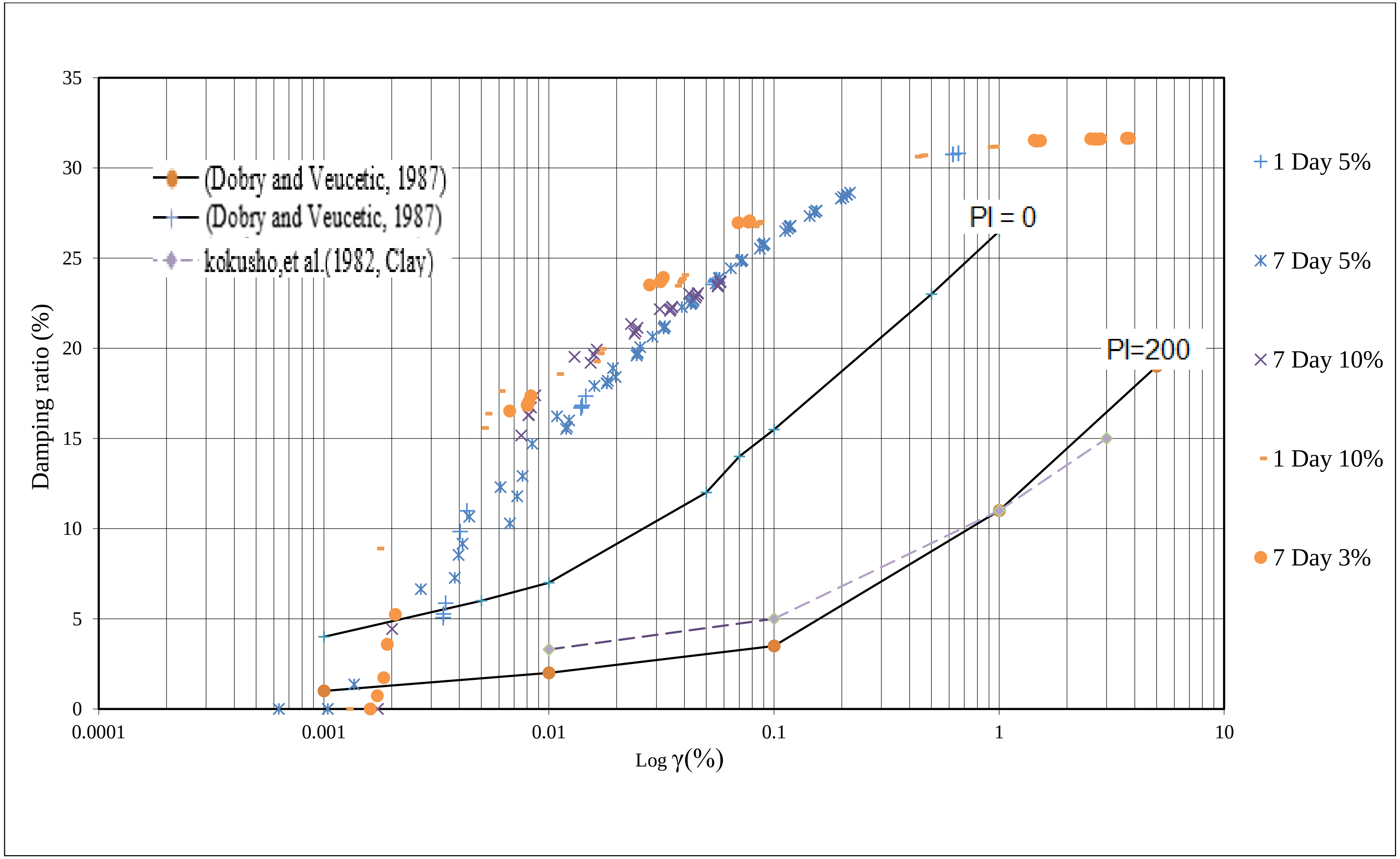

Figure 6.11 : Variation of damping ratio and shear strain for different clays and reinforced sand with P.B. with diffrent ratio

Figure 6.12shows the result of cyclic triaxial test on polyurethane-bitumen (100%). A stress-strain relation is shown in first figure, the second figure shows the cyclic stress vs. number of cycles, in the first 5 cycles amount of stress is ±0.037 and increased to ±3.2 at last 5 cycles. The elasticity value of polyurethane-bitumen is near to 0.5 Mpa.

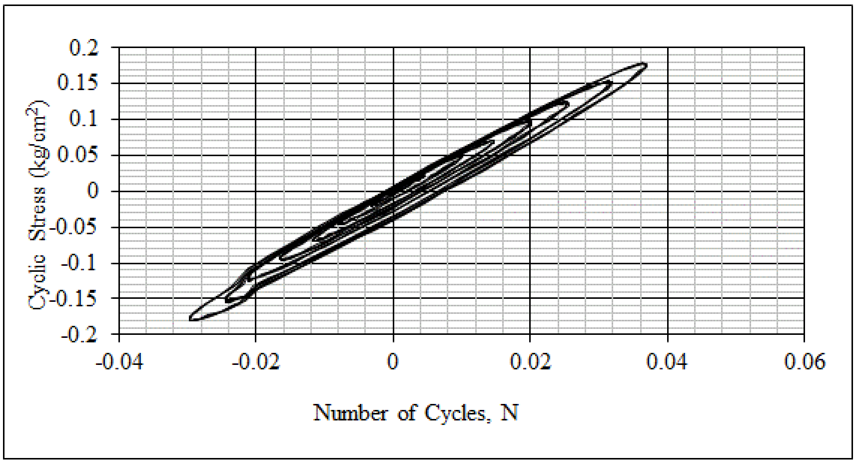

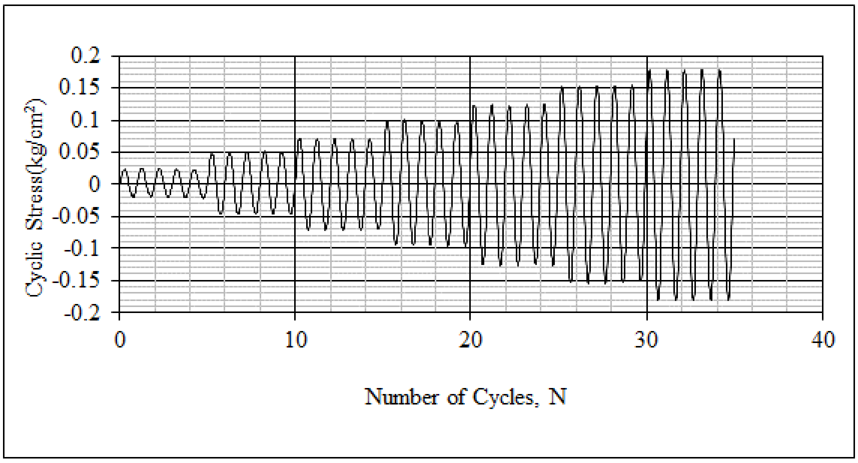

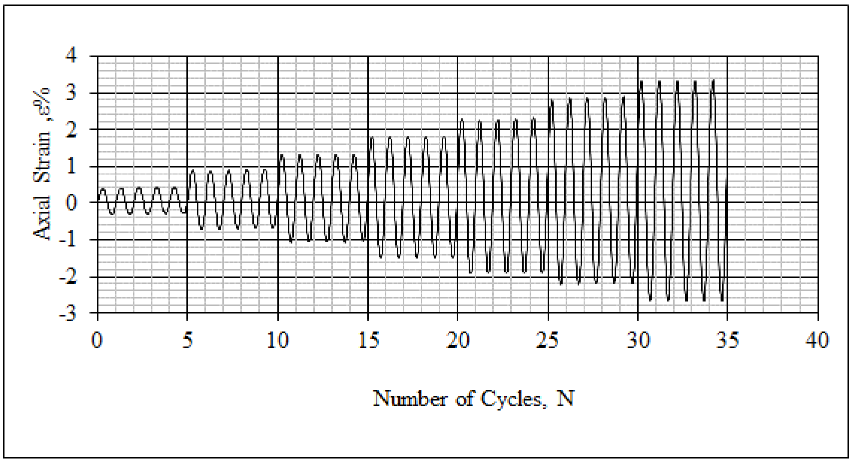

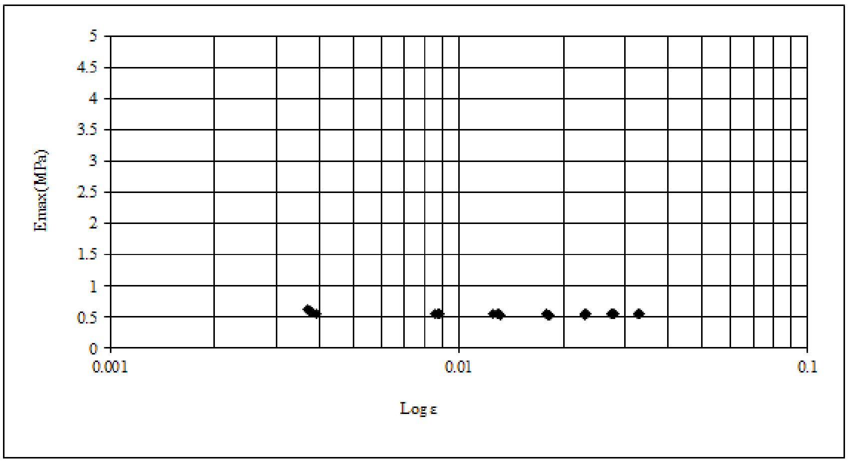

Figure 6.12 : Experimental result of Cyclic Triaxal test for Polyurethane_bitumen

6.2 Unconfined Axial Loading Test Results

To study the effect of time on stress-strain behavior of the mixture sand specimens, unconfined axial loading tests have been conducted to the samples after 1st day, 7th , 30th day and 110th,150th and 200th days. Table 6.7, shows the experimental results of unconfined axial loading test for 12 samples at different curing times.

Table 6.7 Experimental result of unconfiend axial loading test

Test Name	P.B (%)	Curing time (Day)	Date	γ_d	σ_{max}(kg/cm²)	C(Kpa)
M31	3	1	25.12.2013	1.57	0.33	16.5
M51	5	1	21.11.2013	1.64	1.197	59.85
M101	10	1	03.04.2014	1.76	1.61	80.5
M37	3	7	26.12.2014	1.51	0.895	44.75
M57	5	7	21.11.2013	1.6	1.66	83
M107	10	7	06.03.2014	1.74	2.72	136
M330	3	30	11.03.2014	1.51	1.09	54.5
M530	5	30	17.04.2014	1.6	4.04	202
M1030	10	30	11.03.2014	1.608	4.66	233
M3M3	3	110	13.08.2014	1.62	0.99	49.5
M5M5	5	150	01.09.2014	1.6	4.69	234.5
M10M7	10	200	01.09.2014	1.73	5.45	272.5

Figures 6.13, 6.14 and 6.15 show the stress-strain relationship for reinforced sand with 3%, 5% and 10% at different curing times. The axial stress of sample increases with increasing the ratio of P.B and also as the curing duration increases the axial stress

increased too. The sample with 10% of polyurethane-bitumen has the higher value of stress for all curing times.

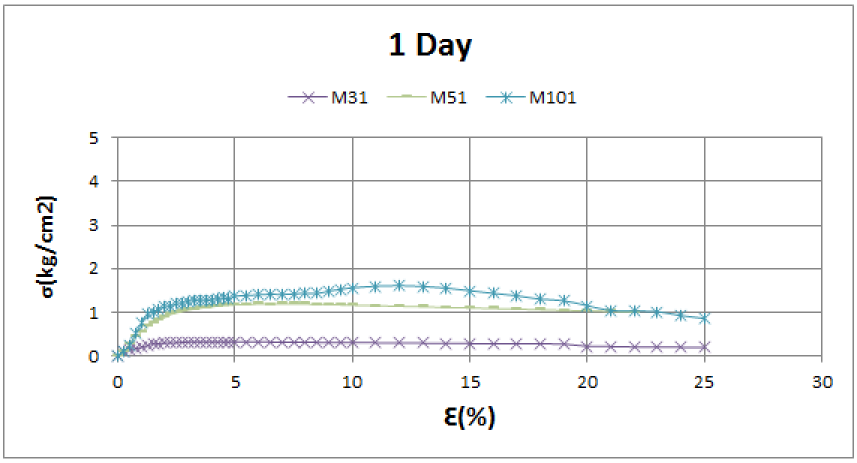

Figure 6.13 : Comparing effect of polyurethane ratio in shear stress in 1st day

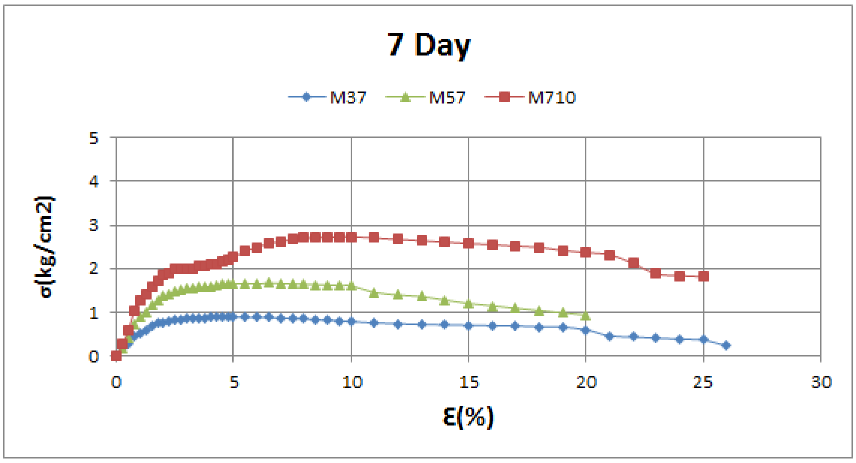

Figure 6.14 : Comparing effect of polyurethane ratio in shear stress in 7th day

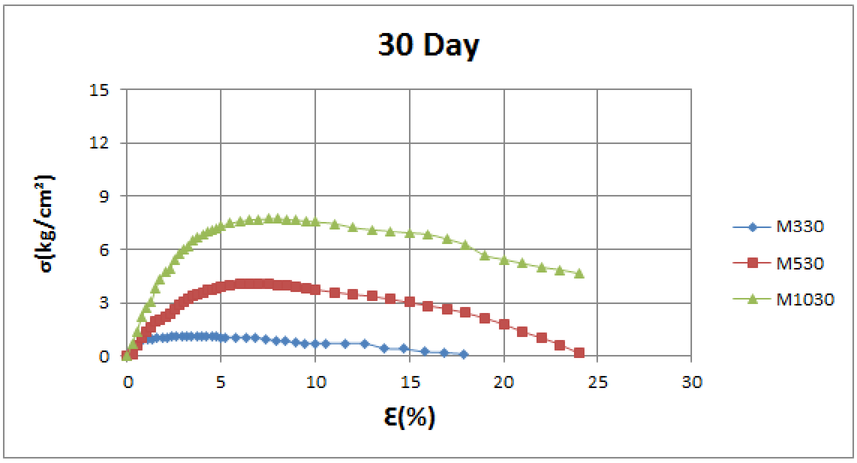

Figure 6.15 : Comparing effect of polyurethane ratio in shear stress in 30th day

Figure 6.16, shows the stress-strain relationship for reinforced sand with 3% at 30th day and 110thday, the peak value of axial stress in both of them is near to 1 kg/cm².

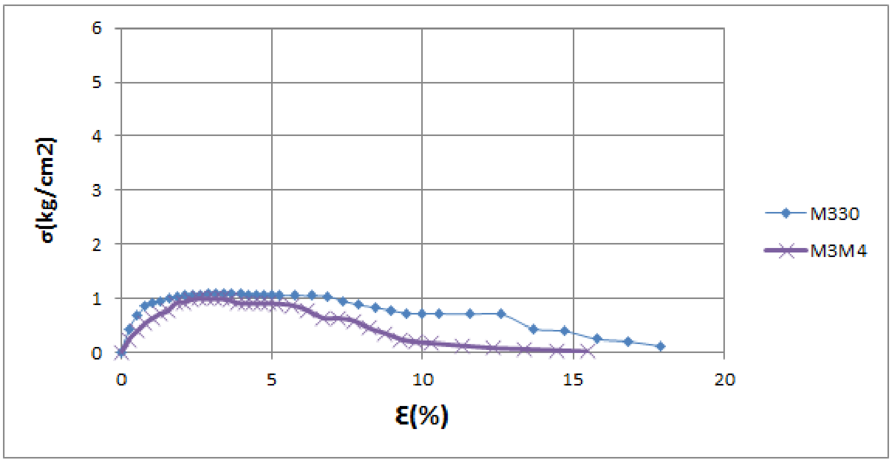

Figure 6.16 : Comparing effect of time in shear stress in 30th day and 4th month for 3% polyurethane

Figure 6.17, shows the stress-strain relationship for reinforced sand with 5% at 30th day and 150th day.

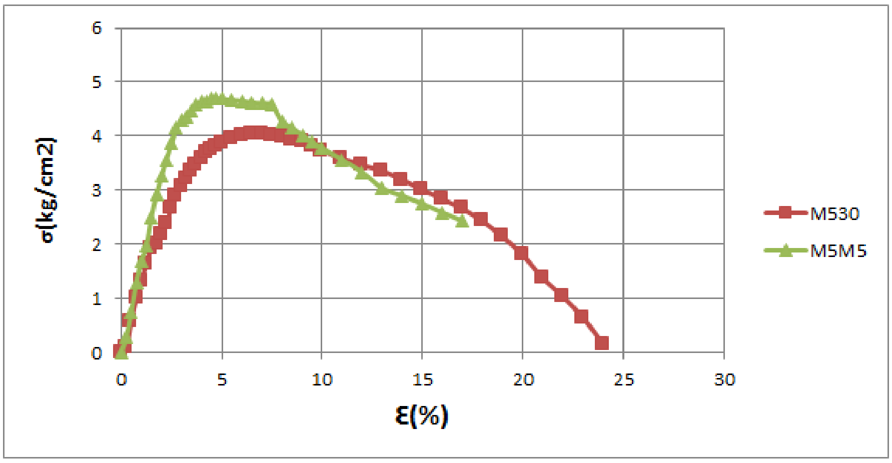

Figure 6.17 : Comparing effect of time in shear stress in 30th day and 5th month for 5% polyurethane

Figure 6.18, shows the stress-strain relationship for reinforced sand with10% at 30th day and 200th day. The peak value of axial stress of sample with 200th day curing time is higher than the sample with 30th day curing time.

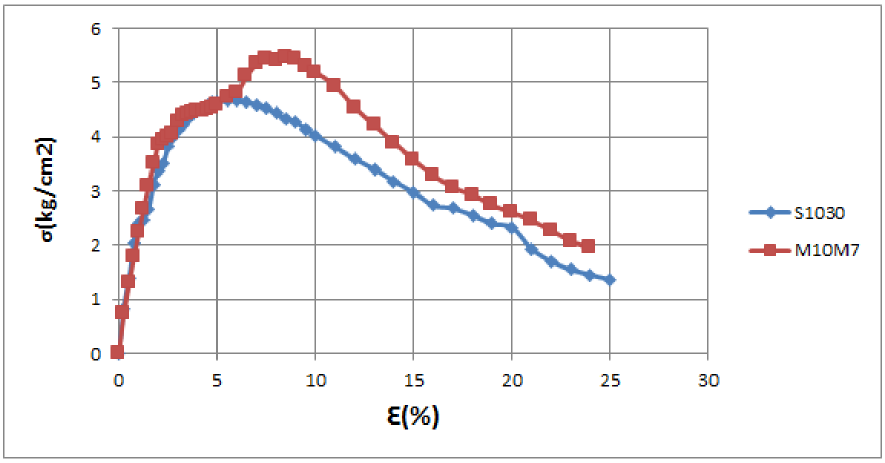

Figure 6.18 : Comparing effect of time in shear stress in 30th day and 7th month for 10% polyurethane

The samples prepared in two different sizes (5cm×10cm and 10cm×20cm) to study the effect of size on axial stress, the unconfined test conducted to samples with 3% and 5% of P.B at first day, as it clear from figure 6.19 and 6.20, there isn't any effect in peak value and also there isn't any significant effect on the stress-strain relation of the reinforced sample.

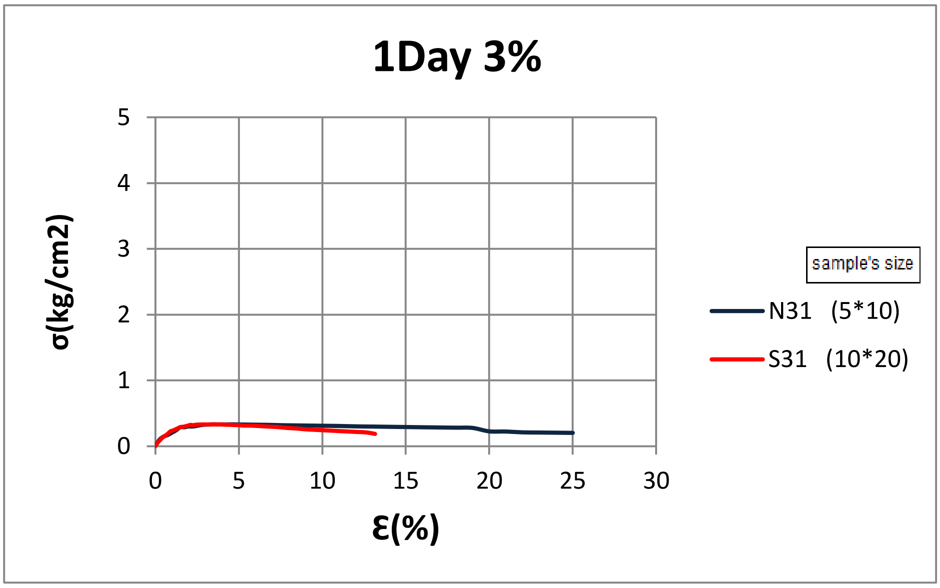

Figure 6.19 : Comparing effect of sample's size in shear stress in first day of curing time for 3% P.B

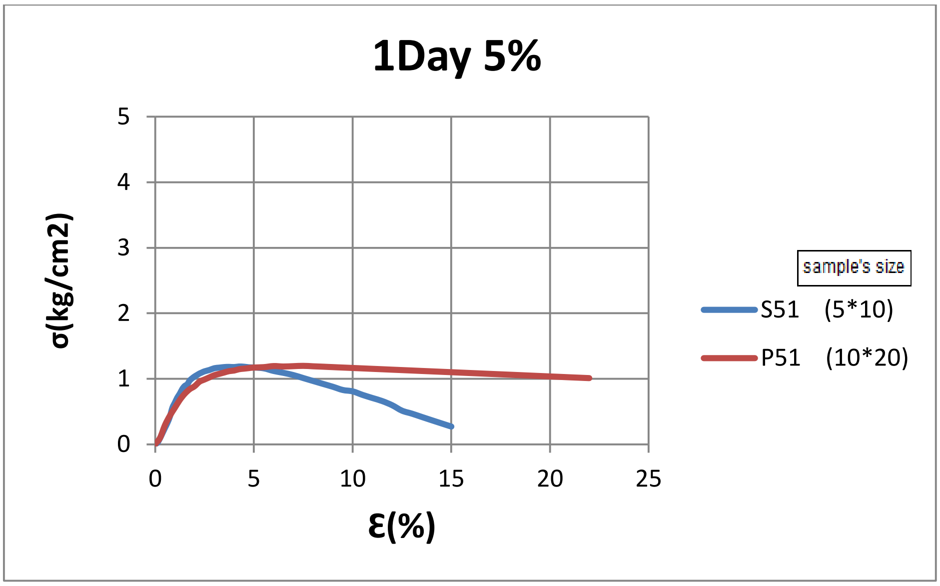

Figure 6.20 : Comparing effect of sample's size in shear stress in first day of curing time for 5% P.B

The axial strain versus curing time for 12 samples with different curing time and different proportion of P.B ratio are plotted in figure 6.21. There is an improvement in the peak strength, the polyurethane ratio have a significant effect on axial stress, the value of axial stress increase from 0.33 kg/cm²(first day of sample with 3% P.B) to 1.69 kg/cm²(first day of sample with 10% of P.B). The figure reveals that time have an important effect too, with increasing the curing time the strength increased.

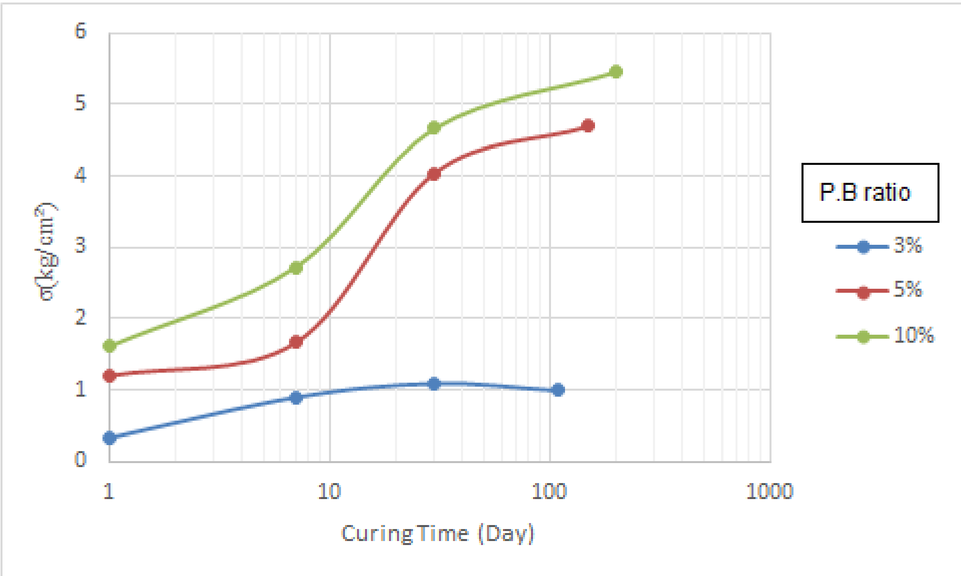

Figure 6.21 : effect of time in axial stress

Figure 6.22 shows cohesion intercept of reinforced samples, this figure clearly presents the effect of polyurethane-bitumen ratio and curing time on samples, with increasing the P.B ratio the cohesion intercept increase and also the samples with higher curing time have the higher cohesion intercept.

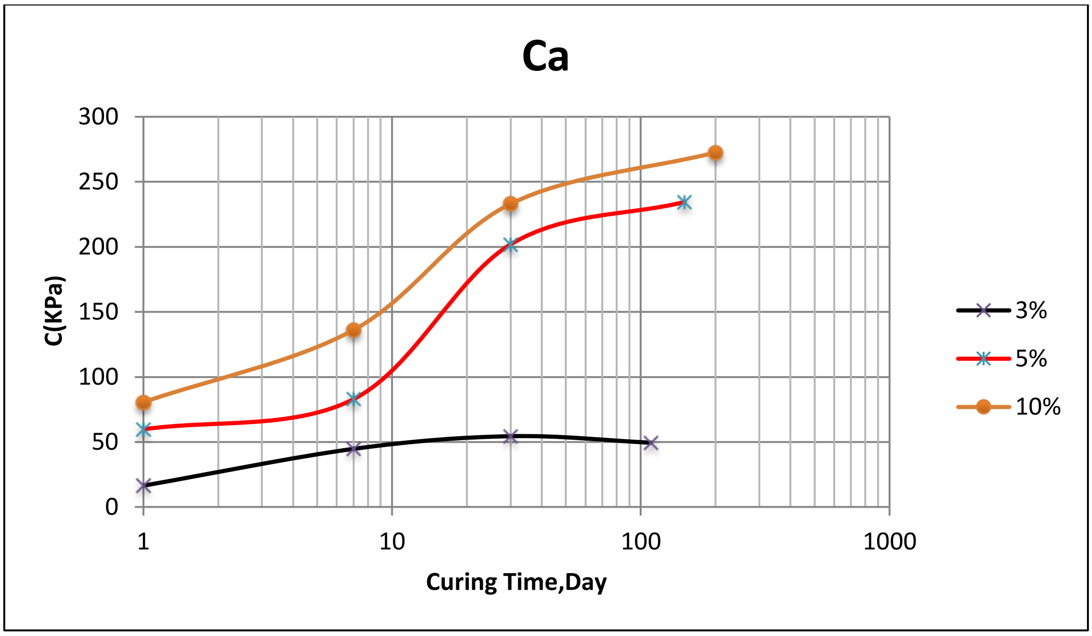

Figure 6.22 : Cohesion intercept of reinforced sand samples with different P.B. ratio obtained from unconfined axial test

6.3 Triaxial Test Results

At the triaxial test program, reinforced sand specimens are prepared at the 3%, 5% and 10% of P.B and tested on unsaturated condition. The specimens are subjected to deviator loading right after they are placed in the triaxial system. The unsaturated specimens are tested at the confining pressure of 1 kg/cm^2, 2kg/cm² and 3kg/cm². The results are shown in table 6.8. These results demonstrate that undrained strength of sand have been improved by increasing the polyurethane ratio, and also the P.B inclusion improved the axial stress, friction angles and the effective stress cohesion intercepts significantly.

Table 6.8 Experimental Result of Trixial Loading Test

sample name	P.B (%)	Confining Pressure(kg/cm²)	Curing time(Day)	W (Kg)	ɣ	σmax (kg/cm2)	Cu	φ(˚)
P311	3	100	1	299.6	1.5268	1.486178	0	26.5
P312	3	200	1	311.2	1.5860	3.0888002		
P313	3	300	1	315.8	1.6092	4.6429849		
P371	3	100	7	316.3	1.6117	2.8248861	0.5	27.5
P372	3	200	7	320.5	1.6332	4.2103539		
P373	3	300	7	320.5	1.6332	5.7081014		
P37301	3	100	30	311.5	1.5872	3.2852724	0.7	22.5
P37302	3	200	30	312.7	1.6015	4.3761618		
P37303	3	300	30	313.5	1.5974	5.4645583		
P511	5	100	1	325.4	1.6582	2.0842833	0.2	29.5
P512	5	200	1	327.4	1.6685	3.7706413		
P513	5	300	1	330.2	1.6827	5.4108873		
P571	5	100	7	328.1	1.6721	5.0204220	1	28.9
P572	5	200	7	332.3	1.6934	6.7005633		
P573	5	300	7	337.9	1.7220	8.6759185		
P5301	5	100	30	321.2	1.6369	5.6913413	1.4	24.5
P5302	5	200	30	323.3	1.6476	7.0285577		
P5303	5	300	30	324.4	1.6529	8.7513910		
P1011	10	100	1	325.5	1.6609	2.9771397	0.3	31.5
P1012	10	200	1	328.9	1.6784	4.9243817		
P1013	10	300	1	330.4	1.6858	7.4237651		
p1071	10	100	7	334.0	1.7023	7.2206070	1.2	33.5
P1072	10	200	7	335.7	1.7110	8.7670073		
P1073	10	300	7	337.6	1.7202	11.871268		
P10301	10	100	30	343.6	1.7509	9.7035365	2.5	24.6
P10302	10	200	30	343.1	1.7486	10.293780		
P10303	10	300	30	346.5	1.7659	11.914105		

Figure 6.23 shows the stress-strain response of reinforced sand specimens including 3% of P.B. The test conducted at first day. The Mohr- Coulomb circles for the reinforced sand is shown in figure 6.24. While the cohesion intercept is calculated as zero, the shear strength angle is calculated as 26.5°.

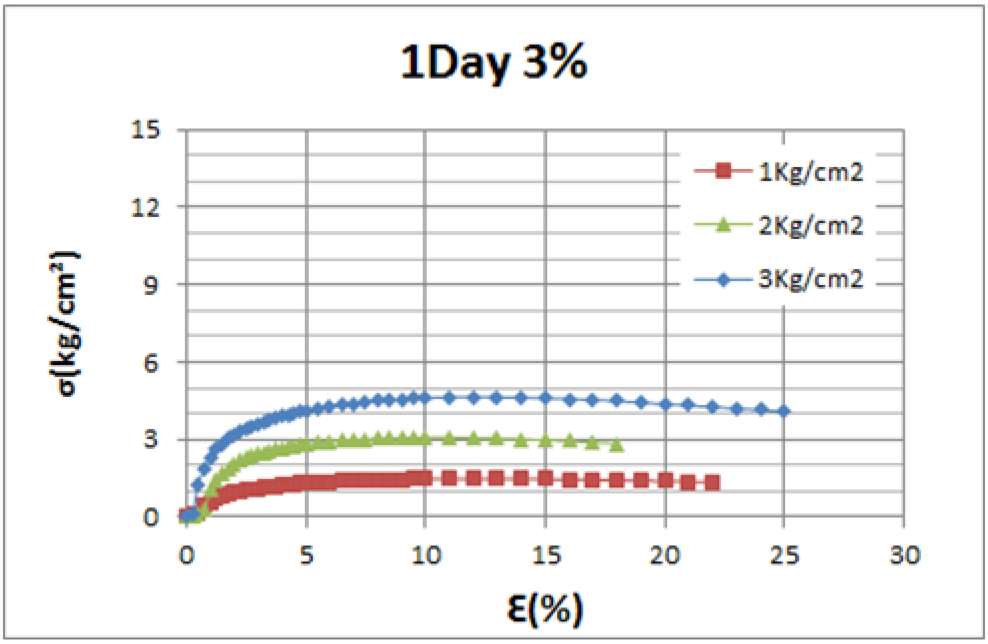

Figure 6.23 : Stress-Strain response of specimens reinforced with 3% of polyurethane at different confining stresses at 1st day

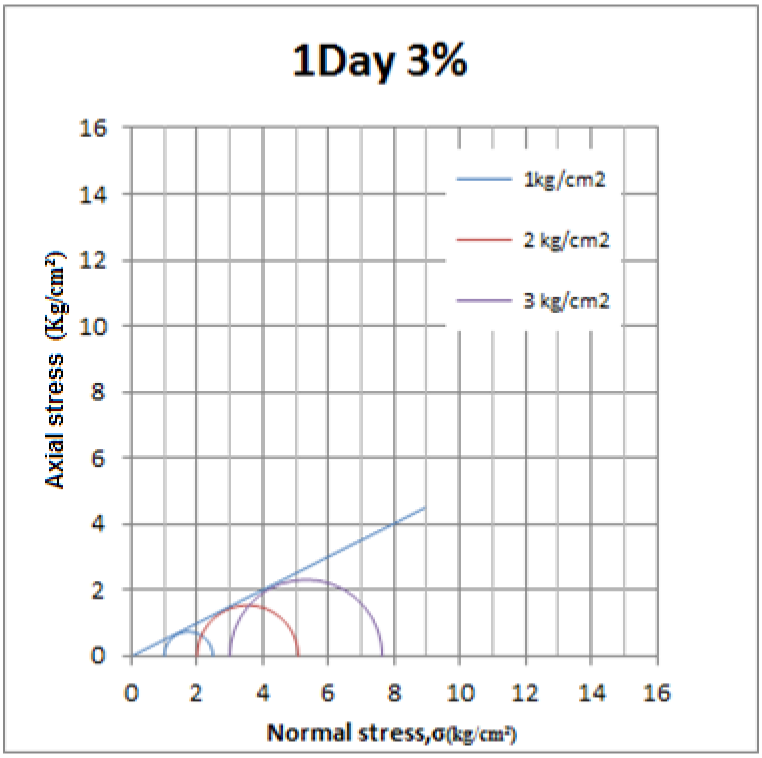

Figure 6.24 : Axial stress-Normal stress graph for sample with 3% of P.B at 1st day

Figure 6.25vshows the stress-strain response of reinforced sand specimens including 5% of P.B at the first day. Mohr- Coulomb circles for the reinforced sand is shown in figure 6.26. While the cohesion intercept is calculated as 0.2 kg/cm², the failure envelope is calculated as 29.5°.

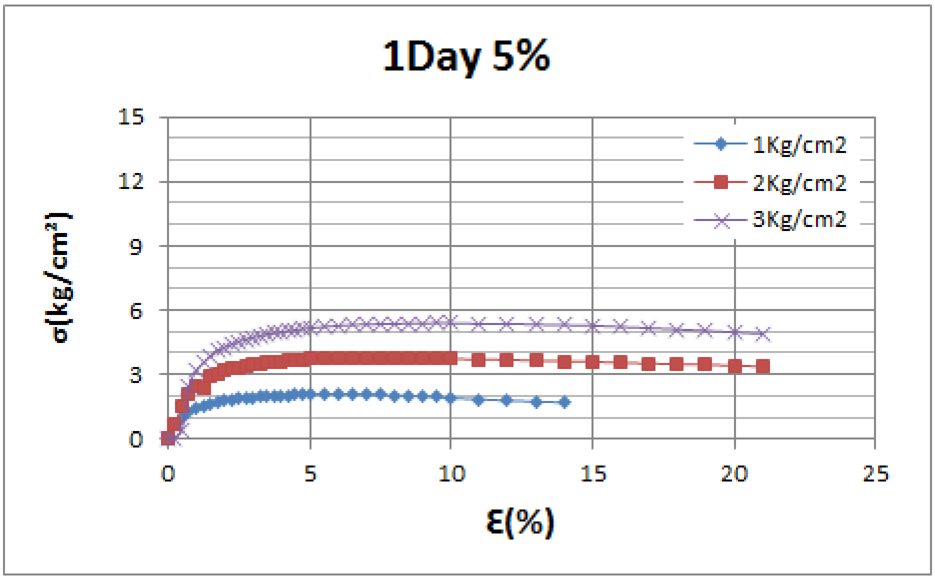

Figure 6.25 : Stress-Strain response of sample with 5% of P.B at different confining stresses at 1st day

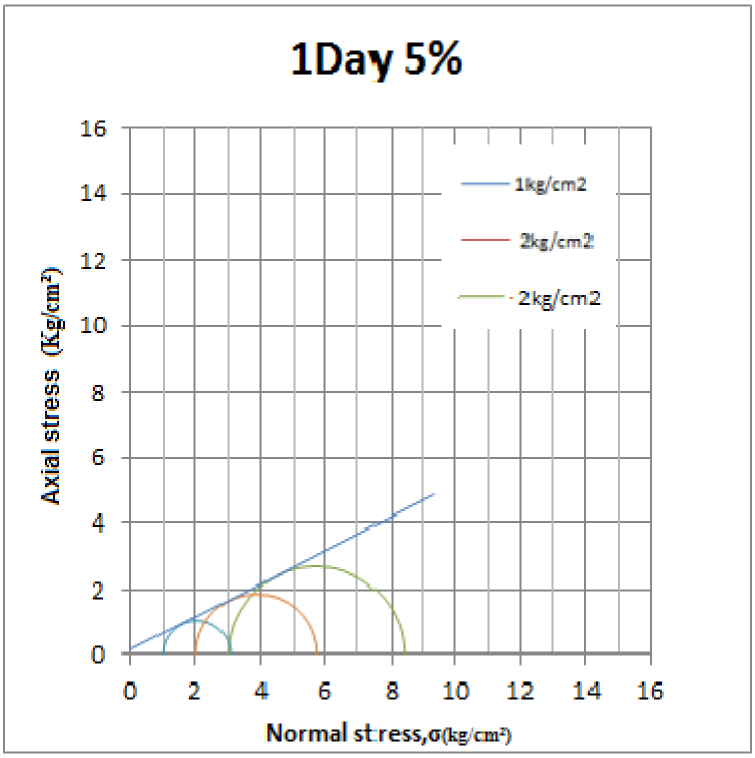

Figure 6.26 : Axial stress-Normal stress graph for sample with 5% of P.B at 1st day

Figure 6.27 shows the stress-strain response of reinforced sand specimens including 10% of P.B at the first day. The Mohr- Coulomb circles for the reinforced sand is shown in figure 6.28. While the cohesion intercept is calculated as 0.3 kg/cm², the failure envelope is calculated as 31.5°.

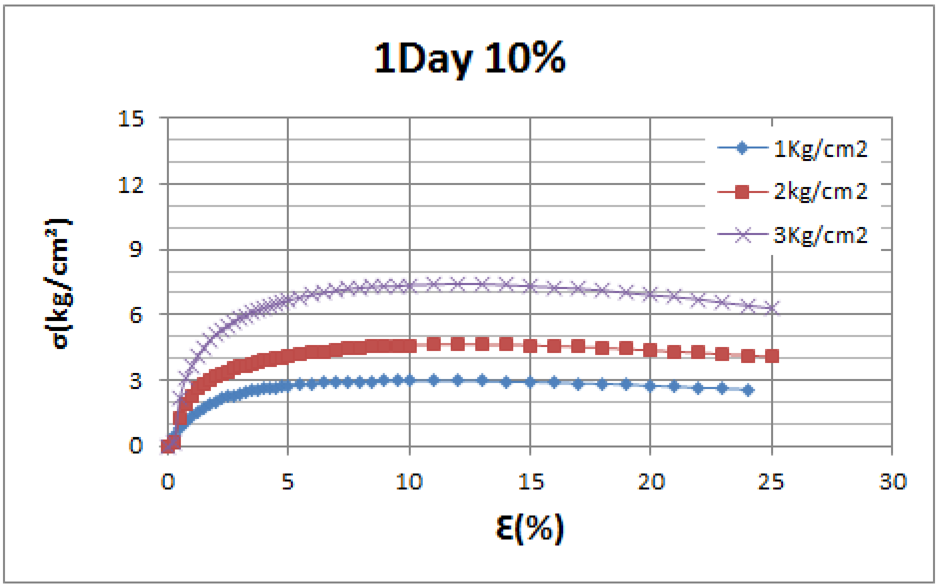

Figure 6.27 : Stress-Strain response of specimens reinforced with 10% of polyurethane at different confining stresses at 1st Day

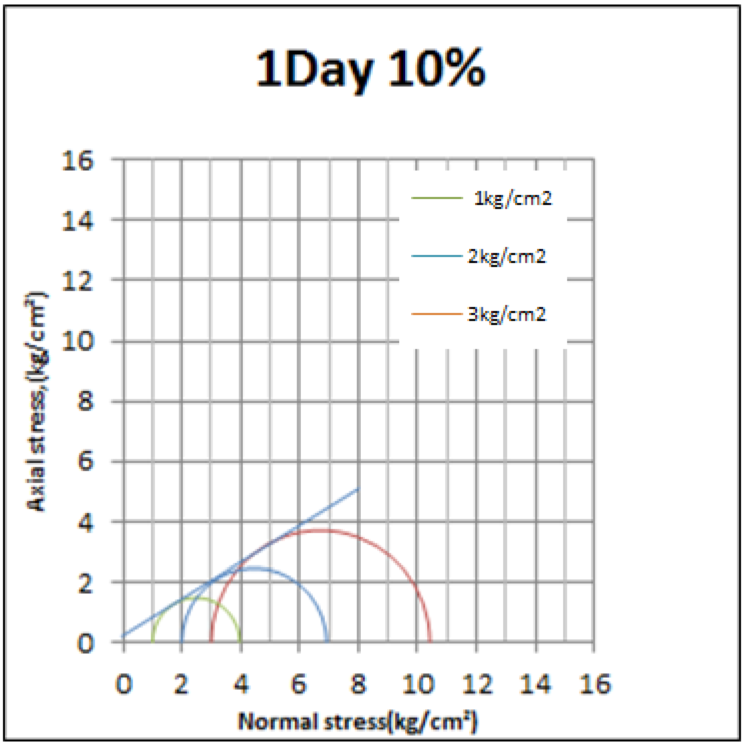

Figure 6.28 : Axial stress-Normal stress graph for sample with 3% of P.B at 1st day

Figure 6.29 shows the stress-strain response of reinforced sand specimens including 3% of P.B at the 7th day. The Mohr -Coulomb circles for the reinforced sand is shown in Figure 6.30. While the cohesion intercept is calculated as 0.5 kg/cm², the failure envelope is calculated as 27.5°.

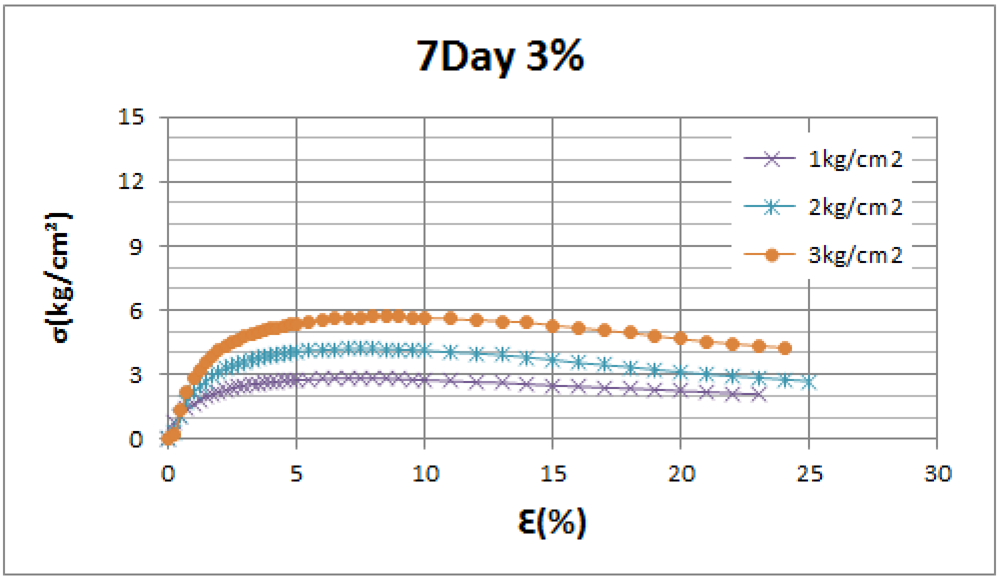

Figure 6.29 : Stress-Strain response of specimens reinforced with 3% of polyurethane at different confining stresses at 7th day

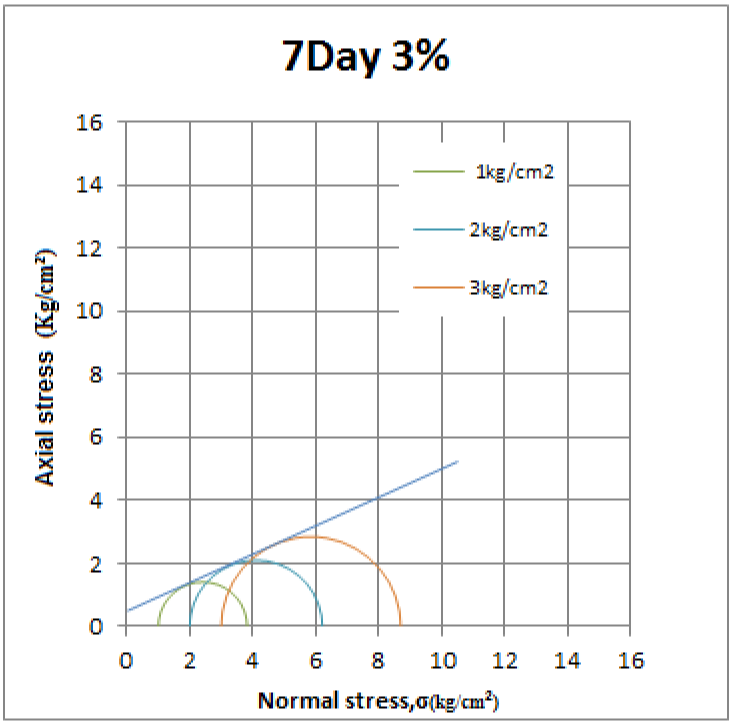

Figure 6.30 : Axial stress-Normal stress graph for sample with 3% of P.B at 7th day

Figure 6.31 shows the stress-strain response of reinforced sand specimens including 5% of P.B at the 7th day. The Mohr- Coulomb circles for the reinforced sand is shown in figure 6.32. While the cohesion intercept is calculated as 1 kg/cm², the failure envelope is calculated as 28.9°.

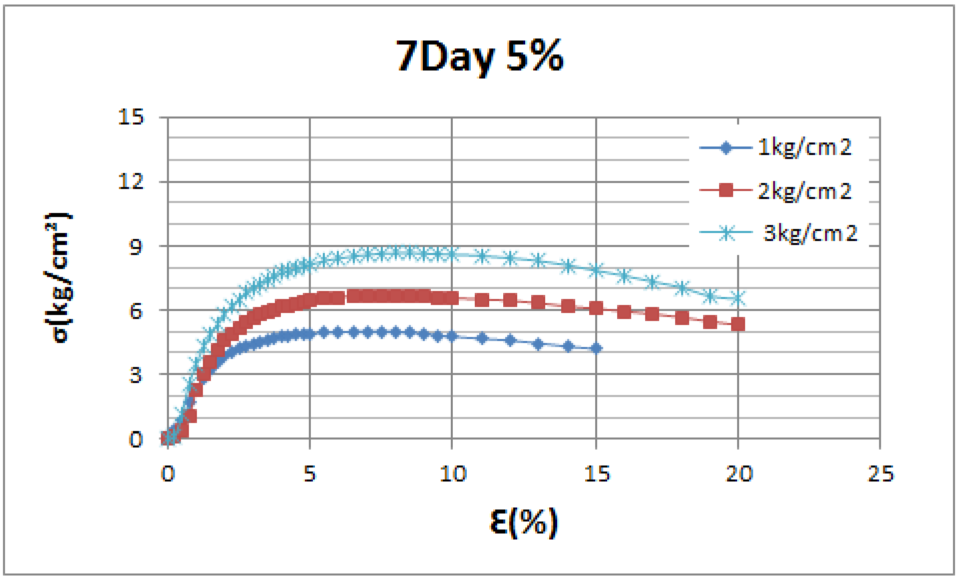

Figure 6.31 : Stress-Strain response of specimens reinforced with 5% of polyurethane at different confining stresses at 7th day

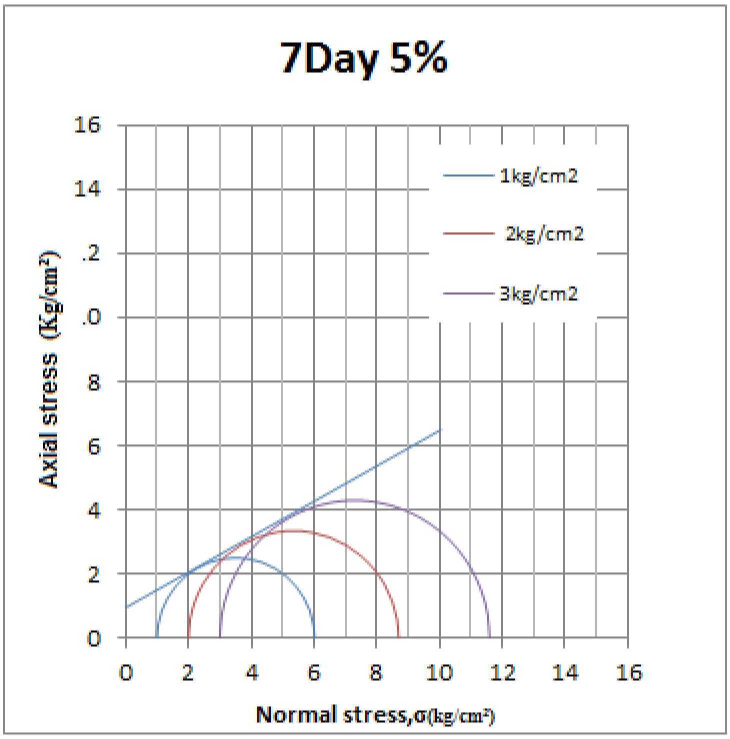

Figure 6.32 : Axial stress-Normal stress graph for sample with 5% of P.B at 7th day

Figure 6.33 shows the stress-strain response of reinforced sand specimens including 10% of P.B at the 7th day. The Mohr-Coulomb circles for the reinforced sand is shown in Figure 6.34. While the cohesion intercept is calculated as 1.2 kg/cm², the failure envelope is calculated as 33.5°.

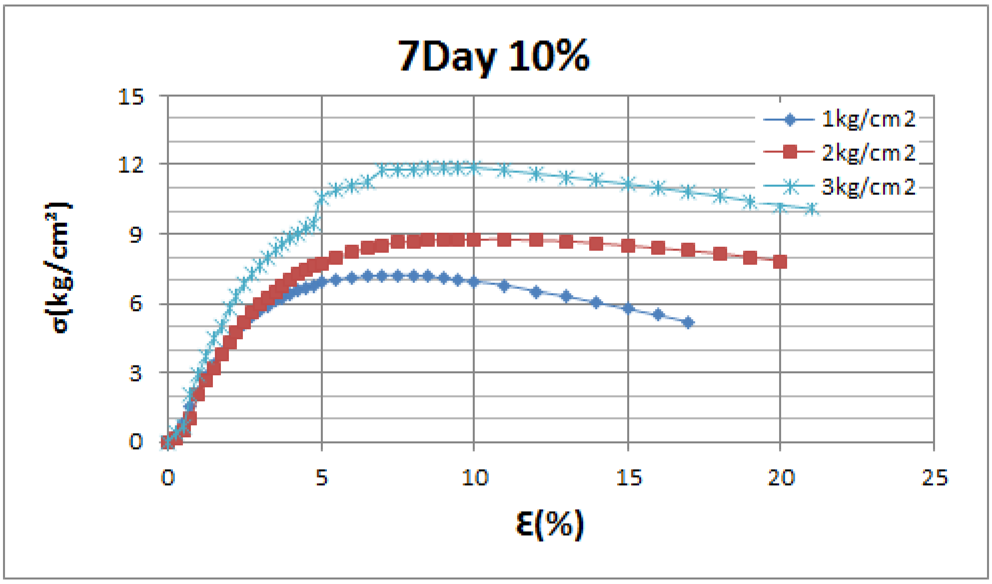

Figure 6.33 : Stress-Strain response of specimens reinforced with 10% of polyurethane at different confining stresses at 7th day

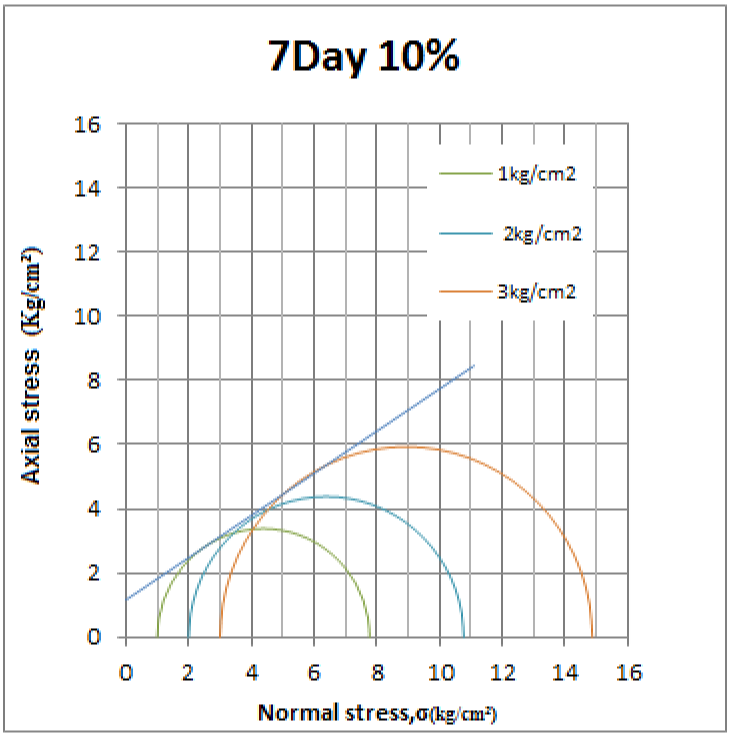

Figure 6.34 : Axial stress-Normal stress graph for sample with 10% of P.B at 7th day

Figure 6.35 shows the stress-strain response of reinforced sand specimens including 3% of P.B at the 30th day. The Mohr- Coulomb circles for the reinforced sand is shown in figure 6.36. While the cohesion intercept is calculated as 0.7 kg/cm², the failure envelope is calculated as 22.5°.

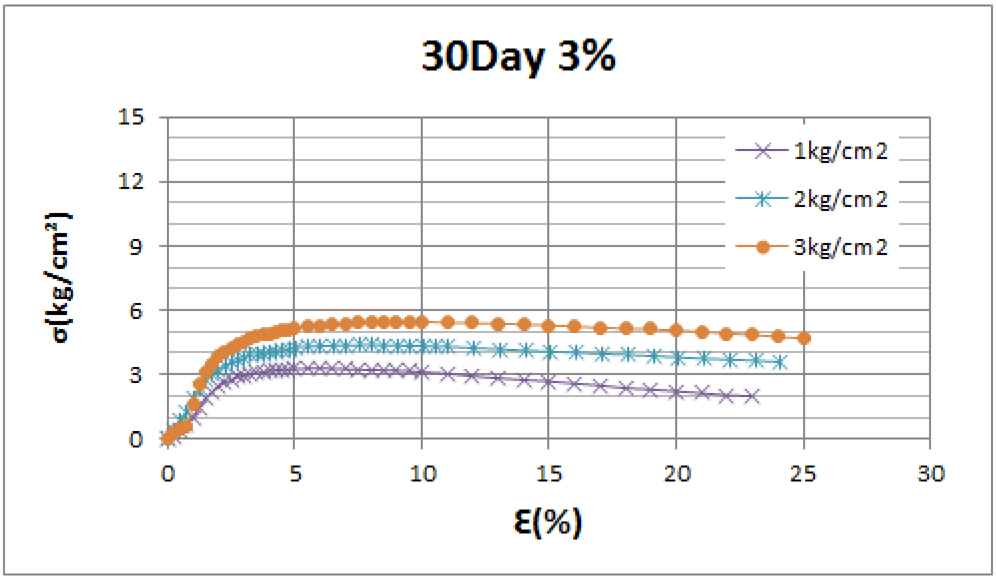

Figure 6.35 : Stress-Strain response of specimens reinforced with 3% of polyurethane at different confining stresses at 30th day

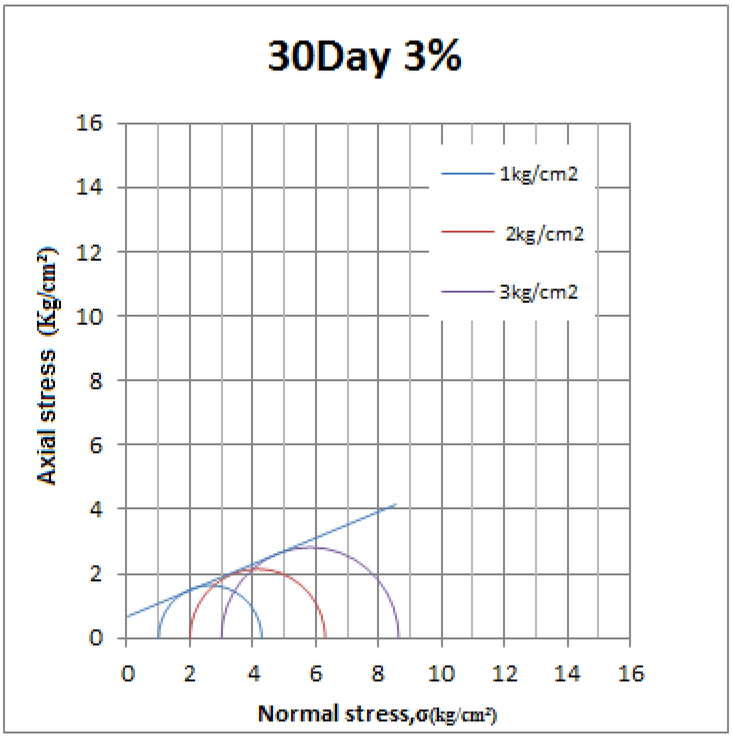

Figure 6.36 : Axial stress-Normal stress graph for sample with 3% of P.B at 30th day

Figure 6.37 shows the stress-strain response of reinforced sand specimens including 5% of P.B at the 30th day. The Mohr- Coulomb circles for the reinforced sand is shown in figure 6.38. While the cohesion intercept is calculated as 1.4 kg/cm², the failure envelope angle is calculated as 24.5°.

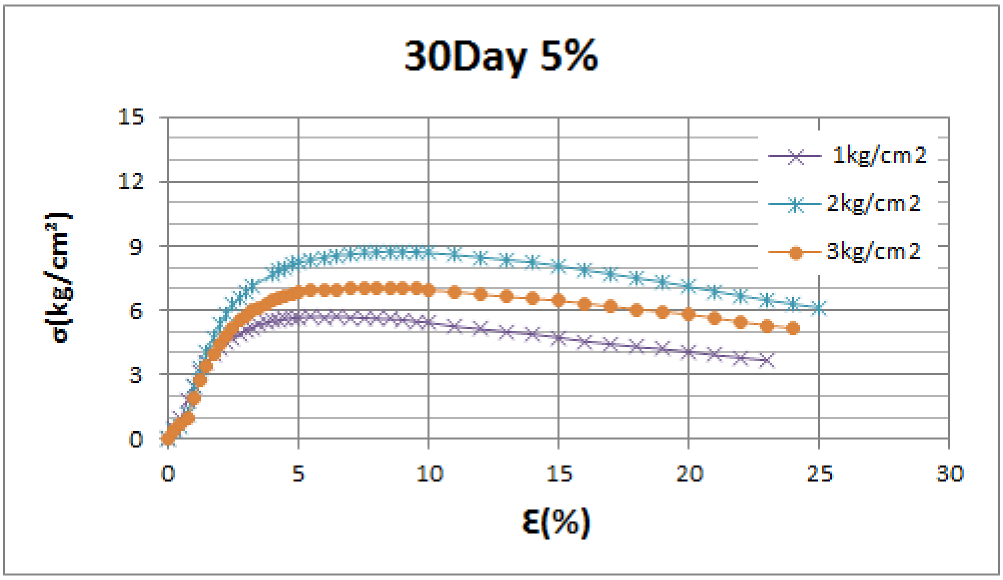

Figure 6.37 : Stress-Strain response of specimens reinforced with 5% of polyurethane at different confining stresses at 30th day

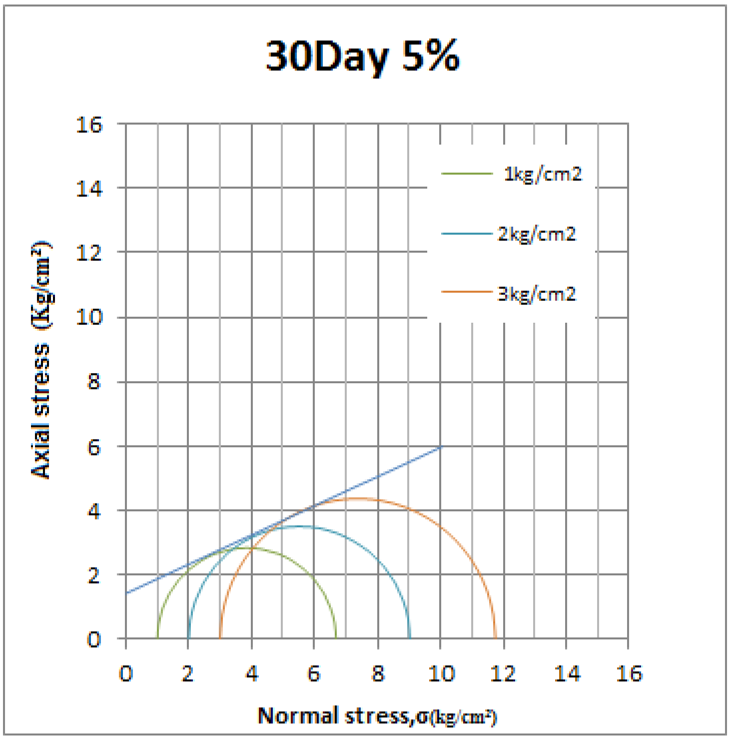

Figure 6.38 : Axial stress-Normal stress graph for sample with 5% of P.B at 30th day

Figure 6.39 shows the stress-strain response of reinforced sand specimens including 10% of P.B at the 30th day. The Mohr- Coulomb circles for the reinforced sand is shown in figure 6.40. While the cohesion intercept is calculated as 2.5kg/cm², the failure envelope is calculated as 24.6°.

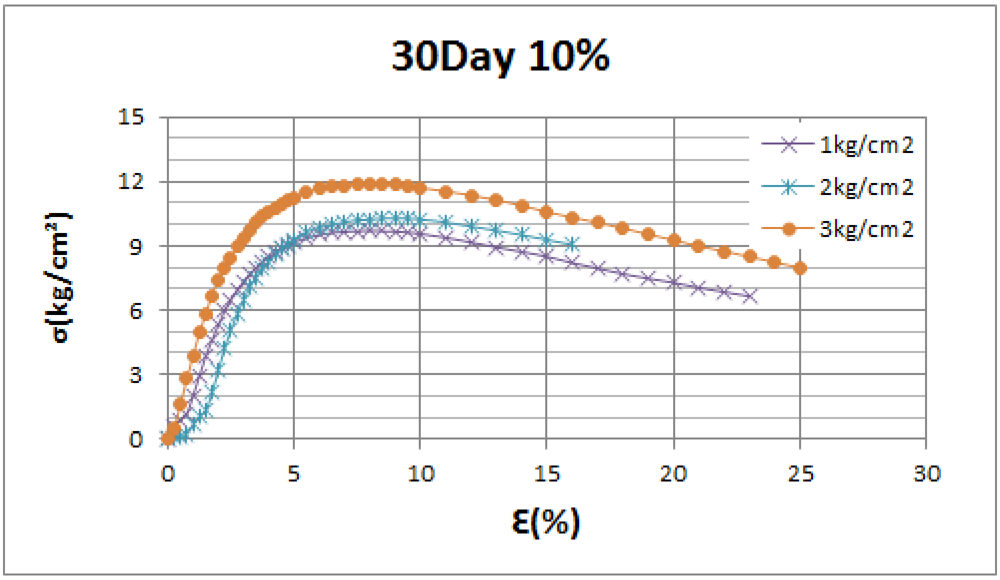

Figure 6.39 : Stress-Strain response of specimens reinforced with 10% of polyurethane at different confining stresses at 30^{th} day

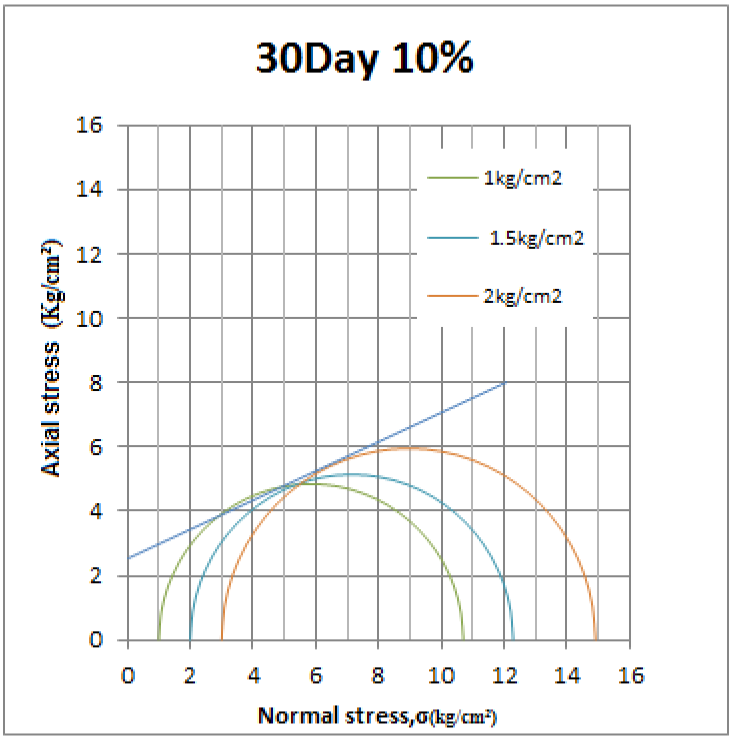

Figure 6.40 : Axial stress-Normal stress graph for sample with 10% of P.B at 30^{th} day

Figure 6.41, 6.42 and 6.43 show the maximum stress response of reinforced sand specimens including P.B contents of 3%, 5% and 10% in different curing times and different confining pressure. It can be seen that the P.B addition improved the static behavior of sand considerably. As the P.B content increased, the recorded peak value is also increased at higher curing time.

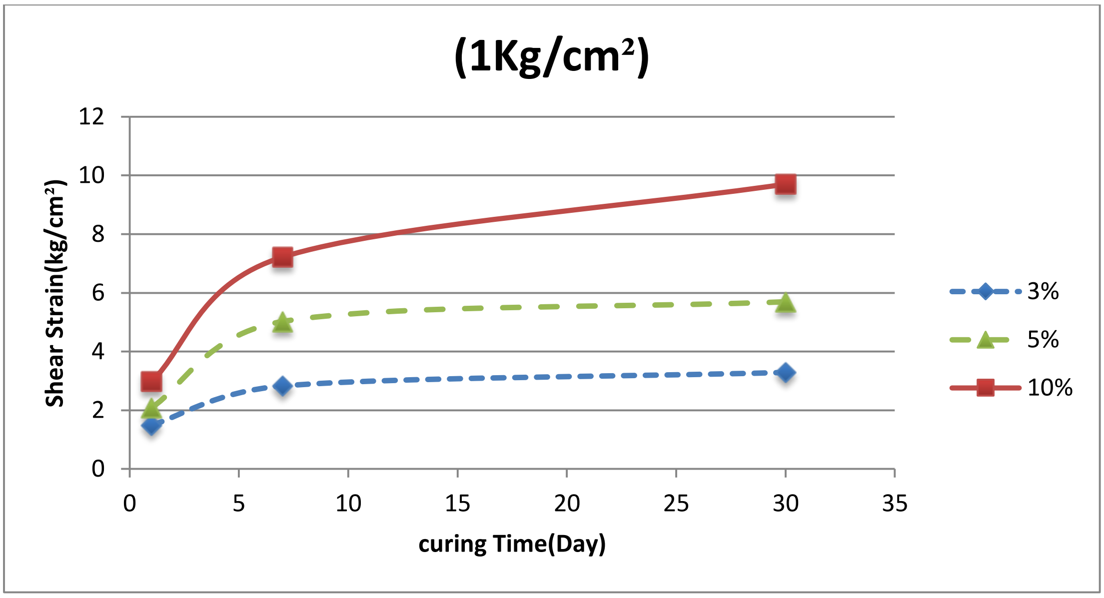

Figure 6.41 : Axial stress-Curing time response for reinforced sand samples with different P. B ratio at the normal stress of $\sigma = 1$ Kg/cm²

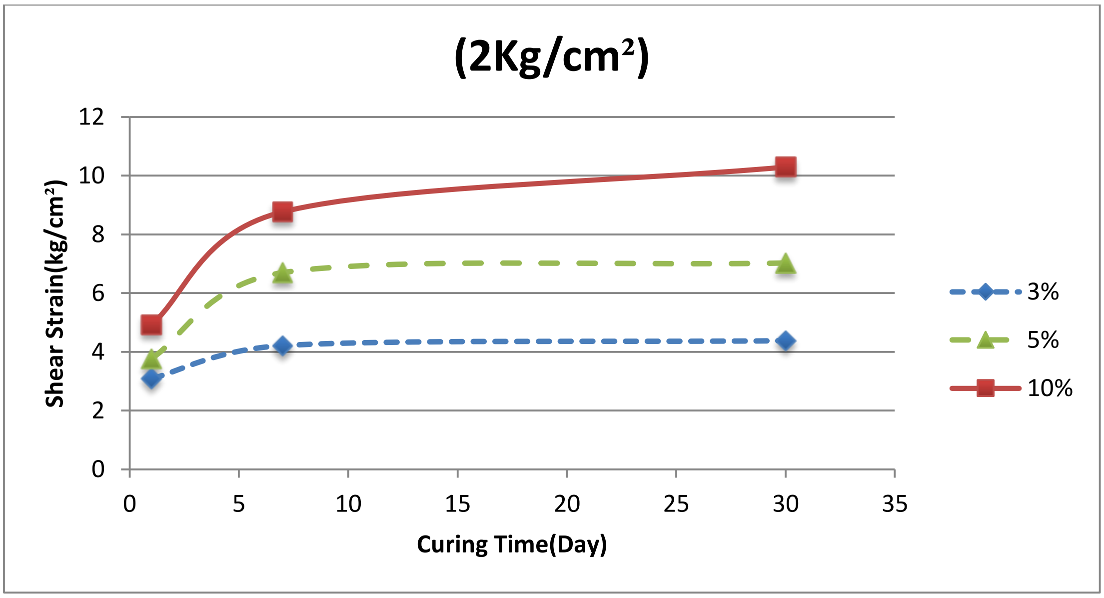

Figure 6.42 : Axial stress-Curing time response for reinforced sand samples with different P.B ratio at the normal stress of $\sigma = 2$ Kg/cm²

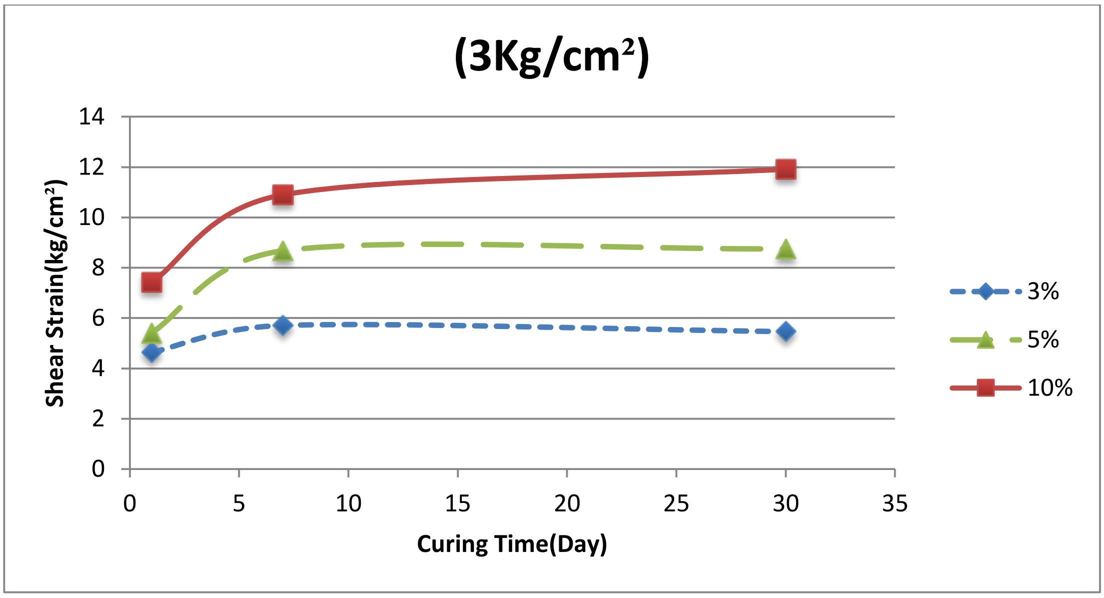

Figure 6.43 : Axial stress-Curing Time response for reinforced sand samples with different P. B ratio at the normal stress of $\sigma = 3$ Kg/cm²

Figure 6.44 shows cohesion intercept of reinforced samples, this figure clearly presents the effect of polyurethane-bitumen ratio and curing time on samples, with increasing the P.B ratio the cohesion intercept increase and also the samples with higher curing time have the higher cohesion intercept.

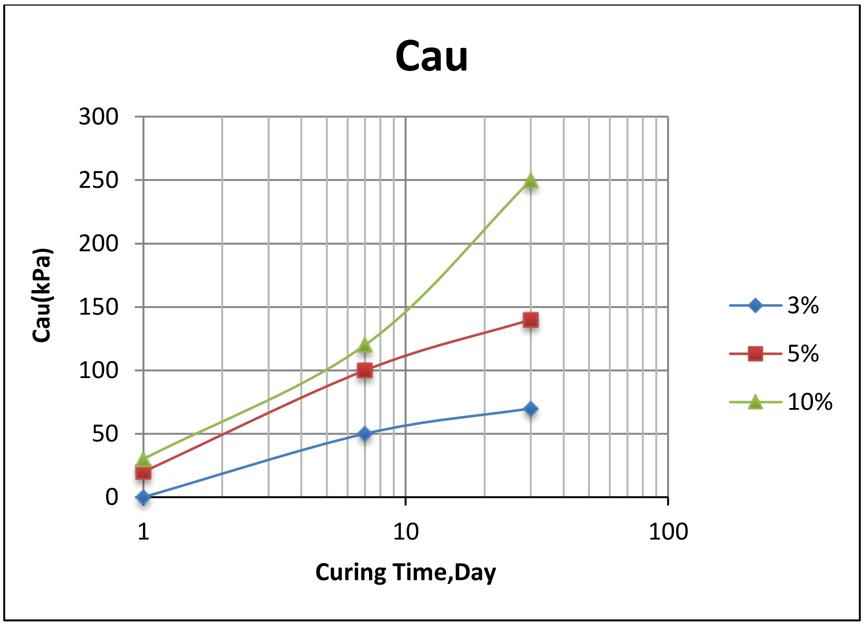

Figure 6.44 : Cohesion intercepts of reinforced sand samples with different P.B. ratio obtained from UU tests

Figure 6.45 shows failure envelope of reinforced samples with different polyurethane ratio at different curing time. With increasing the P.B ratio the failure envelope increase but samples with same P.B ratio have a smaller failure envelope in 30^{th} days than first days, and also the samples in 7^{th} days have a failure envelope near to first days.

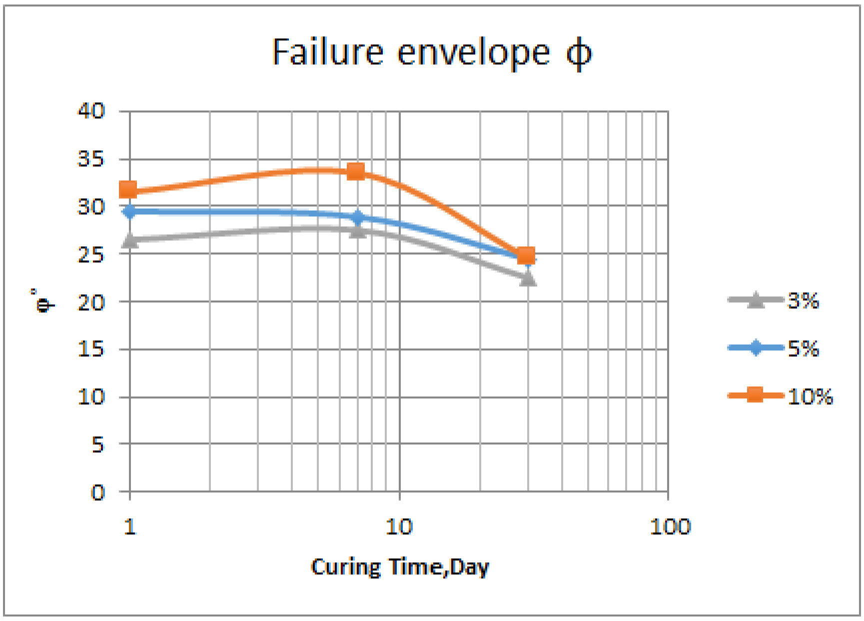

Figure 6.45 : Failure envelope of reinforced sand samples with different P.B. ratio obtained from UU test

7. CONCLUSIONS

The objective of the present thesis is soil improvement of sands against liquefaction. This study was undertaken to investigate the influence of polyurethane - bitumen percentage and curing time conditions on the sandy liquefiable soils. The effect of polyurethane-bitumen inclusion on maximum young modulus, the damping ratio, and the axial strength of sand investigated with laboratory study. Analysis of the dynamic triaxial test, static triaxial tests and unconfined axial test on reinforced specimens have discussed.

Dynamic triaxial test to measure young modulus and damping ratio of reinforced sand sampled with different amount of P.B at different curing time carried out in this thesis. The results illustrate that Emax value and damping ratio of sand increase with additional P.B and also the time have important effect on elasticity modulus, by increasing the curing time the value of elasticity modulus and damping ratio increased. The results of damping ratio compared with Toyoura sand, lower bound and upper bound of Seed and Idriss sand samples and also with some clay's samples, results demonstrate that the reinforced specimens with polyurethane-bitumen have the higher damping ratio value.

The result of unconsolidated-undrained triaxial test reveal that both the cohesion intercept and failure envelope increased when the P.B ratio increased. The combinations improve the behavior of the sand against liquefaction phenomena, but the samples with same P.B ratio have a smaller failure envelope in 30^{th} days than first days, and also the samples in 7^{th} days have a failure envelope near to first days.

Results of unconfined axial test carried out on reinforced samples at different curing time with different additional polyurethane-bitumen to the sand provided that as the ratio of polyurethane-bitumen increase the peak axial stress increased at every curing time. As the P.B content increased up to 10%, the engineering properties of sand improved in significant ways. Also the unconfined axial test conducted on two different sizes of samples and the results have shown there is no significant affect on stress-strain behavior. By comparing the calculated cohesion in unconfined axial test and triaxial test has been observed that there are some differences in values of cohesion its clear that the cohesion has been effected by structure of speicmen.

REFERENCES

Das, B. M. (1993) : Principles of Soil Dynamics. Boston: PWS-KENT Publishing Company.

GovindaRaju, L. *(2005). PhD Thesis, Indian Institute of Science, Bangalore.*

Head, K. H. *(1998): Manual of Soil Laboratory Testing. London: Pentech Press.*

Hanumantharao, C. and Ramana, G.V. (2008). Dynamic soil properties for microzonation of Delhi, India, Journal of Earth System and Science, Vol. 117, S2, 719–730

Ishihara, K. and Koseki, J. (1989). *Cyclic shear strength of fines containing sands, Earthquake and Geotechnical Engineering, Japanese Society of Soil* Mechanics and Foundation Engineering, Tokyo, 101 106.

Jafari M.K, Shafiee A. and Ramezankhahi, *(2002) Dynamic properties of fine grained soils in south of Tehran; Soil Dynamic and Earthquake Eng.*

Kokusho, T. *(1980). Cyclic triaxial test of dynamic soil properties for wide strain range, Soils and Foundations, Vol. 20, No.2, 45-60.*

Kramer, S.L. (*1996). Geotechnical Earthquake Engineering, Prentice Hall, New Jersey (NJ), 653***.**

Kramer, S.L. and Seed, H.B. *(1988). Initiation of soil liquefaction under static loading conditions, Journal of Geotechnical Engineering, ASCE, Vol. 114, No. 4, 412–430.*

Mulilis, J.P. *(1975). The Effects of Method of Sample Preparation on the Cyclic Stress Strain behaviour of Sands, EERC Report 75-18, College of Engineering, University of California ,Berkeley.*

Peacock, W.H., and Seed, H. B*. (1968), "Sand Liquefaction Under Cyclic Loading Simple Shear Conditions," Journal of the Soil Mechanics and Foundations Division, ASCE, Vol. 94, No. SM3, pp. 689 708.*

Ramberg, W., Osgood, W. R. *(1943). Description of stress-strain curves by three parameters, Technical note 902, National Advisory Committee on Aeronautics.*

Seed, H. B., and Lee, K. L. (1966). *"Liquefaction of Saturated Sands DuringCyclic Loading,".*

Seed, H. B. *(1979). "Soil Liquefaction and Cyclic Mobility* Evaluation for Level *Ground During Earthquakes," Journal of the Geotechnical Engineering Division, ASCE, Vol. 105, No. GT2.*

Seed, H. B., and Peacock, W. H. *(1971). "The Procedure for Measuring Soil Liquefaction Characteristics," Journal of the Soil Mechanics and Foundations Division , ASCE, Vol. 97, No. SM8.*

Seed, H.B., Tokimatsu, K., Harder, L.F., and Chung, R.M. *(1985). Influence of SPT procedures in soil liquefaction resistance evaluations, Journal of Geotechnical Engineering, Vol. III, No. 12.*

Silver, M.L. and Ishihara, K., *(1977). Comparison between the strength of undisturbed and reconstituted sands from Niigata, Japan, Contract Report, U.S. Army Engineer waterways experiment station, Corps of Engineers, Vicksburg, Miss.*

Tatsuoka, F., Yasuda, S., Iwasaki, T. and Tokida, K. *(1980). Normalised dynamic undrained strength of sands subjected to cyclic and random loading, Soil and Foundations, Vol. 20, No.*

U. S. Army Corps of Engineers Washington, D. C. *20314-1000,1970*

Vucetic, M. and Dobry, R. *(1991). Effect of soil plasticity on cyclic response. Journal of Geotechnical Engineering, ASCE, Vol. 117, No. 1, 89–107.*

Wong, R.T., Seed, H.B. and Chan, C.K., *(1975). Cyclic loading liquefaction of gravelly soils. Journal of Geotechnical Engineering, ASCE, Vol.101, No.GT6.*

Yoshimi, Y., and Oh-oka, H. *(1973). "A Ring Torsion Apparatus for Simple Shear Tests," Proceedings, 8th International Conference on Soil Mechanics and Foundation Engineering, Vol. 1.2, Moscow, USSR.*